Differential Wye Modular Multilevel AC Converter (DW-M2AC) for Direct AC/AC Power Conversion

by

Shehan Selaka Herathge

A thesis submitted in partial fulfillment of the requirements for the degree of

Master of Science

in

Energy Systems

Department of Electrical and Computer Engineering
University of Alberta

Abstract

Direct AC/AC MMCs are used in a wide variety of power system applications such as interconnecting asynchronous grids with different frequencies, renewable energy integrations and medium voltage variable frequency motor drives. Due to the advantages such as lower component count and lesser control complexity led by a low number of control states currents, the development of direct AC/AC MMCs with a lower number of arms has been a research trend in the recent literature. This research work proposes a direct AC/AC MMC with a simpler converter design (low number of arms) that has an integrated transformer to provide necessary galvanic isolation. A defining feature of the DW-M2AC is the adoption of a novel power transfer mechanism where the transformer windings carry current with multiple frequency components, while the core is rated only for a single AC frequency flux similar to conventional AC power systems transformers. This multi-tasking of the transformer provides a lower total semiconductor effort and, due to an inherent voltage boosting effect, makes the DW-M2AC more suitable for applications where high AC voltage step ratios are needed. This research work also presents a control strategy based on dq reference frame with decoupled control of differential mode and common mode currents in converter arms. The DW-M2AC's performance is tested under different scenarios using simulations. The simulation results are used to study the converter power transferring capability in fixed frequency grid connected operation and variable frequency operation. A scaled down 208/104 V, 1 kW three-phase laboratory prototype is developed and the converter operating principle is further validated by conducting a series of experiments.

To my mother and father…

Acknowledgements

First and foremost, I would like to express my sincere gratitude towards my supervisor, Professor Gregory Kish who accepted me to be one of his MSc students. Without this opportunity given by him, I probably would not have embarked on this journey as a graduate student in University of Alberta, gathering expertise in technical things and hands-on experience in laboratory experiments. He has always been a supportive supervisor in every part of the research work and his guidance and technical expertise helped me a lot to complete my research successfully. The time and effort he put into review the thesis and ideas on technical writings are quite remarkable for the success of this thesis work. I also wish to give my sincere gratitude to the members of the thesis examination committee, Professor Ryan (Yunwei) Li and Professor Ali Khajehoddin, for the time they took to review this work and their valuable feedback.

Most importantly, I would like to thank my parents who are the two pillars of my success, for their endless efforts and sacrifices to make the person who I am today. I always remember my mother, who is no longer among us, for believing in my potential and giving her blessings to pursue my dreams in a country far away from home. And I am forever in debt to my father who always takes care of my needs and for building a strong foundation in my life. Also, I would like to mention my school teachers, university professors who led the foundation for a good background in Electrical Engineering and technical know-how.

Special thanks go to Chatumal and Vishwa for helping me out in various occasions during my academic works and research, and I am forever thankful for their generous contributions. Also, I would like to thank my colleagues Anjana and Yuan for sharing their knowledge and help during the laboratory experiments. I am incredibly grateful to the many people, friends who I met in Edmonton and UofA for making my graduate life an enjoyable and memorable one.

Finally, I would like to thank University of Alberta for creating a nice working atmosphere full of diverse and supportive community.

~ Shehan Herathge, August 2022

Contents

List of Tables

List of Figures

List of Abbreviations

AC	Alternating Current
B2B MMC	Back-to-Back Modular Multilevel Converter
CHBC	Cascaded H-Bridge Converter
DC	Direct Current
DCC	Diode Clamped Converter
DW-M2AC	Differential Wye Modular Multilevel AC Converter
FBSM	Full Bridge Sub Module
FCC	Flying Capacitor Converter
FFTS	Fractional Frequency Transmission System
HBSM	Half Bridge Sub Module
HVDC	High Voltage Direct Current
KVL	Kirchhoff's Voltage Law
M3C	Modular Multilevel Matrix Converter
MMC	Modular Multilevel Converter
MVD	Medium Voltage Drive
NLC	Nearest Level Control
NPCC	Neutral Point Clamped Converter
PWM	Pulse Width Modulation
SHE	Selective Harmonic Elimination
SM	Sub Module
SMMC	Sparse Modular Multilevel Converter
SVM	Space Vector Modulation
THD	Total Harmonic Distortion
VFD	Variable Frequency Drive
VSC	Voltage Source Converter
WECS	Wind Energy Conversion System
Y-MMC	Y-connected Modular Multilevel Converter

Chapter 1

Introduction

In the last several years the energy conversion process in grid applications has drastically improved with the advancement of semiconductor devices and power electronics. Power electronic based converters play a vital role in every major phase of today's power systems including generation, transmission, and distribution. The increasing demand for renewable energy integration and microgrid applications is driving the extensive use of power converters as the power conversion interface with the grid.

Two-level Voltage Sourced Converters (VSC) are widely used in low voltage applications due to their structural simplicity with lesser components. But when it comes to high voltage and high-power applications, multilevel converters have some prominent advantages over two level VSCs. Some of the benefits that multilevel converters have can be pointed as; lower harmonic distortion and hence reduced demand for filtering, lower dv/dt and lower stresses on semiconductor components [1],[2].

There are several classes of multilevel converters that can be found in the literature. One such multilevel converter is the Diode Clamped Converter (DCC) which uses clamping diodes and cascaded DC capacitors to build up the DC link voltage. The three-level Neutral Point Clamped Converter (NPCC) [3] is the most popular variant under DCCs which has gained success in many commercial applications. Another multilevel converter topology is the Flying Capacitor Converter (FCC) [4] which use capacitors in between clamping points. The Cascaded H-Bridge Converter (CHBC) [5] can also provide multiple levels of voltage by using multiple cascaded H-bridge cells fed by separate DC sources.

In addition to these, the Modular Multilevel Converter (MMC) has gained immense popularity in the category of multilevel converters due to its modular and scalable design and the suitability for high power applications. A brief overview of the broader class of MMCs is given in the following section.

1.1 Modular Multilevel Converters

The MMC was first introduced by Prof. R. Marquardt and A. Lesnicar [6] as a new class of multilevel converter well suited for high voltage applications with modular design. As of today, the MMC and its topological variants are widely used in different power electronics related applications such as Medium Voltage Drives (MVD) [7], active filters [8], integration of renewable energy sources to the electrical grid [9],[10] and perhaps most notably, in High Voltage Direct Current (HVDC) transmission [11],[12]. MMCs receive wide acceptance in electrical power industry due to their advantages over conventional VSCs such as modular design, scalability, low harmonic content, redundancy and lower switching losses [13],[14].

The main feature of the MMC is the cascaded connection of a large number of low-voltage power cells. These power cells are called submodules, each containing a capacitor as the energy storage element that eliminates the requirement of having a single large capacitor in parallel with the DC link. Half Bridge Sub Module (HBSM) based MMCs are currently the most mature and economical MMC topology, but they have some drawbacks such as inability to clear the DC side short circuit current. Full Bridge Sub Module (FBSM) based MMCs are also available as they are inherently capable of blocking DC faults although with higher cost and losses due to the higher number of switches and diodes used in a single submodule [15]. Figure 1.1 shows the switch arrangement of a half bridge submodule and a full bridge submodule. In the half bridge cell, the capacitor can be inserted or bypassed resulting in two levels of output voltages; $+V_C$ and 0. In the full bridge cell, the capacitor can be positively inserted, negatively inserted, or bypassed resulting in three levels of output voltages; $+V_C$, $-V_C$ and 0.

Unlike in other multilevel converters such as NPCC and FCC, the number of output levels can be easily increased by simply adding more submodules in series within the MMC. Having a higher number of submodules leads to higher levels in the output voltage which helps to reduce the Total Harmonic Distortion (THD) and ultimately helping to minimize the filtering requirement. Utilizing more submodules also helps to reduce the voltage ratings of the individual semiconductor switches, which is beneficial in high voltage applications.

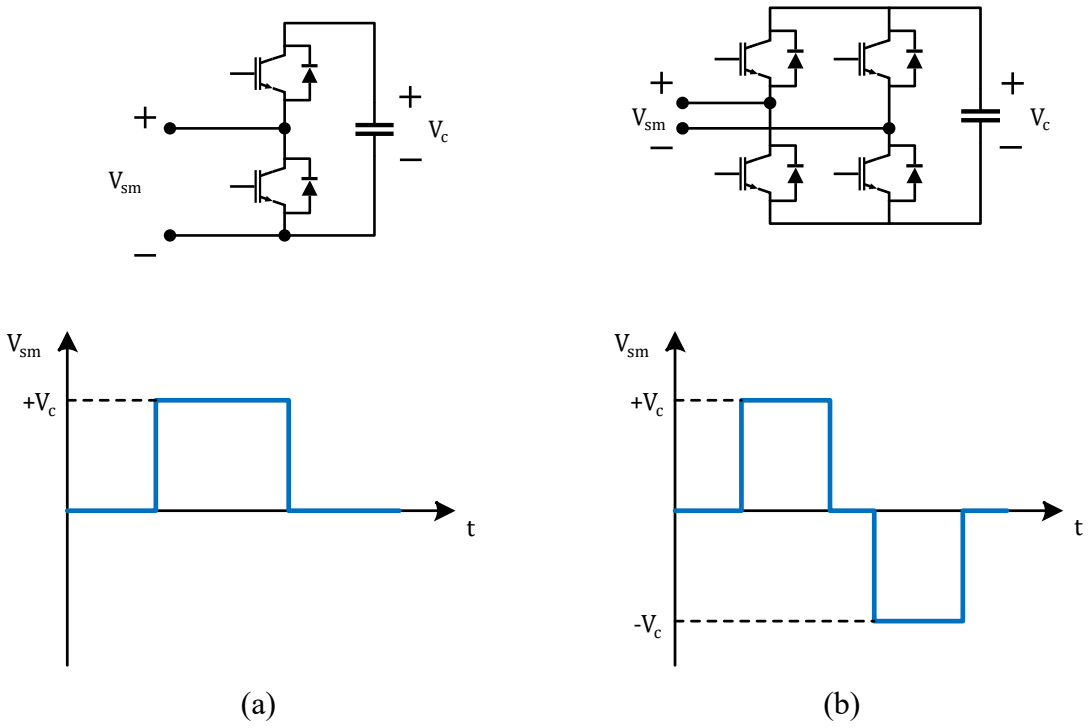

Figure 1.1: (a) Half Bridge Submodule (b) Full Bridge Submodule used in MMC

Figure 1.2 shows the schematic of a conventional three-phase MMC used in AC/DC conversion. The submodule string is a series connection of N number of half bridge or full bridge cells. A submodule string with an arm reactor is referred to as a phase arm (or branch) of the converter. The arm reactors in MMC play a vital role by controlling the rapid changes in arm currents and avoiding the direct parallel connection of submodule capacitors with the DC link [1]. The other benefits of arm reactors include; helping to avoid the resonance with arm capacitors, reducing di/dt of fault currents and limiting magnitudes of internally circulating currents. Also, in the controlling aspect, arm reactor allows the operation of a branch as a controlled current source. In this particular configuration, each set of upper and lower phase arms can be considered as a phase leg of the MMC.

Various modulation techniques have been proposed for MMCs. In general, these techniques can be divided into two main categories depending on the switching frequency. Nearest Level Control (NLC) and Selective Harmonic Elimination (SHE) can be given as some examples for the first category where the switching frequency is near the fundamental frequency. In the second

category, a high switching frequency is used. Multicarrier Pulse Width Modulation (PWM) and Space Vector Modulation (SVM) are some examples for the second category. Among these techniques, NLC is an attractive method due to the ease of implementation in HVDC applications where a high number of submodules is used. Multicarrier PWM techniques are also popular, but implementation complexity goes up as the number of submodules increases.

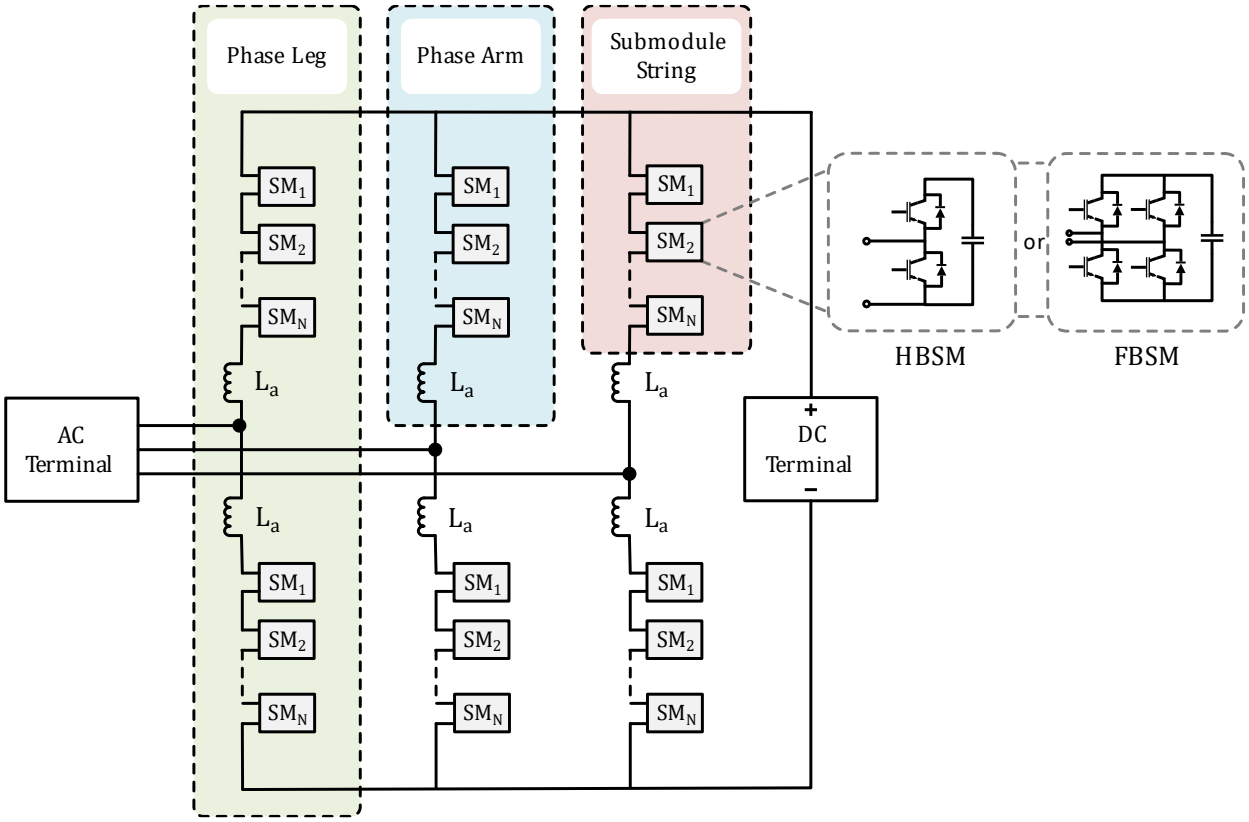

Figure 1.2: Schematic diagram of a three-phase MMC

Modulation techniques alone are not sufficient in MMCs when providing gate signals for the submodule strings. Since there are large number of capacitors inserted or bypassed periodically, submodules need to be selected properly in order to keep the average capacitor voltage of each submodule at an equal value over time. To handle this problem, capacitor voltage balancing techniques are also needed in MMC modulation. The sort and selection method is the most popular technique used for capacitor voltage balancing [6],[16]. In this method, capacitors are sorted according to their measured voltages. Depending on the current flow direction in the

arms, if the capacitors need to be charged (current must flow into the capacitor) then the capacitors with the lowest voltages will be inserted first, and if discharge needs to happen (current must flow out of the capacitor) the capacitors with highest voltages will be inserted first.

The MMC concept is used in many different topologies performing a wide range of power conversions from DC/DC, DC/AC and AC/AC. The following section gives a brief introduction about MMC based AC/AC converters.

1.2 AC/AC Modular Multilevel Converters

AC/AC MMCs can be divided into two main categories; indirect and direct converters. Indirect conversion is where two-stage power conversion happens, first from AC to DC and then DC to AC. Back-to-Back (B2B) MMC [17],[18] is an example of an indirect AC/AC converter. Modular Multilevel Matrix Converter (M3C) [19], Hexverter [20] and Y-connected MMC (Y-MMC) [21] are a few examples for direct AC/AC converters. In general, direct AC/AC converters are only capable of connecting two AC systems of different frequencies. Same or near frequency operation is somewhat difficult to achieve due to large capacitor voltage fluctuations [22]. However, there are some cases where same or near frequency operation is also possible by redistributing energy between arms by using circulating currents [23],[24]. In [25], a MMC topology was recently introduced that allows direct AC/AC power conversion between different voltage levels in a single frequency AC system. Another challenge inherent to AC/AC MMC operation is that the excessive low frequency fluctuations in capacitor voltages during low frequency operation especially at the starting of a motor [26]. There are some methods proposed in the literature to mitigate this issue such as injection of different high frequency currents [27],[28].

AC/AC converters are widely used in applications such as in railway traction systems [29], grid integration of wind turbines [30], railway power conditioning applications [31], grid connected power flow controller [32], Fractional Frequency Transmission Systems (FFTS) [33] and high power medium voltage motor drives [34],[35].

A detailed description of prominent 3ph-3ph AC/AC MMC topologies is given below.

1.2.1 Back-to-Back MMC (B2B MMC)

The B2B MMC consists of two bi-directional AC/DC MMCs connected in back-to-back configuration via an intermediate DC link (see Figure 1.3). As mentioned earlier, power conversion happens in two stages hence this topology falls under the category of indirect AC/AC converter. This topology has no limitation on frequency separation since the DC link decouples the two stages, and hence it can be used in same frequency operation as well. Typically, B2B MMCs use half bridge cells as their submodules in the arms. This is because of the DC voltage component appearing across the arms, avoiding the need for inserting negative voltages in the arm voltages [36]. However, B2B MMC topologies which use full bridge submodules [37] or combination of both submodule types (Hybrid B2B MMC) [38] can also be found in the literature.

As shown in the Figure 1.3, B2B MMC has twelve arms in total. Compared to other prominent AC/AC converter topologies (where M3C has nine arms and Hexverter has six arms) this can negatively affect the cost effectiveness the B2B MMC in terms of semiconductor and capacitor ratings and cost. However, reference [39] shows that the B2B MMC requires lesser semiconductor ratings but needs higher capacitor ratings compared to M3C. Because of the symmetry of the dual converter setup, both step-down and step-up options are available at either side of the AC/AC converter. The operation and control of the B2B MMC is relatively straight forward as it employs two bidirectional AC/DC MMCs. In terms of power transferring mechanism, the active power input of system 1 must be equal to the active power output to the system 2 (at steady-state) while regulating the capacitor voltage values of each submodule. The B2B MMC inherently experiences fluctuations in capacitor voltages when it is used for generating lower frequencies at the output side. In order to tackle this problem, there are several solutions given by various researchers. These solutions include methods such as injecting high frequency common mode voltages and additional circulating currents between arms, which can lead to higher current ratings of the semiconductor used in the converter [27],[40].

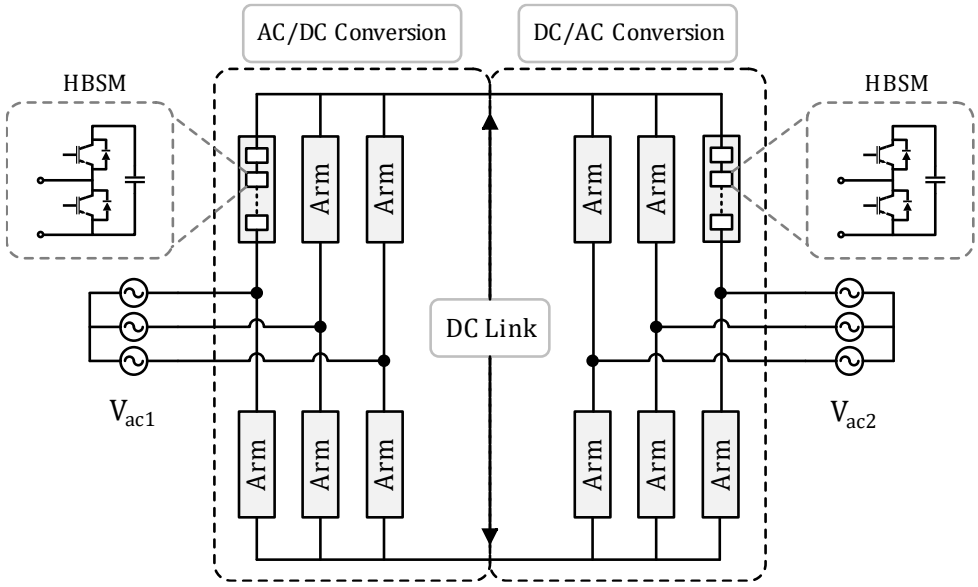

Figure 1.3: Configuration of the B2B MMC

1.2.2 Modular Multilevel Matrix Converter (M3C)

The M3C can be used to connect two AC systems with different frequencies without using an intermediate DC link. Hence it is referred to as a direct AC/AC converter. Figure 1.4 shows the circuit configuration of the M3C. The M3C has nine arms which consist of full bridge submodules. Unlike in the B2B MMC, the M3C does not have a DC link hence full bridge submodules are needed to inject positive and negative voltages in the converter arms. The controlling of M3C can be somewhat a challenging task due to complex arm interconnections. Capacitor voltages of each arms need to be regulated properly in order to ensure adequate power transfer between system 1 and system 2. This is done by controlling four linearly independent circulating currents which are internal to converter arms but not appear at the input or output sides of the converter [41]. In low frequency operation, the capacitor voltage fluctuations in the M3C are lower compared to the B2B MMC for the same installed energy storage. This makes the M3C a promising topology for high power variable speed motor drive applications. However, due to the complexity in controls and high component count, the M3C is more costly to build. Therefore, it is still not largely employed in commercial applications.

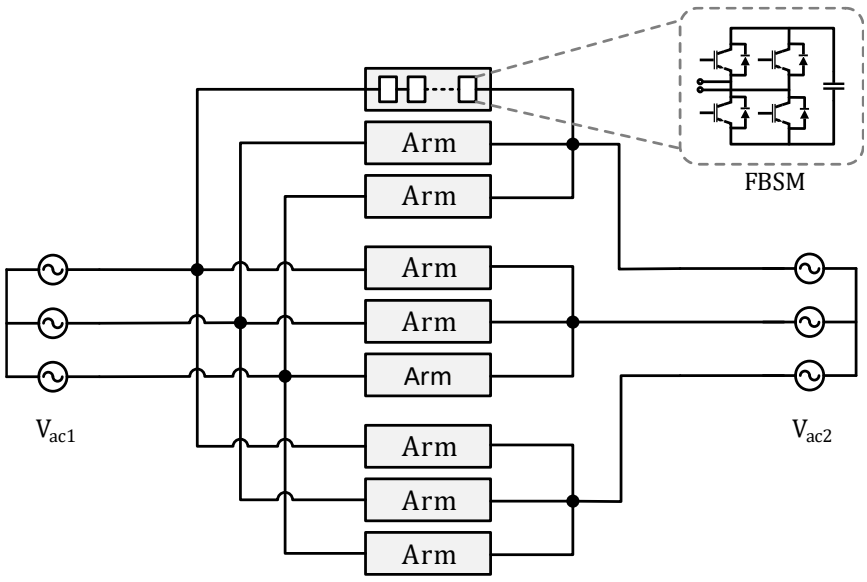

Figure 1.4: Configuration of the M3C

1.2.3 Hexagonal Modular Multilevel Converter (Hexverter)

The Hexagonal MMC (also referred as Hexverter) directly connects two three phase systems without having a central DC link, similar to the M3C. The Hexverter consists of six branches connected in a hexagonal ring shape as shown in Figure 1.5. This can be seen as a simplification of the matrix converter of Figure 1.4 with reduced number of converter arms. The phases of the two AC systems are connected alternatively to the connection points of branches in the ring as depicted in Figure 1.5. In this way, one phase of an AC system is connected to two phases of the other AC system by two branches. Like in the M3C, the Hexverter also needs to have full bridge cells in its arms allowing the synthesis of both positive and negative voltages. Compared to the M3C and B2B MMC, the Hexverter has the lowest number of arms and hence equipment volume and cost are significantly reduced. On par with the M3C, the Hexverter exhibits superior performance in low frequency operations therefore it is best suitable for applications such as variable frequency drives and wind energy integrations.

Another direct AC/AC converter topology named as Hex-Y converter is proposed in [42] by adding 3 additional star connected branches to the Hexverter structure in Figure 1.5. By doing this, the Hex-Y converter can benefit from having three linearly independent circulating current loops contrary to only one available in the Hexverter.

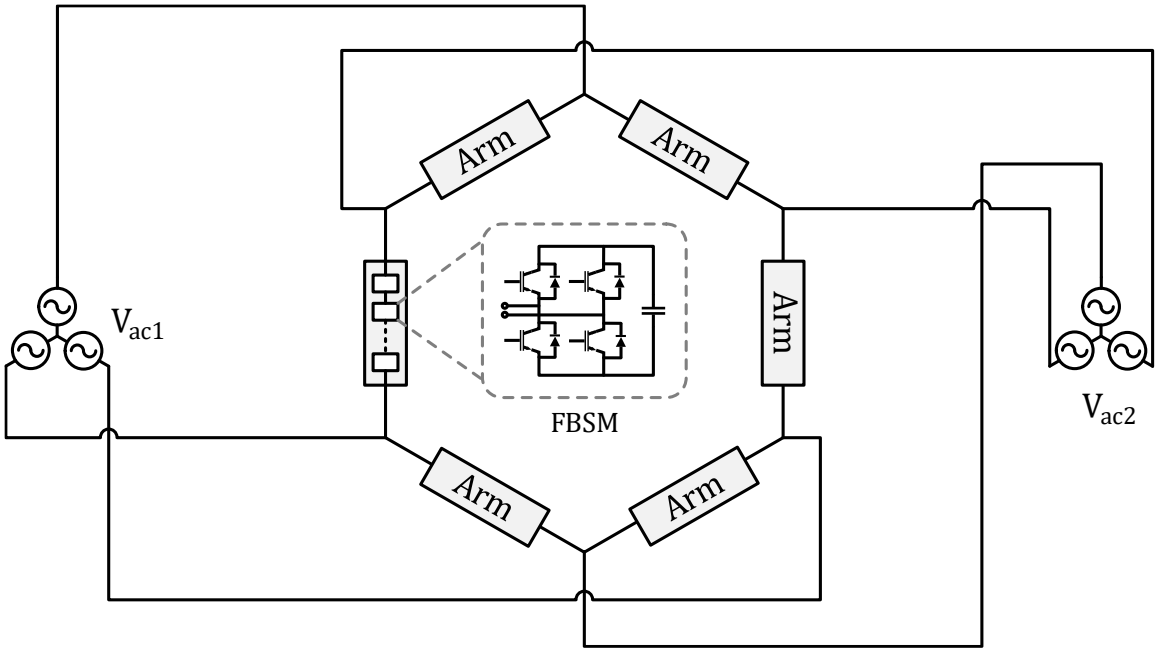

Figure 1.5: Configuration of the Hexverter

The M3C, Hexverter and Hex-Y converters are highlighted here as direct AC/AC MMCs due to their widespread prominence in the literature. However, other direct AC/AC modular converters have also been proposed. One such direct AC/AC converter is the Sparse Modular Multilevel Converter (SMMC), which is based on an alternative configuration of half bridge and full bridge submodules [43]. Reference [44] proposes a Three-port Nonagonal MMC which has nine bridge arms connected from end to end.

1.3 Motivation

In power system applications where two AC systems are connected, AC/AC converters are used as an intermediate device as shown in Figure 1.6a. These two AC systems can be same frequency or different frequency systems, and most of the time with two different voltage levels (indicated here by V_{ac1}, V_{ac2}). Therefore, the AC/AC converter employed here should have the ability to perform voltage stepping and frequency conversion if necessary. Alternatively, a transformer can be used along with an AC/AC converter to step-up or step-down the voltage levels while providing necessary galvanic isolation, Figure 1.6b. In this case voltage stepping can solely be done by the transformer or by a combination of both converter and transformer. The converter topology proposed in this thesis work will have a similar configuration as shown in Figure 1.6c, where the transformer is integrated to the converter. By integrating the transformer at the arm level of the MMC, the function of the arm inductors and AC side line filters can be merged to the leakage inductance of the transformer [45].

In high voltage applications, when transformers with high turns ratio are used they will have some designing challenges such as high insulation cost, dielectric losses in insulation and increased core losses [46]. Alternatively, voltage stepping can be done by the converter itself and it can increase more stress on semiconductor devices of converters.

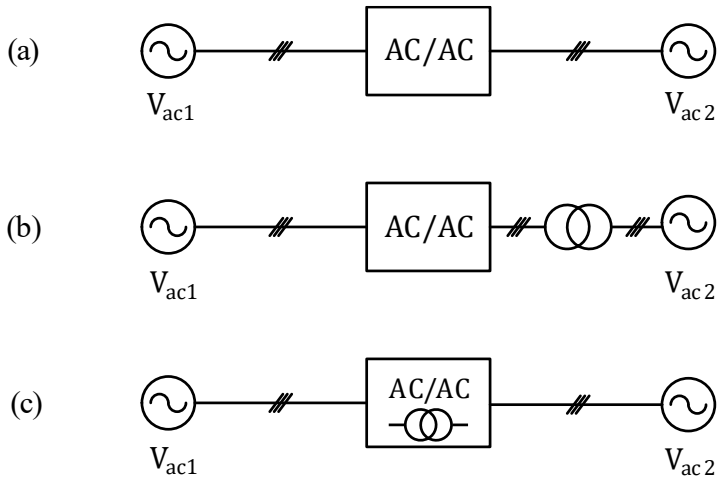

Figure 1.6: Different AC system connections using AC/AC converters (a) without isolation transformer (b) with isolation transformer (c) with integrated transformer

Figure 1.7 shows the semiconductor effort (normalized to input power) vs. AC voltage step ratio plot for three different AC/AC MMCs; M3C, Hexverter and the converter presented in this thesis, the DW-M2AC (a detailed derivation and analysis of the semiconductor effort is presented in the section 2.4.1). The AC voltage step ratio is defined in this work as $G_v = \frac{V_{ac2}}{V_{ac1}}$. In Figure 1.7, the proposed DW-M2AC has an integrated 1:1 transformer (see Figure 1.6c) while the other two converters are also given 1:1 transformers for fair comparison. As shown in Figure 1.7, the semiconductor effort will increase when the voltage step ratio increases. For the M3C and Hexverter, the semiconductor effort is lowest when the voltage step ratio is 1 and for DW-M2AC the semiconductor effort is lowest when the voltage step ratio is 2. Therefore, it is important that if the converter is operated at an operating point where its semiconductor effort is lowest, and rest of the voltage boosting is done by a transformer. In that case, a transformer integrated converter topology that can facilitate lesser turns ratio will have a significant place among the AC/AC power converters.

As mentioned earlier, the B2B MMC has 12 arms while the M3C and Hexverter have 9 and 6 arms respectively. More branches in the converter means the mechanical construction will be more difficult and the cost for measuring devices and control electronics will be high. Therefore, a converter with lesser number of arms can be benefited from cost saving from physical construction and measuring equipment and hence will be more cost effective in terms of total system cost when implemented in commercial applications.

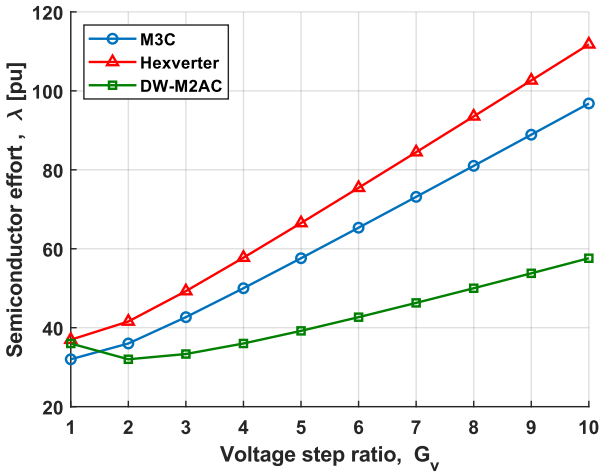

Figure 1.7: Semiconductor effort for converters where all the converters are having a 1:1 transformer

1.4 Thesis Scope

A new modular multilevel converter topology for AC/AC conversion integrated with galvanic isolation is presented in this thesis. This new topology is termed as Differential Wye Modular Multilevel AC Converter (DW-M2AC) due to the differential arrangement of wye connected arms. In addition to the galvanic isolation, the DW-M2AC is more suitable for applications where high voltage AC step ratio is needed. A comparative analysis is done to compare the semiconductor effort and magnetics requirement of the DW-M2AC against two of prominent direct AC/AC MMCs; the M3C and Hexverter. The DW-M2AC uses a novel power transfer mechanism where the transformer windings carry current with multiple frequencies, but the core only needs to be rated for a single AC frequency flux due to the flux cancellation happening at the center-tapped winding. Other salient features can be mentioned as; reduced requirement of arm inductance, lower semiconductor effort and control simplicity due to lower number of converter arms. The operation of the proposed converter is validated through simulations and some design specific case studies have been carried out with controlling mechanisms. The power transferring capability of the DW-M2AC is demonstrated using an experimental setup for different input and output frequencies.

Chapter 2

Overview of Differential Wye Modular Multilevel AC Converter (DW-M2AC)

In this chapter an overview of the proposed DW-M2AC is given with the general structure of the converter topology. Also, operating principles of the converter are discussed including the dynamic modelling and explanation on internal power transfer mechanisms. Later, the operating principle of the converter is validated through simulations. In addition, a comparative analysis against existing prominent direct AC/AC MMCs is done based on semiconductor effort, magnetics requirement and energy storage requirement. Finally, salient features of the proposed DW-M2AC are presented.

2.1 DW-M2AC System Architecture

The general structure of the DW-M2AC is shown in Figure 2.1. This structure consists of a three-phase center tapped transformer and six arms (two arms per phase leg). Each arm is a stack of Full Bridge Submodules (FBSM). Since the injected arm voltages are subjected to bidirectional voltages it is necessary to use Full Bridge Submodules. Two arms of a single-phase leg are differentially connected across the center-tapped windings on the converter side of the three-phase transformer. The arms of the three phases are connected as wye connection at left side and right side of the converter (labeled as point L and point R) hence gives the name for this converter topology as Differential Wye Modular Multilevel AC Converter. The differentially connected converter arms can impose both a common mode and differential mode voltage across the center-tapped windings. These two voltage components interact with the two AC system voltages, V_{g1} and V_{g2} respectively, to achieve the desired AC side power injections. AC system 1 is connected to the primary side of the transformer at the center tapped position and AC system 2 is connected to the secondary side of the transformer. By this means, two AC systems are galvanically isolated and the transformer itself is integrated to the converter operation.

A salient feature of the DW-M2AC compared to other MMCs is that, since the transformer windings are in series with the converter arms, the leakage inductance of the transformer can be used as the arm inductance. This can help to reduce the cost of employing separate arm inductors for the converter.

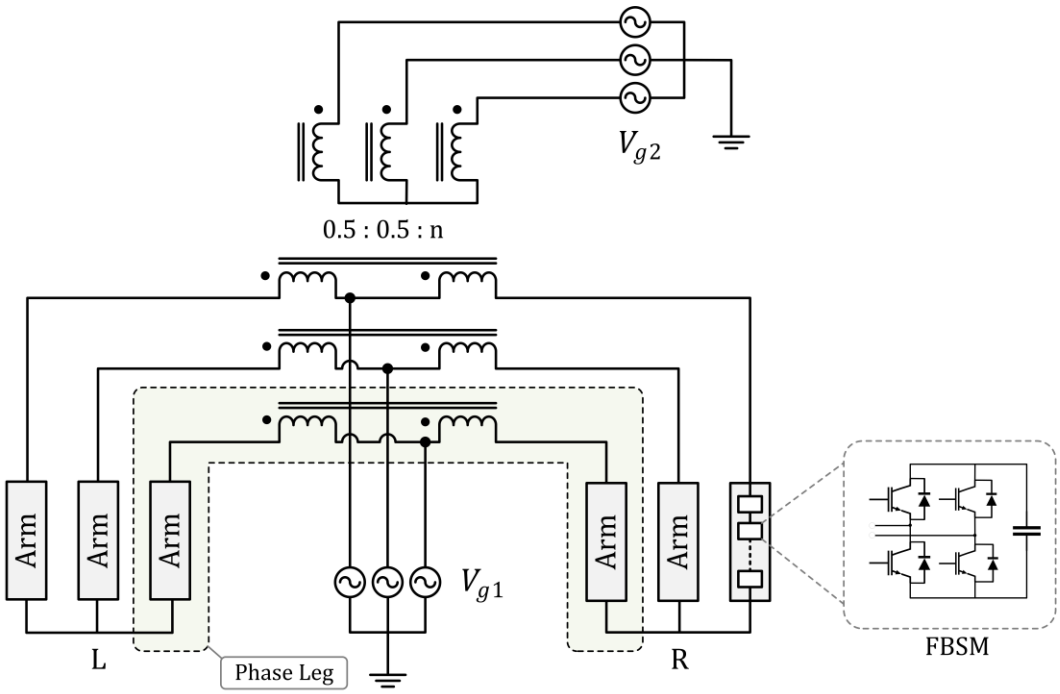

Figure 2.1: General structure of the three phase DW-M2AC for direct AC/AC conversion

The proposed DW-M2AC is a direct AC/AC converter that can be employed in different applications, such as:

1. An AC/AC converter for asynchronous grids of different frequencies (e.g., to interconnect 50 Hz and 60 Hz grids). Due to the integrated transformer structure, galvanic isolation is achieved and bidirectional power flow is possible between the two AC grids. Additionally, reactive power can also be provided to the grids or absorbed from grids as needed.
2. An AC/AC converter for Variable Frequency Drive (VFD) applications. The AC port 2 can be connected to the grid and the AC port 1 can be connected to the motor drive. In this way, flux is produced in the transformer core using a fixed frequency while the transformer primary winding (connected to AC port 1) is responsible for variable frequency operation.

3. A frequency changer in Fractional Frequency Transmission Systems (FFTS). For example, the DW-M2AC can be used as a frequency tripler where 50/3 Hz power transmitted through a transmission line is converted back to 50 Hz power at the grid side. FFTS is a popular technique used in offshore wind energy integration applications where higher power transferring capability is achieved using a fractional frequency in transmission lines [47].

2.2 DW-M2AC Operating Principle

The DW-M2AC operating principle is most easily described using the single-phase version of the DW-M2AC. Considering the single-phase circuit of the converter, dynamic equations are derived and later these will be triplicated to get the complete model for the three-phase topology.

2.2.1 Dynamic Modelling

For analyzing the single-phase version of the DW-M2AC, arm currents and arm voltages can be broken into differential and common mode components as depicted by Figure 2.2. The symbol 'Δ' denotes differential mode components and the symbol 'Σ' denotes common mode components. The arm voltage of the left branch synthesizes a common mode voltage of v_{Σ} and differential mode voltage of v_{Δ} and both have the same polarity. The arm voltage of the right branch synthesizes a common mode voltage of v_{Σ} and differential mode voltage of v_{Δ} but they have opposite polarities. The relationship of arm voltages with the differential mode and common mode components are,

$$v_{arm,L} = v_{\Sigma} + v_{\Delta} \tag{2.1}$$

$$v_{arm,R} = v_{\Sigma} - v_{\Delta} \tag{2.2}$$

$$v_{\Delta} = \frac{v_{arm,L} - v_{arm,R}}{2} \tag{2.3}$$

$$v_{\Sigma} = \frac{v_{arm,L} + v_{arm,R}}{2} \tag{2.4}$$

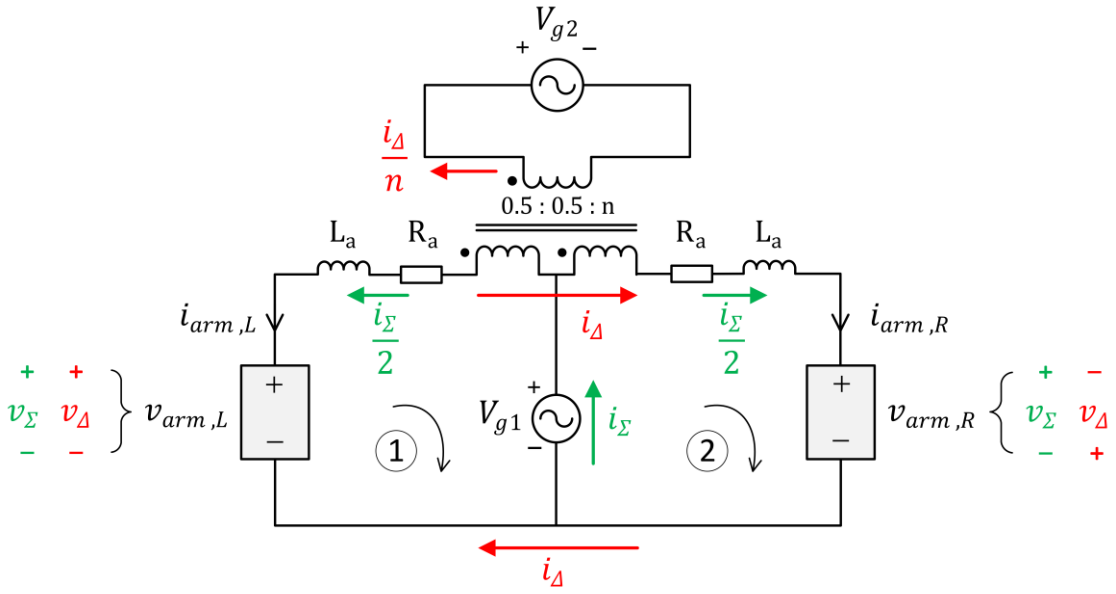

Figure 2.2: Schematic diagram of the single-phase version of DW-M2AC

According to the voltages imposed by converter arms as shown in Figure 2.2, the resulting differential mode current i_Δ operates with fundamental frequency of f_2 while common mode current i_Σ operates with fundamental frequency of f_1. The relationship of arm currents with the differential mode and common mode components are,

$$i_{arm,L} = \frac{i_\Sigma}{2} - i_\Delta \tag{2.5}$$

$$i_{arm,R} = \frac{i_\Sigma}{2} + i_\Delta \tag{2.6}$$

$$i_\Delta = \frac{i_{arm,R} - i_{arm,L}}{2} \tag{2.7}$$

$$i_\Sigma = i_{arm,L} + i_{arm,R} \tag{2.8}$$

According to (2.5) and (2.6), it is evident that the arm currents carry currents of two different frequencies. Although transformer primary winding carries current with two different frequency components, there is no common mode flux produced in the transformer core due to the $\frac{i_\Sigma}{2}$ component. This is because of the windings arrangement where common mode currents are

flowing in opposite directions and the flux will be cancelled out. That is, the $\frac{i_\Sigma}{2}$ in one center-tapped winding produces a flux which opposes the flux produced by the $\frac{i_\Sigma}{2}$ in the other center-tapped winding. The net flux in the transformer core has a single frequency component only, which is due to the differential mode current i_Δ. Note that, R_a denotes the arm resistance and L_a captures both arm choke inductance and the transformer leakage inductance for ease of modelling.

The step-by-step process for obtaining converter dynamic equations using Figure 2.2 is given below.

By applying KVL to loop (1),

$$v_{arm,L} + R_a i_{arm,L} + L_a \frac{d}{dt}\left(i_{arm,L}\right) - \frac{V_{g2}}{2n} - V_{g1} = 0 \tag{2.9}$$

By applying KVL to loop (2),

$$V_{g1} - \frac{V_{g2}}{2n} - R_a i_{arm,R} - L_a \frac{d}{dt}\left(i_{arm,R}\right) - v_{arm,R} = 0 \tag{2.10}$$

By adding (2.9) and (2.10),

$$\left(v_{arm,L} - v_{arm,R}\right) - 2\left(\frac{V_{g2}}{2n}\right) + R_a\left(i_{arm,L} - i_{arm,R}\right) + L_a \frac{d}{dt}\left(i_{arm,L} - i_{arm,R}\right) = 0 \tag{2.11}$$

$$2v_\Delta - \frac{V_{g2}}{n} - 2R_a i_\Delta - 2L_a \frac{d}{dt}(i_\Delta) = 0 \tag{2.12}$$

Further simplifying the above equation, differential mode dynamics of the converter can be obtained as follows,

$$v_\Delta - \frac{V_{g2}}{2n} - R_a i_\Delta - L_a \frac{d}{dt}(i_\Delta) = 0 \tag{2.13}$$

By subtracting (2.9) and (2.10),

$$\left(v_{arm,L} + v_{arm,R}\right) - 2V_{g1} + R_a\left(i_{arm,L} + i_{arm,R}\right) + L_a \frac{d}{dt}\left(i_{arm,L} + i_{arm,R}\right) = 0 \tag{2.14}$$

$$2v_{\Sigma} - 2V_{g1} + R_a i_{\Sigma} + L_a \frac{d}{dt}(i_{\Sigma}) = 0 \tag{2.15}$$

Further simplifying the above equation, common mode dynamics of the converter can be obtained as follows,

$$v_{\Sigma} - V_{g1} + \frac{R_a}{2} i_{\Sigma} + \frac{L_a}{2} \frac{d}{dt}(i_{\Sigma}) = 0 \tag{2.16}$$

Equations (2.13) and (2.16) contain only differential mode and common mode components, respectively. Using these decoupled dynamic equations, differential mode current i_{Δ} and common mode current i_{Σ} (which are analogous to grid currents i_{g2} and i_{g1} respectively) can be controlled independently and this will be further discussed in Chapter 3.

2.2.2 Internal Power Transfer Mechanism

Since the DW-M2AC is connected through two AC systems with different frequencies, the converter arms should absorb power from one frequency and release power in the other frequency (or vice versa). The submodules in the arms only have capacitive energy storage and therefore, the average power consumed at steady-state by each arm should be equal to zero. Using this property, the internal power transfer mechanism can be explained as follows.

Common mode and differential mode quantities for voltages and currents can be defined as follows.

$$v_{\Sigma} = \hat{V}_{\Sigma} \cos(\omega_{\Sigma} t + \theta_{v\Sigma}) \tag{2.17}$$

$$v_{\Delta} = \hat{V}_{\Delta} \cos(\omega_{\Delta} t + \theta_{v\Delta}) \tag{2.18}$$

$$i_{\Sigma} = \hat{I}_{\Sigma} \cos(\omega_{\Sigma} t + \theta_{i\Sigma}) \tag{2.19}$$

$$i_{\Delta} = \hat{I}_{\Delta} \cos(\omega_{\Delta} t + \theta_{i\Delta}) \tag{2.20}$$

For the left arm, the instantaneous power is

$$P_{arm,L} = v_{arm,L} \times i_{arm,L} \tag{2.21}$$

$$P_{arm,L} = (v_\Sigma + v_\Delta)\left(\frac{i_\Sigma}{2} - i_\Delta\right) = v_\Sigma \frac{i_\Sigma}{2} - v_\Sigma i_\Delta + v_\Delta \frac{i_\Sigma}{2} - v_\Delta i_\Delta \tag{2.22}$$

For the right arm, the instantaneous power is

$$P_{arm,R} = v_{arm,R} \times i_{arm,R} \tag{2.23}$$

$$P_{arm,R} = (v_\Sigma - v_\Delta)\left(\frac{i_\Sigma}{2} + i_\Delta\right) = v_\Sigma \frac{i_\Sigma}{2} + v_\Sigma i_\Delta - v_\Delta \frac{i_\Sigma}{2} - v_\Delta i_\Delta \tag{2.24}$$

For the left arm, when imposing steady-state requirement $P_{arm,L} = 0$,

$$\langle P_{arm,L} \rangle = \frac{1}{T}\int_1^T \left(v_\Sigma \frac{i_\Sigma}{2} - v_\Sigma i_\Delta + v_\Delta \frac{i_\Sigma}{2} - v_\Delta i_\Delta\right) dt = 0 \tag{2.25}$$

$$\begin{aligned}\langle P_{arm,L} \rangle = \frac{1}{T}\int_1^T \Bigg(&\frac{\hat{V}_\Sigma \hat{I}_\Sigma}{2}\cos(\omega_\Sigma t + \theta_{v\Sigma})\cos(\omega_\Sigma t + \theta_{i\Sigma}) - \hat{V}_\Sigma \hat{I}_\Delta \cos(\omega_\Sigma t + \theta_{v\Sigma})\cos(\omega_\Delta t + \theta_{i\Delta}) \\ &+ \frac{\hat{V}_\Delta \hat{I}_\Sigma}{2}\cos(\omega_\Delta t + \theta_{v\Delta})\cos(\omega_\Sigma t + \theta_{i\Sigma}) - \hat{V}_\Delta \hat{I}_\Delta \cos(\omega_\Delta t + \theta_{v\Delta})\cos(\omega_\Delta t + \theta_{i\Delta})\Bigg) dt = 0\end{aligned} \tag{2.26}$$

$$\frac{\hat{V}_\Sigma \hat{I}_\Sigma}{2}\cos(\theta_{v\Sigma} - \theta_{i\Sigma}) - \hat{V}_\Delta \hat{I}_\Delta \cos(\theta_{v\Delta} - \theta_{i\Delta}) = 0 \tag{2.27}$$

Consequently, the steady-state power balance relationship for the left arm is

$$\frac{\hat{V}_\Sigma \hat{I}_\Sigma}{2}\cos(\theta_{v\Sigma} - \theta_{i\Sigma}) = \hat{V}_\Delta \hat{I}_\Delta \cos(\theta_{v\Delta} - \theta_{i\Delta}) \tag{2.28}$$

Similarly, when imposing steady-state requirement $P_{arm,R} = 0$,

$$\langle P_{arm,R} \rangle = \frac{1}{T}\int_1^T \left(v_\Sigma \frac{i_\Sigma}{2} + v_\Sigma i_\Delta - v_\Delta \frac{i_\Sigma}{2} - v_\Delta i_\Delta\right) dt = 0 \tag{2.29}$$

$$\begin{aligned}\langle P_{arm,R} \rangle = \frac{1}{T}\int_1^T \Bigg(&\frac{\hat{V}_\Sigma \hat{I}_\Sigma}{2}\cos(\omega_\Sigma t + \theta_{v\Sigma})\cos(\omega_\Sigma t + \theta_{i\Sigma}) + \hat{V}_\Sigma \hat{I}_\Delta \cos(\omega_\Sigma t + \theta_{v\Sigma})\cos(\omega_\Delta t + \theta_{i\Delta}) \\ &- \frac{\hat{V}_\Delta \hat{I}_\Sigma}{2}\cos(\omega_\Delta t + \theta_{v\Delta})\cos(\omega_\Sigma t + \theta_{i\Sigma}) - \hat{V}_\Delta \hat{I}_\Delta \cos(\omega_\Delta t + \theta_{v\Delta})\cos(\omega_\Delta t + \theta_{i\Delta})\Bigg) dt = 0\end{aligned} \tag{2.30}$$

$$\frac{\hat{V}_\Sigma \hat{I}_\Sigma}{2}\cos(\theta_{v\Sigma} - \theta_{i\Sigma}) - \hat{V}_\Delta \hat{I}_\Delta \cos(\theta_{v\Delta} - \theta_{i\Delta}) = 0 \tag{2.31}$$

The steady-state power balance relationship for the right arm is

$$\frac{\hat{V}_\Sigma \hat{I}_\Sigma}{2}\cos(\theta_{v\Sigma} - \theta_{i\Sigma}) = \hat{V}_\Delta \hat{I}_\Delta \cos(\theta_{v\Delta} - \theta_{i\Delta}) \tag{2.32}$$

According to (2.28) and (2.32), it can be concluded that each arm processes half of the power exchanged between AC systems 1 and 2. Moreover, each arm absorbs power in one frequency and releases power in another frequency. The internal power transfer in the converter can be graphically represented as in Figure 2.3.

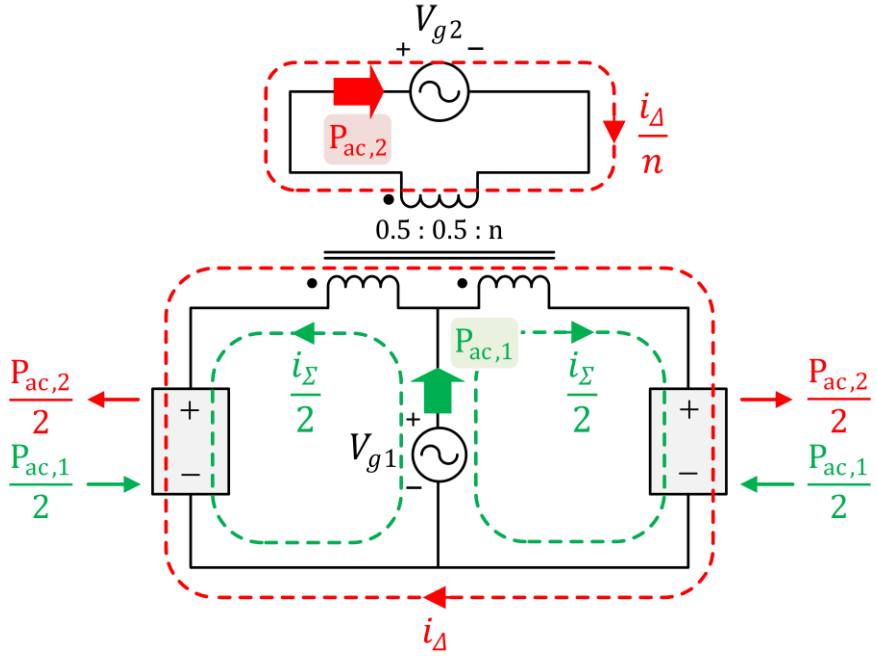

Figure 2.3: Internal power transfer mechanism of the DW-M2AC

2.3 Simulation Validation of the DW-M2AC Operating Principle

In this section the DW-M2AC operating principle is validated by performing a simulation based on the single-phase circuit of the DW-M2AC, Figure 2.4. In this model, AC system 1 (supply side) is represented using an AC voltage source connected to the center-tapped position of the primary winding of the transformer and AC system 2 (load side) is represented using a resistive load connected to the secondary winding of the transformer. In accordance with the notation used in section 2.2.1, the common mode current i_{Σ} is the system 1 (supply side) current (i_{g1}) and differential mode current i_{Δ} is the system 2 (load side) current (i_{g2}).

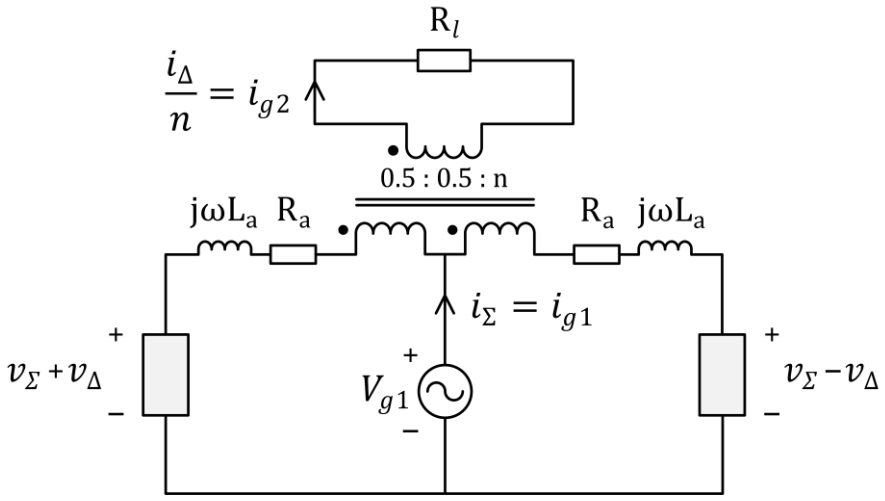

Figure 2.4: Single-phase simulation model of the DW-M2AC

As discussed in the previous section, the converter arms absorb power in the frequency corresponding to i_{Σ} and release power in the frequency corresponding to i_{Δ}. This is for real power transfer from source to load. Using this insight, the circuit shown in Figure 2.4 can be split into two circuits for easier analysis as shown in Figure 2.5a and Figure 2.5b. As shown in each subfigure, the circuits on the left-hand side can be further simplified into the circuits on the right-hand side.

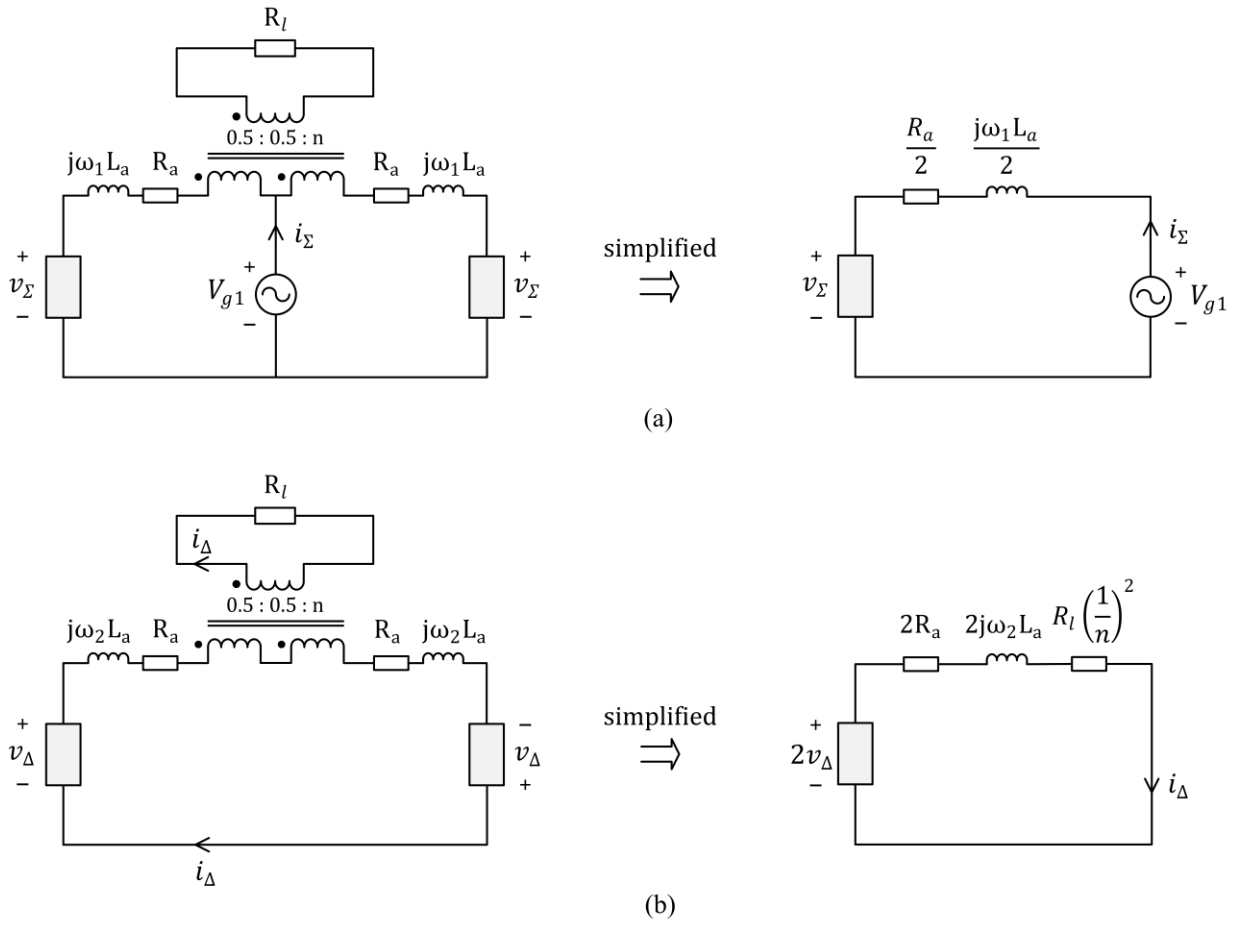

Figure 2.5: Decoupled equivalent circuits for (a) common mode quantities and (b) differential mode quantities

Considering the common mode circuit in Figure 2.5a, a phasor equation for steady-state i_Σ can be obtained as,

$$\bar{I}_\Sigma = \frac{\bar{V}_{g1} - \bar{V}_\Sigma}{\frac{R_a}{2} + \frac{j\omega_1 L_a}{2}} \tag{2.33}$$

This yields the steady-state common mode voltage phasor $\bar{V}_\Sigma$, which needs to be imposed by converter arms.

$$\bar{V}_\Sigma = \bar{V}_{g1} - \frac{1}{2}\bar{I}_{g1}(R_a + j\omega_1 L_a) \tag{2.34}$$

Also, by considering the differential mode circuit in Figure 2.5b, a phasor equation for i_Δ can be obtained as,

$$\bar{I}_\Delta = \frac{2\bar{V}_\Delta}{2R_a + R_l\left(\frac{1}{n}\right)^2 + j\omega_2 L_a} \tag{2.35}$$

The average power of the two equivalent circuits should be equal at steady-state, which gives the following dot product relationship,

$$\bar{V}_\Sigma \bar{I}_\Sigma = 2\bar{V}_\Delta \bar{I}_\Delta \tag{2.36}$$

$$\bar{V}_\Sigma \times \left(\frac{\bar{V}_{g1} - \bar{V}_\Sigma}{\frac{R_a}{2} + \frac{j\omega_1 L_a}{2}}\right) = 2\bar{V}_\Delta \times \left(\frac{2\bar{V}_\Delta}{2R_a + R_l\left(\frac{1}{n}\right)^2 + j\omega_2 L_a}\right) \tag{2.37}$$

By simplifying (2.37), the steady-state differential mode voltage phasor $\bar{V}_\Delta$ that needs to be imposed by converter arms can be obtained as,

$$\bar{V}_\Delta = \sqrt{\frac{\bar{V}_\Sigma\left(\bar{V}_{g1} - \bar{V}_\Sigma\right)}{4} \times \frac{2R_a + R_l\left(\frac{1}{n}\right)^2 + j\omega_2 L_a}{\frac{R_a}{2} + \frac{j\omega_1 L_a}{2}}} \tag{2.38}$$

Using (2.34) and (2.38), numerical values for common mode and differential mode arm voltage components can be calculated for a given converter design. Then, via simulation, $v_\Sigma + v_\Delta$ is injected as the left arm voltage and $v_\Sigma - v_\Delta$ is injected as the right arm voltage using ideal voltage sources (see Figure 2.6). The model of Figure 2.6 is valid as long as the average powers absorbed by the voltage sources in the arms are equal to zero. For this idealized simulation, the frequencies of the two AC systems are arbitrary selected as 50 Hz and 60 Hz respectively and the rest of the parameters used in the simulation model are given in Table 2.1.

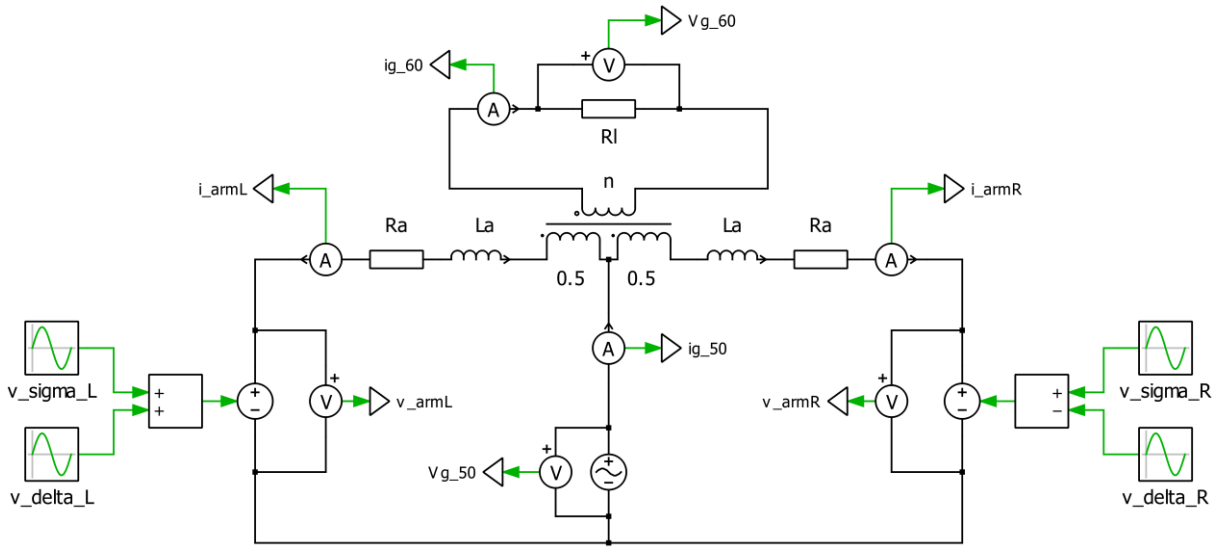

Figure 2.6: Schematic diagram of the simulation model

Table 2.1: Parameters for the simulation model

AC system 1 frequency (f_1)	50 Hz
AC system 1 power ($P_{ac,1}$)	1 MW
AC system 1 voltage (V_{g1})	1000 V rms
AC system 2 frequency (f_2)	60 Hz
Voltage gain ratio (V_{g2}/V_{g1})	2
Transformer turns ratio (n)	1
Arm resistance (R_a)	10 mΩ
Arm inductance (L_a)	1 mH
Load resistance (R_l)	4 Ω

2.3.1 Simulation Results

Figure 2.7 shows steady-state simulation results based on the model of Figure 2.6 and parameters in Table 2.1. As shown, the supply side and load side voltage & currents have two distinct frequencies, 50 Hz and 60 Hz, respectively. This is achieved by injecting the proper common mode and differential mode voltages in the converter arms based on (2.34) and (2.38). According to the chosen power level of 1MW, the supply voltage (V_{g1}) is 1000 V rms and hence

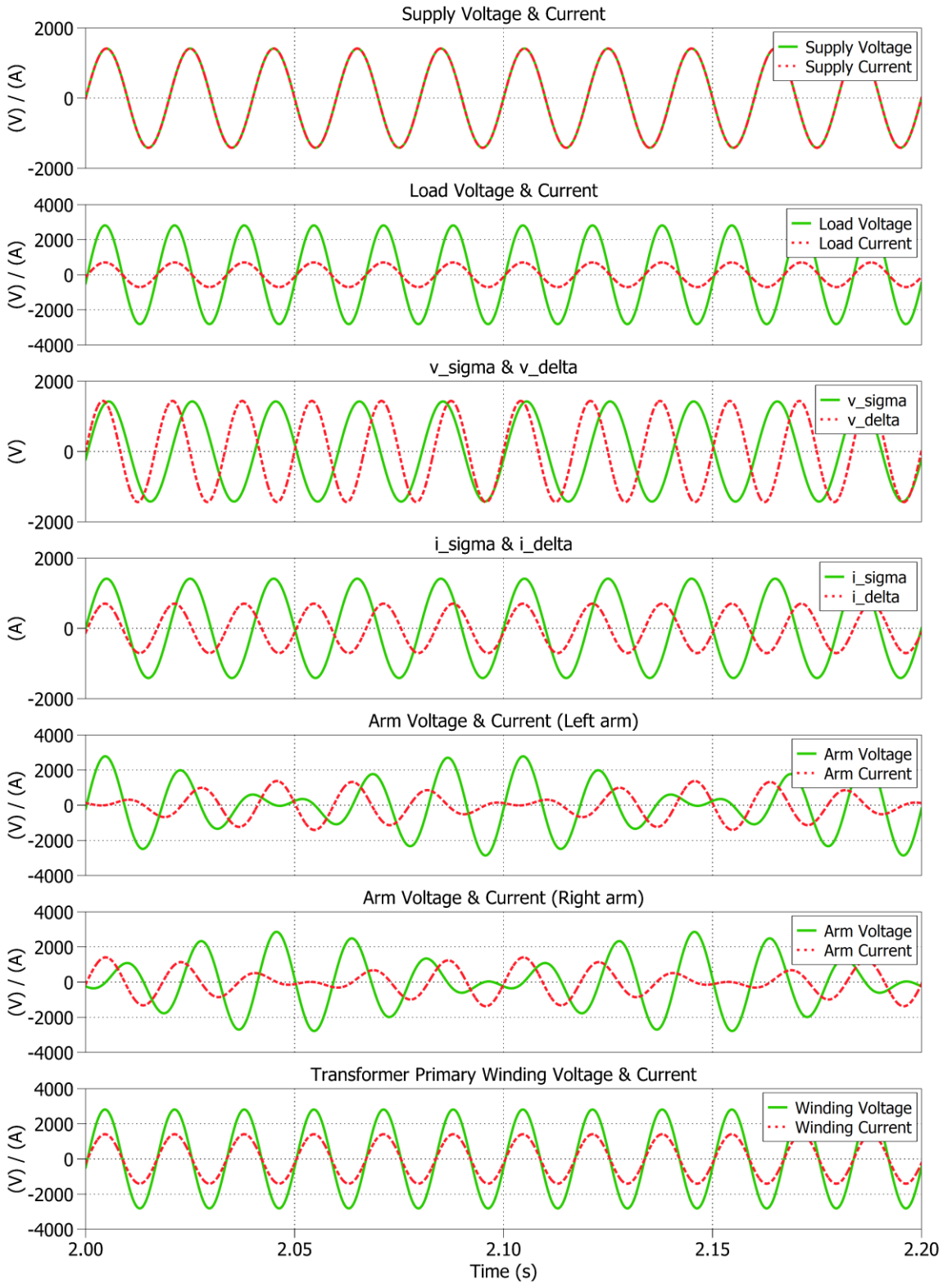

Figure 2.7: Simulation results for DW-M2AC single-phase operation (idealized)

the supply current (i_{g1}) is 1000 A rms. Taking into account the voltage drops due to arm inductance and resistance, load voltage and load current are valued at closer to 2000 V rms and 500 A rms respectively. It can be clearly seen from the graphs that the arm current is having two frequency components of 50 and 60 Hz. Although the transformer winding carries a current comprised of two frequency components, there is only a differential mode voltage of one frequency (60 Hz) appeared across the primary winding of the transformer. According to these results, operating principle of the DW-M2AC can be validated and a detailed analysis of the converter operation with different case study scenarios is presented in Chapter 3.

2.4 Comparative Analysis

The proposed DW-M2AC is compared with two prominent direct AC/AC MMCs; the M3C and Hexverter, by considering the semiconductor effort, magnetics requirement and energy storage requirement. The M3C and Hexverter are selected for this comparison because these are the two prominent direct AC/AC MMCs found in the literature which also exhibit similarity in power transfer mechanisms and submodule type used (i.e., Full bridge submodules).

2.4.1 Semiconductor Effort

One of the main metrics used in this comparison is the semiconductor effort, as it significantly contributes to the cost of the converter. Two main parameters which determines the semiconductor ratings are the switch blocking voltage and switch current stress. The current rating of the semiconductors is determined by the peak value of the arm current, $\hat{I}_{arm}$. For the voltage rating of the semiconductors, switching transients and voltage fluctuations in submodule capacitors need to be accounted but for simplicity it is assumed that the combined voltage rating of semiconductors will be directly proportional to the peak value of the arm voltage, $\hat{V}_{arm}$. In order to compare the semiconductor effort in different topologies, the combined power rating of all semiconductors, S_{sm}, can be normalized with respect to the rated power of the converter. Therefore, the equation for the semiconductor effort, λ $[pu]$ can be given as in (2.39) [36].

$$\lambda\,[pu] = \frac{S_{sm}}{S_{conv}} = \frac{n_{arm} n_{sw} \hat{V}_{arm} \hat{I}_{arm}}{S_{conv}} \tag{2.39}$$

where n_{arm} is the number of arms, n_{sw} is the number of switches per submodule, and S_{conv} is the rated power of the converter. For simplicity, it is assumed that the rated power is equal to S_{conv} at both input and output (i.e., losses are neglected) and this yields,

$$S_{conv} = 3\frac{\hat{V}_1 \hat{I}_1}{2} = 3\frac{\hat{V}_2 \hat{I}_2}{2} \tag{2.40}$$

Also, AC voltage step ratio is defined as,

$$G_v = \frac{\hat{V}_2}{\hat{V}_1} \tag{2.41}$$

Here, $\hat{V}_1$ and $\hat{I}_1$ refer to converter input side peak AC voltage and AC current whereas $\hat{V}_2$ and $\hat{I}_2$ refer to converter output side peak AC voltage and AC current. A summary of calculation of the semiconductor effort for three converter topologies is presented in Table 2.2. Note that $\lambda\,[pu]$ is a function of G_v.

Table 2.2: Semiconductor effort calculation

M3C	Hexverter	DW-M2AC
$\hat{V}_{arm} = \hat{V}_1 + \hat{V}_2 = (1 + G_v)\hat{V}_1$	$\hat{V}_{arm} = \hat{V}_1 + \hat{V}_2 = (1 + G_v)\hat{V}_1$	$\hat{V}_{arm} = \hat{V}_1 + \hat{V}_2/2 = (1 + G_v/2)\hat{V}_1$
$\hat{I}_{arm} = \frac{1}{3}(\hat{I}_1 + \hat{I}_2) = \frac{1}{3}\left(1 + \frac{1}{G_v}\right)\hat{I}_1$	$\hat{I}_{arm} = \frac{1}{\sqrt{3}}(\hat{I}_1 + \hat{I}_2) = \frac{1}{\sqrt{3}}\left(1 + \frac{1}{G_v}\right)\hat{I}_1$	$\hat{I}_{arm} = \frac{\hat{I}_1}{2} + \hat{I}_2 = \left(\frac{1}{2} + \frac{1}{G_v}\right)\hat{I}_1$
$\frac{S_{sm}}{S_{conv}} = \frac{9 \times 4 \times \frac{1}{3}\left(2 + G_v + \frac{1}{G_v}\right)\hat{V}_1\hat{I}_1}{S_{conv}}$ $\lambda\,[pu] = 8\left(2 + G_v + \frac{1}{G_v}\right)$	$\frac{S_{sm}}{S_{conv}} = \frac{6 \times 4 \times \frac{1}{\sqrt{3}}\left(2 + G_v + \frac{1}{G_v}\right)\hat{V}_1\hat{I}_1}{S_{conv}}$ $\lambda\,[pu] = 8 \times \frac{2}{\sqrt{3}}\left(2 + G_v + \frac{1}{G_v}\right)$	$\frac{S_{sm}}{S_{conv}} = \frac{6 \times 4 \times \left(1 + \frac{G_v}{4} + \frac{1}{G_v}\right)\hat{V}_1\hat{I}_1}{S_{conv}}$ $\lambda\,[pu] = 8\left(2 + \frac{G_v}{2} + \frac{2}{G_v}\right)$

Unlike the M3C and Hexverter, the DW-M2AC has a transformer integrated within the converter. Therefore, for fair comparison, it is assumed that a transformer is used with other topologies as well. That is, all three converters provide galvanic isolation. This evaluation is presented based on two scenarios. During scenario 1, all the converters have a 1:1 transformer so that the AC voltage stepping is done entirely by the converter. In scenario 2, an optimal operating point for all converters is identified in such a way that the transformer turns ratio is picked so the converters can operate with minimized semiconductor effort.

Figure 2.8 and Figure 2.9 show the semiconductor effort, $\lambda[pu]$ vs. voltage step ratio, G_v plots obtained for the two scenarios. As shown in Figure 2.8, semiconductor effort for the M3C, Hexverter and DW-M2AC increases with the voltage step ratio. For the M3C and Hexverter, the semiconductor effort is lowest at voltage step ratio of 1, valued at 32 and 36.95, respectively. However, semiconductor effort for the DW-M2AC has a minimum point at G_v equals to 2 and thereafter it gradually increases. This point ($G_v = 2$) can be identified as the optimal operating point for the DW-M2AC where the semiconductor effort is minimized. An important insight from Figure 2.8 is that the semiconductor effort for the DW-M2AC is less, compared to the other two topologies at higher voltage step ratios. According to the Figure 2.9, where the transformer turns ratio is selected to achieve minimum $\lambda\,[pu]$ at all values of G_v, the M3C and DW-M2AC have a lower semiconductor effort compared to the Hexverter.

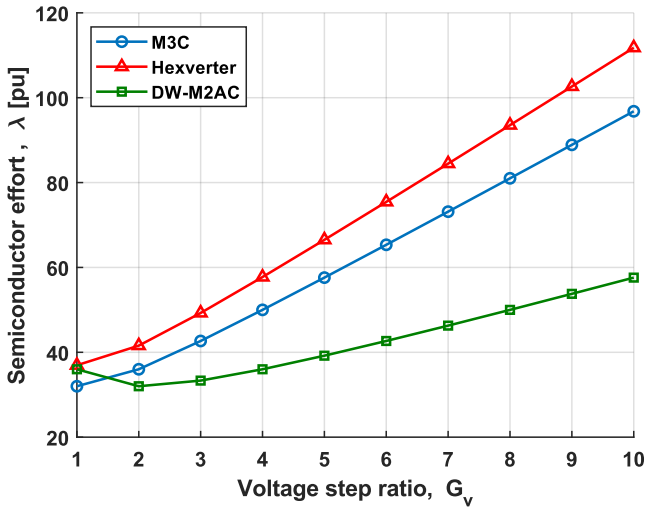

Figure 2.8: Semiconductor effort for the M3C, Hexverter and DW-M2AC when all the converters use a 1:1 transformer

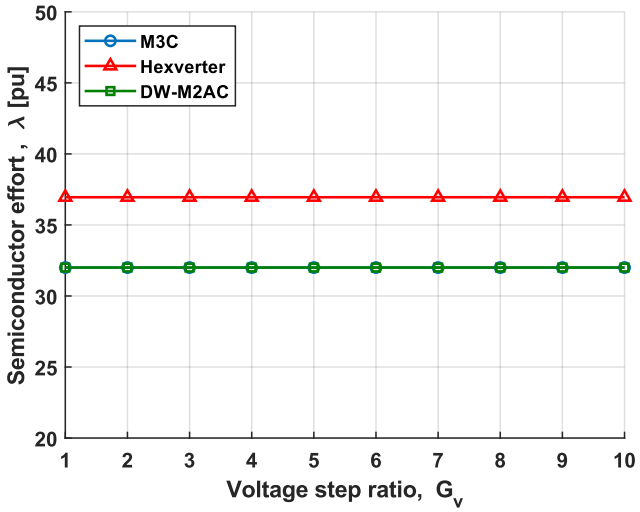

Figure 2.9: Semiconductor effort for the M3C, Hexverter and DW-M2AC when converters are operating at the optimal operating point where the λ $[pu]$ is minimized by suitable selection of transformer turns ratio

Figure 2.10 shows the plot for the transformer turns ratio, n vs. AC voltage step ratio, G_v when converters are operating at their optimal operating point where the semiconductor effort is minimized. A notable fact is that the integrated transformer in DW-M2C only requires half of the turns ratio compared to a transformer used by M3C and Hexverter due to the inherent voltage doubling effect. This will give a significant benefit for the DW-M2AC over other two topologies when it comes to the applications where higher voltages step ratio is needed.

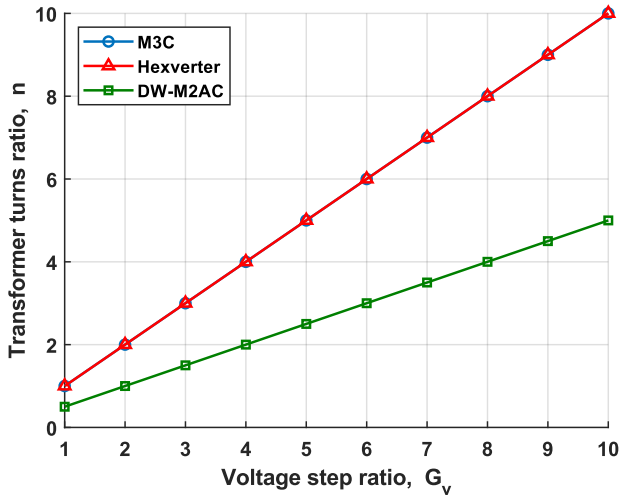

Figure 2.10: Transformer turns ratio required for M3C, Hexverter and DW-M2AC when they are designed for the optimal operating point

2.4.2 Magnetics Requirement

This section quantifies and compares the transformer core sizing used in the three considered AC/AC topologies. The size of a transformer core is represented by the area product, A_p. This metric can be calculated by summing the product of rms voltage and rms current of each winding as shown in the equation (2.42) [48].

$$A_p = 3\left(V_{rms,p}.I_{rms,p} + V_{rms,s}.I_{rms,s}\right) \tag{2.42}$$

The area product normalized to the apparent power, A_p $[pu]$, for a 3-phase transformer used with the M3C, Hexverter and DW-M2AC is plotted against the voltage step ratio, G_v, and presented in Figure 2.11. For a conventional transformer (such as a 1:n transformer used with the M3C and Hexverter i.e., n is the transformer turns ratio) the per unitized area product is equals to 1 irrespective of the voltage step ratio. Therefore, $A_p[pu]$ for a transformer used with the M3C and Hexverter will be a constant line equals to 1 as shown in Figure 2.11. In the case of the integrated 0.5:0.5:n transformer used in the DW-M2AC, the transformer primary winding carries a current containing two frequency components hence the rms value of the winding current is $\sqrt{2}$ times higher than a normal case. This leads to an increased area product for the transformer as shown in Figure 2.11, where the A_p $[pu]$ for the transformer in the DW-M2AC is valued at 1.207.

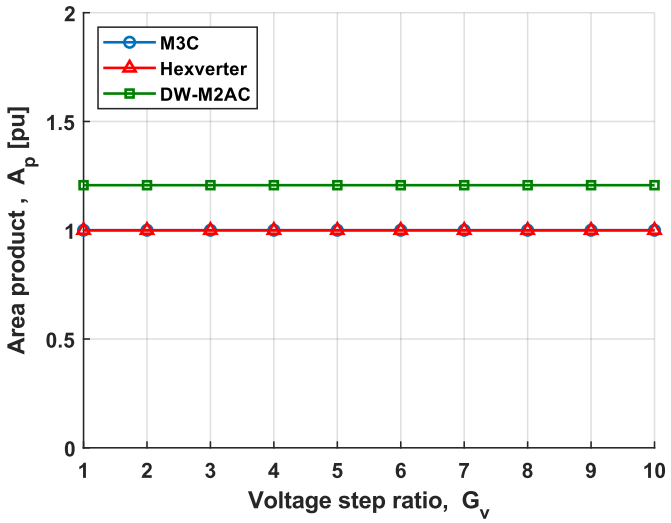

Figure 2.11: Area product for the transformers used with M3C, Hexverter and DW-M2AC

2.4.3 Energy Storage Requirement

The total energy storage requirement of each topology is evaluated based on the sum of the peak-to-peak energy variations in the converter arms. For this comparison, total peak-to-peak energy variation data points for the M3C and Hexverter are extracted from the work done in [36]. The total energy storage requirement for the DW-M2AC is obtained by conducting simulations, using similar operating conditions as mentioned in [36]. The operating conditions at which the comparison is made are listed in Table 2.3.

Table 2.3: Operating conditions for comparison of total peak-to-peak energy variation

	$V_{LL}(\text{rms})$	$S_{conv,3\phi}$	φ	Frequency
AC System 1	6.0 kV	10 MVA	+15°	10,20,30,40 Hz
AC System 2	6.6 kV	10 MVA	- 15°	50 Hz

Total peak-to-peak energy variations for M3C, Hexverter and DW-M2AC for different operating points (i.e., system 1 frequency (f_1) equals to 40 Hz, 30 Hz, 20 Hz and 10 Hz) are presented in Table 2.4. These results indicate that the proposed DW-M2AC has a lower energy storage requirement compared to the other topologies. Note that all three topologies require a higher energy storage when system 1 frequency (f_1) is getting lower, as would be expected. However, a more comprehensive analysis needs to be carried out to better investigate the relative energy storage requirements of these converters, which is not covered in the scope of this thesis.

Table 2.4: Total peak-to-peak energy variations for M3C, Hexverter and DW-M2AC

		Total peak-to-peak energy variation (kJ/MVA)		
f_1	f_2	M3C	Hexverter	DW-M2AC
40 Hz	50 Hz	13.75	15.25	8.52
30 Hz	50 Hz	11.75	16.25	9.47
20 Hz	50 Hz	13.75	20	11.12
10 Hz	50 Hz	21.25	30	18.35

Based on the result of the comparative analysis, assuming that all the converters are operated at the optimal operating point where their respective semiconductor effort is minimalized and the M3C and Hexverter are also provided with a transformer for galvanic isolation, the following statements can be concluded.

- Compared to the Hexverter, the DW-M2AC has a 13.5% less semiconductor effort but the area product of the integrated transformer is higher by a margin of 20.7% compared to a transformer used with the Hexverter or M3C.
- The DW-M2AC and M3C both have the lowest overall semiconductor effort.
- The DW-M2AC has somewhat lower arms energy storage requirement, based on comparison with operating points described in [36].

But it should be noted that, especially for applications where high AC voltage step ratio is needed, the DW-M2AC needs a 50% less turns ratio for the integrated transformer compared to other two topologies with a transformer.

2.5 Salient Features of the DW-M2AC

As discussed in the previous section, the proposed DW-M2AC has a significant advantage over other topologies in higher voltage step ratio applications when it comes to the semiconductor effort. Therefore, the DW-M2AC will require lesser amount for semiconductors and hence it will reduce the cost of the converter. However, to decide the overall cost effectiveness of the converter topology, a detailed analysis should be done considering the transformer construction and sizing of the converter which is not in the scope of this thesis.

Due to the fact that the windings of the integrated center-tapped transformer are in series with the DW-M2AC arms, a requirement for separate arm inductors is not essential as the leakage inductance of the transformer can take the role of the arm reactors. Typically arm reactors of a converter occupy significant space in the converter station, therefore by having smaller arm reactors will help to save space in the converter station.

In terms of controlling complexity, the DW-M2AC requires lesser number of voltage and current sensors compared to the M3C due to the reduced number of arms. (i.e., M3C has 9 arms while DW-M2AC has only 6 arms). Also, reduced number of converter arms means there will be fewer state currents to control. In addition to that, having lesser number of arms will reduce the mechanical construction cost of the converter and the space in the converter station.

2.6 Summary

The system architecture of the DW-M2AC and the operating principle is presented in this chapter. Similar to most prominent AC/AC MMCs, the DW-M2AC also uses full bridge submodules. The integrated transformer in the DW-M2AC provides galvanic isolation when interconnecting two different AC systems. One side of the transformer winding is configured as a center-tapped winding which allows the flux cancelation although the winding contains currents with two different frequencies. This allows the integrated transformer to be used similar to a conventional power transformer where the core only needs to be rated for one fixed frequency flux. The operating principle of the DW-M2AC is validated using a simulation model of the single-phase circuit of the converter. A comparative analysis is done based on three main metrics namely; semiconductor effort, magnetics requirement and energy storage requirement, to evaluate the economical aspect of the converter. For this analysis two of the prominent direct AC/AC converter which are the M3C and Hexverter, are used to compare with the DW-M2AC. The results from this analysis indicate that the DW-M2AC has a lower semiconductor effort compared to the Hexverter which has similar number of arms as the DW-M2AC. Also, the DW-M2AC only needs a half of turns ratio for the integrated transformer compared to other two topologies with a transformer, which makes it more suitable for high AC voltage step ratio applications.

Chapter 3

DW-M2AC Control Strategy and Simulations

The goals of the control scheme of the DW-M2AC are to regulate the active and reactive power exchange between the two AC systems, while keeping the submodule capacitor voltages at the desired nominal value. These objectives are achieved by the three main control loops detailed in the following subsections, based on the overall controller structure shown in Figure 3.1. The two current controllers are designed based on the dq-reference frame, primarily because it can facilitate variable frequency operations for certain scenarios. In the particular control scenario illustrated in Figure 3.1, the power reference is set at the AC system 1, therefore d and q axis current references for the common mode current controller is set by the active and reactive power

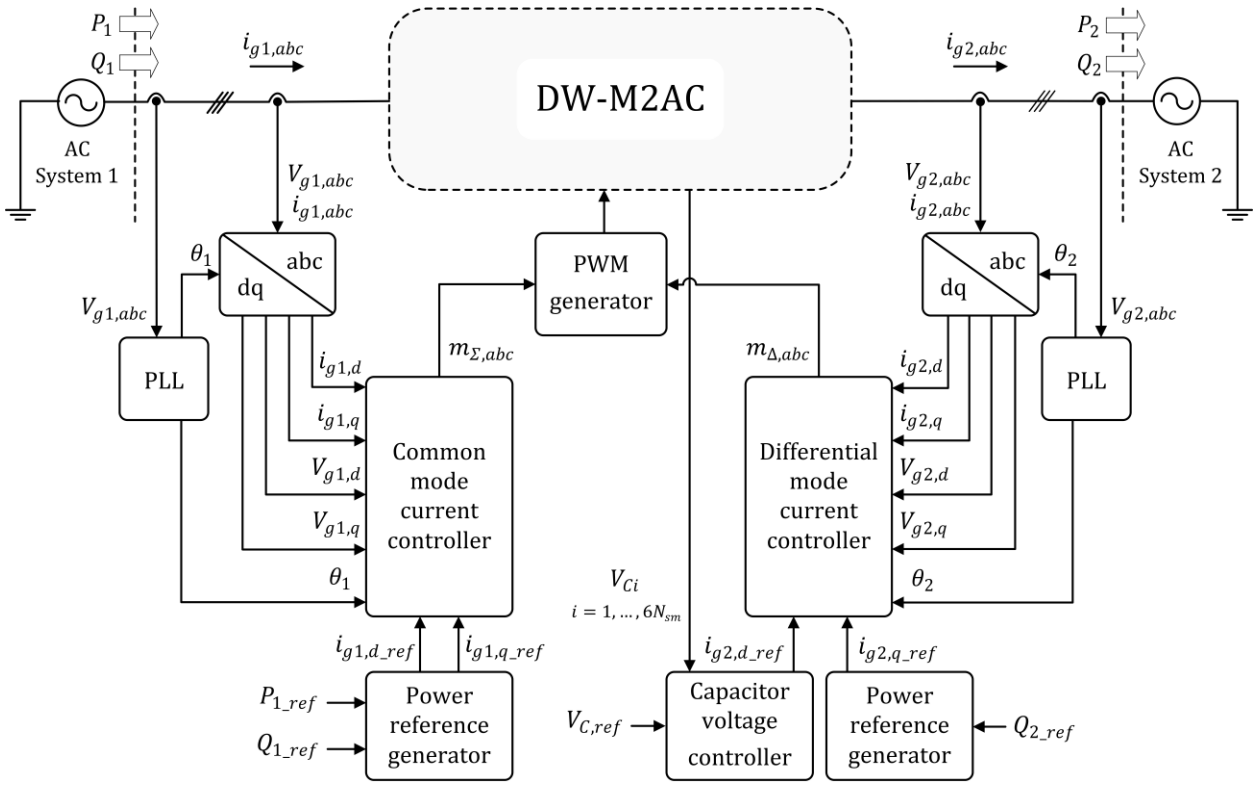

Figure 3.1: The overall controller structure of the DW-M2AC

references. Then, for the differential mode current controller at AC system 2 side, the d-axis current reference is set by the output of the capacitor voltage controller and q-axis current reference is set by the power reference generator. Note that, in scenarios where it is desired to instead control active and reactive power injections at AC system 2, the current references for differential mode current controller would be set by the power reference values while the d-axis current reference for the common mode current controller would be set by the output of the capacitor voltage controller. Voltage balancing of capacitor of each arm is achieved using the well-known sort and selection method [6],[16] and this is implemented inside the PWM signal generator.

3.1 Differential Mode Current Controller

The differential mode current controller regulates the AC system 2 current, i_{g2}, which is equivalent to i_{Δ}/n. The following steps explain the design process of the differential mode controller. The schematic diagram of the differential mode current controller is given in Figure 3.2. As mentioned in Chapter 2, differential mode dynamics for the single-phase model of the DW-M2AC can be obtained as follows.

$$v_{\Delta} - \frac{V_{g2}}{2n} - R_a i_{\Delta} - L_a \frac{d}{dt}(i_{\Delta}) = 0 \tag{3.1}$$

According to (3.1) differential mode dynamics for a 3-phase system can be expressed as,

$$\begin{bmatrix} v_{\Delta,a} \\ v_{\Delta,b} \\ v_{\Delta,c} \end{bmatrix} - \frac{1}{2n}\begin{bmatrix} V_{g2,a} \\ V_{g2,b} \\ V_{g2,c} \end{bmatrix} - R_a \begin{bmatrix} i_{\Delta,a} \\ i_{\Delta,b} \\ i_{\Delta,c} \end{bmatrix} - L_a \frac{d}{dt}\begin{bmatrix} i_{\Delta,a} \\ i_{\Delta,b} \\ i_{\Delta,c} \end{bmatrix} = 0 \tag{3.2}$$

Equation (3.2) can be transformed into dq rotating reference frame that rotates at ω_2, which is the frequency of AC system 2, yielding

$$\begin{bmatrix} v_{\Delta,d} \\ v_{\Delta,q} \end{bmatrix} - \frac{1}{2n}\begin{bmatrix} V_{g2,d} \\ V_{g2,q} \end{bmatrix} - R_a \begin{bmatrix} i_{\Delta,d} \\ i_{\Delta,q} \end{bmatrix} - L_a \frac{d}{dt}\begin{bmatrix} i_{\Delta,d} \\ i_{\Delta,q} \end{bmatrix} - L_a \begin{bmatrix} 0 & -\omega_2 \\ \omega_2 & 0 \end{bmatrix}\begin{bmatrix} i_{\Delta,d} \\ i_{\Delta,q} \end{bmatrix} = 0 \tag{3.3}$$

$$\begin{bmatrix} v_{\Delta,d} \\ v_{\Delta,q} \end{bmatrix} - \frac{1}{2n}\begin{bmatrix} V_{g2,d} \\ V_{g2,q} \end{bmatrix} - R_a \begin{bmatrix} i_{\Delta,d} \\ i_{\Delta,q} \end{bmatrix} - L_a \frac{d}{dt}\begin{bmatrix} i_{\Delta,d} \\ i_{\Delta,q} \end{bmatrix} - \omega_2 L_a \begin{bmatrix} -i_{\Delta,q} \\ i_{\Delta,d} \end{bmatrix} = 0 \tag{3.4}$$

Then, by transforming from the time domain to the Laplace domain,

$$\begin{bmatrix} v_{\Delta,d}(s) \\ v_{\Delta,q}(s) \end{bmatrix} - \frac{1}{2n}\begin{bmatrix} V_{g2,d}(s) \\ V_{g2,q}(s) \end{bmatrix} - R_a \begin{bmatrix} i_{\Delta,d}(s) \\ i_{\Delta,q}(s) \end{bmatrix} - L_a s \begin{bmatrix} i_{\Delta,d}(s) \\ i_{\Delta,q}(s) \end{bmatrix} - \omega_2 L_a \begin{bmatrix} -i_{\Delta,q}(s) \\ i_{\Delta,d}(s) \end{bmatrix} = 0 \tag{3.5}$$

This yields equations (3.6) and (3.7), which are the d and q axis differential mode voltage components that needs to be synthesized by the converter arms.

$$v_{\Delta,d}(s) = (L_a s + R_a) i_{\Delta,d}(s) - (\omega_2 L_a) i_{\Delta,q}(s) + \left(\frac{1}{2n}\right) V_{g2,d}(s) \tag{3.6}$$

$$v_{\Delta,q}(s) = (L_a s + R_a) i_{\Delta,q}(s) + (\omega_2 L_a) i_{\Delta,d}(s) + \left(\frac{1}{2n}\right) V_{g2,q}(s) \tag{3.7}$$

Then the controller outputs and the differential component of the modulating signal, m_Δ, are related for each phase leg by

$$m_{\Delta,abc} = \frac{2v_{\Delta,abc}}{V_{dc}} \tag{3.8}$$

where,

$$V_{dc} = 2\hat{V}_{g1} \tag{3.9}$$

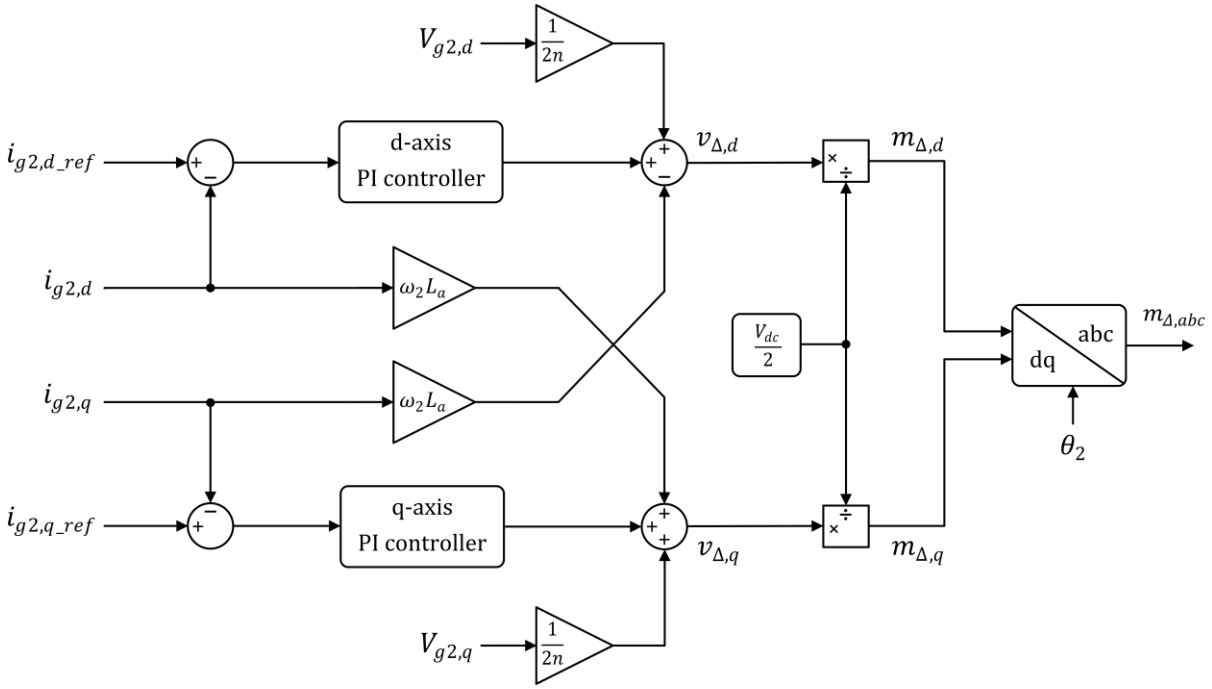

Figure 3.2: Schematic diagram of the differential mode current controller

3.2 Common Mode Current Controller

The common mode current controller regulates the AC system 1 current, i_{g1}, which is equivalent to i_{Σ}. The schematic diagram of the common mode current controller is given in Figure 3.3, and the steps for the design process of the controller are explained below. As mentioned in Chapter 2, the common mode dynamics for the single-phase model of the DW-M2AC are described by

$$v_{\Sigma} - V_{g1} + \frac{R_a}{2} i_{\Sigma} + \frac{L_a}{2} \frac{d}{dt}(i_{\Sigma}) = 0 \tag{3.10}$$

According to (3.10) common mode dynamics for a 3-phase system can be expressed as follows,

$$\begin{bmatrix} v_{\Sigma,a} \\ v_{\Sigma,b} \\ v_{\Sigma,c} \end{bmatrix} - \begin{bmatrix} V_{g1,a} \\ V_{g1,b} \\ V_{g1,c} \end{bmatrix} + \frac{R_a}{2} \begin{bmatrix} i_{\Sigma,a} \\ i_{\Sigma,b} \\ i_{\Sigma,c} \end{bmatrix} + \frac{L_a}{2} \frac{d}{dt} \begin{bmatrix} i_{\Sigma,a} \\ i_{\Sigma,b} \\ i_{\Sigma,c} \end{bmatrix} = 0 \tag{3.11}$$

Equation (3.11) can be transformed into the dq rotating reference frame that rotates at ω_1, which is the frequency of AC system 1, yielding

$$\begin{bmatrix} v_{\Sigma,d} \\ v_{\Sigma,q} \end{bmatrix} - \begin{bmatrix} V_{g1,d} \\ V_{g1,q} \end{bmatrix} + \frac{R_a}{2} \begin{bmatrix} i_{\Sigma,d} \\ i_{\Sigma,q} \end{bmatrix} + \frac{L_a}{2} \frac{d}{dt} \begin{bmatrix} i_{\Sigma,d} \\ i_{\Sigma,q} \end{bmatrix} + \frac{L_a}{2} \begin{bmatrix} 0 & -\omega_1 \\ \omega_1 & 0 \end{bmatrix} \begin{bmatrix} i_{\Sigma,d} \\ i_{\Sigma,q} \end{bmatrix} = 0 \tag{3.12}$$

$$\begin{bmatrix} v_{\Sigma,d} \\ v_{\Sigma,q} \end{bmatrix} - \begin{bmatrix} V_{g1,d} \\ V_{g1,q} \end{bmatrix} + \frac{R_a}{2} \begin{bmatrix} i_{\Sigma,d} \\ i_{\Sigma,q} \end{bmatrix} + \frac{L_a}{2} \frac{d}{dt} \begin{bmatrix} i_{\Sigma,d} \\ i_{\Sigma,q} \end{bmatrix} + \frac{\omega_1 L_a}{2} \begin{bmatrix} -i_{\Sigma,q} \\ i_{\Sigma,d} \end{bmatrix} = 0 \tag{3.13}$$

Then, transforming from the time domain to the Laplace domain yields

$$\begin{bmatrix} v_{\Sigma,d}(s) \\ v_{\Sigma,q}(s) \end{bmatrix} - \begin{bmatrix} V_{g1,d}(s) \\ V_{g1,q}(s) \end{bmatrix} + \frac{R_a}{2} \begin{bmatrix} i_{\Sigma,d}(s) \\ i_{\Sigma,q}(s) \end{bmatrix} + \frac{L_a s}{2} \begin{bmatrix} i_{\Sigma,d}(s) \\ i_{\Sigma,q}(s) \end{bmatrix} + \frac{\omega_1 L_a}{2} \begin{bmatrix} -i_{\Sigma,q}(s) \\ i_{\Sigma,d}(s) \end{bmatrix} = 0 \tag{3.14}$$

This yields equations (3.15) and (3.16), which are the d and q axis common mode voltage components that needs to be synthesized by the converter arms.

$$v_{\Sigma,d}(s) = -\left(\frac{L_a s}{2} + \frac{R_a}{2}\right) i_{\Sigma,d}(s) + \left(\frac{\omega_1 L_a}{2}\right) i_{\Sigma,q}(s) + V_{g1,d}(s) \tag{3.15}$$

$$v_{\Sigma,q}(s) = -\left(\frac{L_a s}{2} + \frac{R_a}{2}\right) i_{\Sigma,q}(s) - \left(\frac{\omega_1 L_a}{2}\right) i_{\Sigma,d}(s) + V_{g1,d}(s) \tag{3.16}$$

Then the controller outputs and the common mode component of the modulating signal, m_{Σ}, are related for each phase leg by

$$m_{\Sigma,\text{abc}} = \frac{2v_{\Sigma,\text{abc}}}{V_{dc}} \tag{3.17}$$

where,

$$V_{dc} = 2\hat{V}_{g1} \tag{3.18}$$

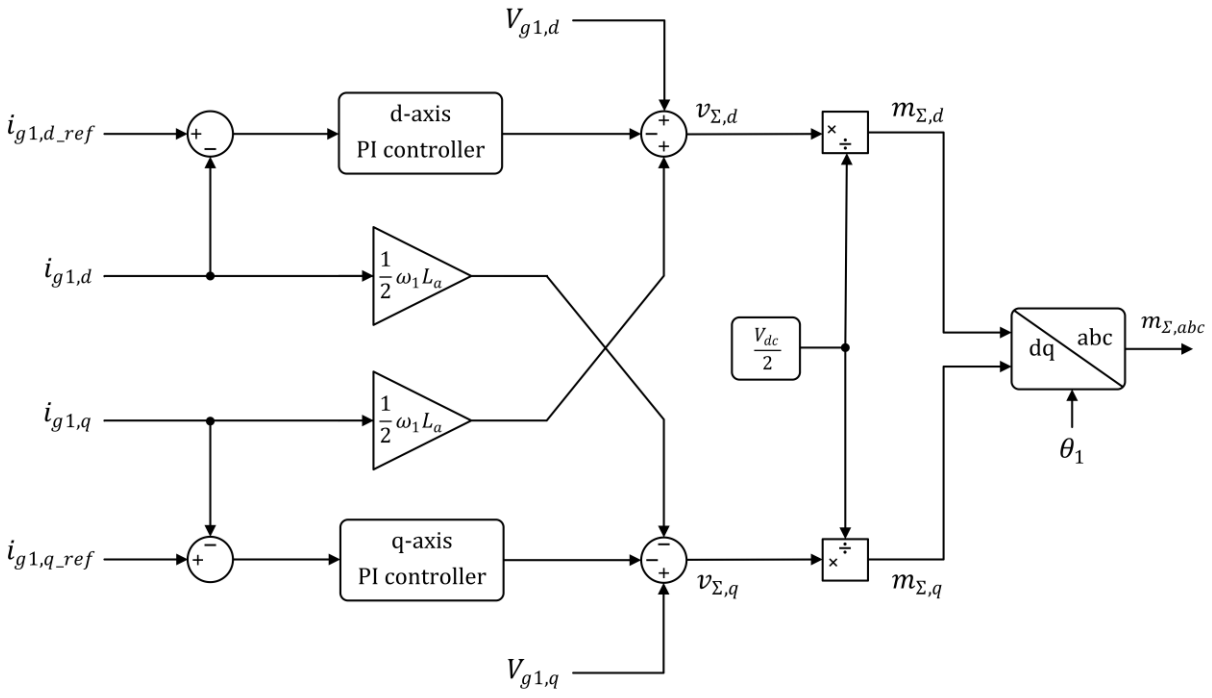

Figure 3.3: Schematic diagram of the common mode current controller

3.3 Capacitor Voltage Controller

The capacitor voltage controller acts as a slower outer control loop for the inner control loop of the differential mode current controller. This ensures the overall power balance of the converter by maintaining the capacitor voltages at a desired steady-state value. In this control structure, the capacitor voltages of each submodule are summed together and average is taken. This average capacitor voltage value is then compared with the $V_{C,ref}$ which has the following relationship.

$$V_{C,ref} = \frac{2\hat{V}_{g1}}{N_{sm}} \tag{3.19}$$

The error is fed through a PI control block which then outputs the d-axis current reference for the inner current loop, shown in Figure 3.4.

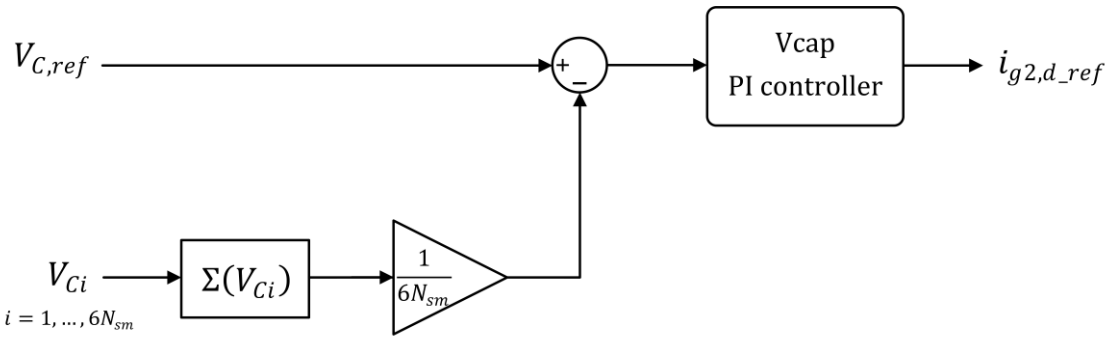

Figure 3.4: Schematic diagram of the capacitor voltage controller

3.4 DW-M2AC Design Case Studies

The performance of the proposed DW-M2AC topology and the developed controls are demonstrated using two design case studies. The simulations are done using a detailed switched model developed in PLECS software. In the first case study, the DW-M2AC is used to connect two AC grids which have differing frequencies. In the second case study, the supply side (side 2) of the DW-M2AC is connected to a fixed frequency AC grid, and the load side (side 1) is connected to a resistive load where the load side can have a variable frequency.

3.4.1 DW-M2AC for Fixed Frequency Grid Connected Operation

In this case study scenario, the low voltage side of the converter is connected to Grid 1 with frequency of 50 Hz while the high voltage side is connected to Grid 2 operating at 60 Hz. This choice imposes the transformer to operate at the higher frequency. Bidirectional power transfer can be achieved given the presence of two grid sources. The converter is rated at 10 MVA and the capacitor average voltages are regulated at 1.6 kV. Switching frequency is selected as 5 kHz and level shifted PWM method is used along with sort and selection algorithm for balancing of each submodule capacitor voltage. The main simulation parameters are listed in Table 3.1.

Table 3.1: Simulation parameters for three-phase grid connected operation

Parameter	Symbol	Value
Three-phase DW-M2AC power rating	$S_{conv,3\emptyset}$	10 MVA
Grid 1 frequency	f_1	50 Hz, 50/3 Hz
Grid 1 voltage (line-line rms)	V_{g1}	6.9 kV
Grid 2 frequency	f_2	60 Hz
Grid 2 voltage (line-line rms)	V_{g2}	13.8 kV
Transformer turns ratio	0.5:0.5:n	0.5:0.5:1
No. of submodules per arm	N_{sm}	7
Submodule capacitance	C_{sm}	10 mF
Average capacitor voltage	V_C	1.6 kV
Arm inductance	L_a	5 mH
Arm resistance	R_a	10 mΩ

Figure 3.5 shows the steady-state grid voltages and currents at the terminals of the DW-M2AC. In this case, real power is flowing from Grid 1 to Grid 2 while the power factor for both sides is unity. The active power reference at Grid 1 side is set at 10 MW and the reactive power is set to zero. Grid 1 and 2 line currents have a rms value of 838 A and 418 A, respectively and the THD value is around 0.8% for both line currents. The line currents exhibit very low THD values mainly due to the fact that a relatively high number of voltage levels is imposed by converter arms (i.e., 7 submodules per arm is used which create 15 voltage levels). Note that, arm reactance used for this design is 0.1 p.u. and it is assumed that transformer leakage reactance is also captured inside the arm inductance, L_a.

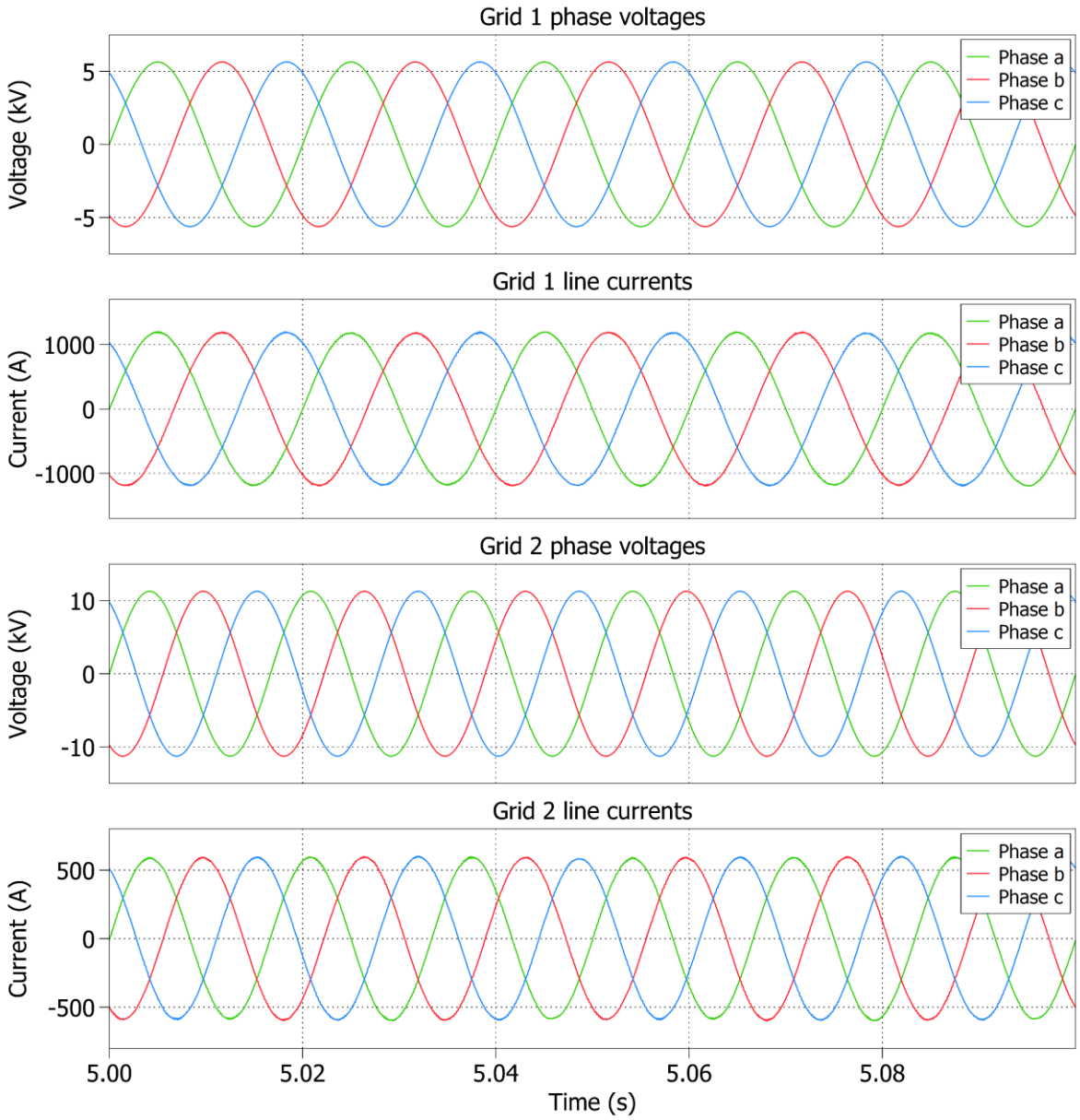

Figure 3.5: Steady-state grid voltage and current waveforms for f_1 = 50 Hz and f_2 = 60 Hz

Figure 3.6a illustrates the behavior of capacitor voltages in left and right arms of phase 'a' of the DW-M2AC. It can be seen that the average capacitor voltage is regulated around 1600 V and the peak-to-peak ripple voltage is around 7.2%. As it can be seen from Figure 3.6b, the arm voltages have 15 voltage levels which are created from 7 submodules used in each arm. The arm current contains currents of both frequencies as depicted in Figure 3.6c, and the max/min peaks are valued at ±1180 V which is equivalent to the summation of Grid 2 current (i_{g2}) and half of Grid 1 current (i_{g1}), i.e., $i_{arm,L} = \frac{i_{g1}}{2} - i_{g2}$ and $i_{arm,R} = \frac{i_{g1}}{2} + i_{g2}$.

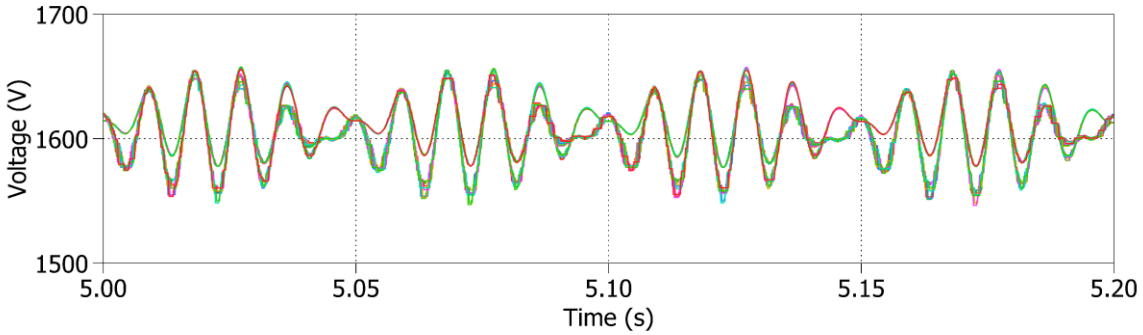

(a) Capacitor voltages in phase 'a'

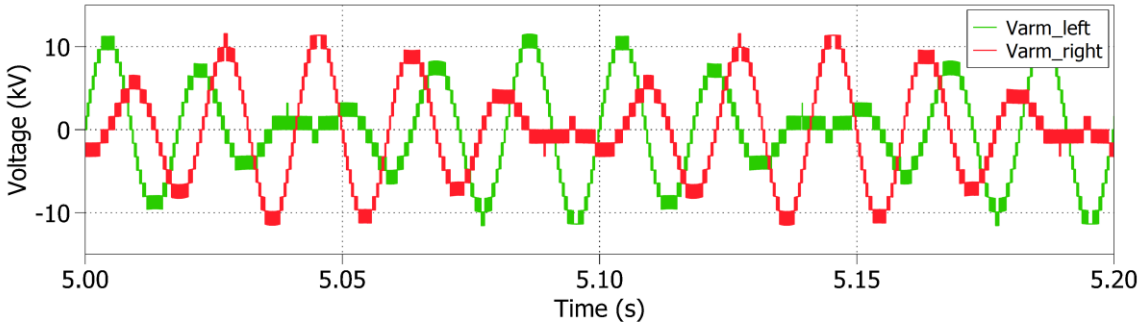

(b) Arm voltages in phase 'a'

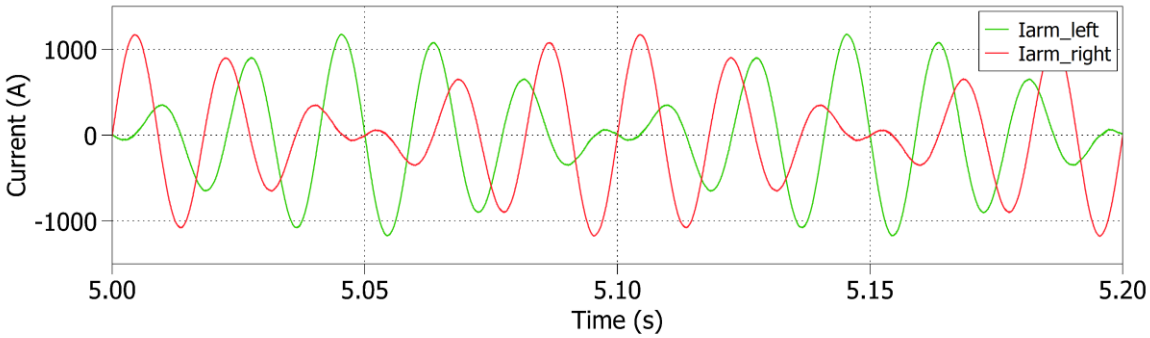

(c) Arm currents in phase 'a'

Figure 3.6: Steady-state DW-M2AC voltage and current waveforms for f_1 = 50 Hz and f_2 = 60 Hz

As mentioned earlier in Chapter 2, the DW-M2AC is also suitable to interface Fractional Frequency Transmission Systems (FFTS) with the grid. This would impose a larger frequency mismatch between the AC systems in comparison to the examined 50/60 Hz interconnect. To confirm that the DW-M2AC can handle such applications, Figure 3.7 shows steady-state results when the DW-M2AC is used to interface a 60 Hz grid and 50/3 Hz fractional frequency transmission line.

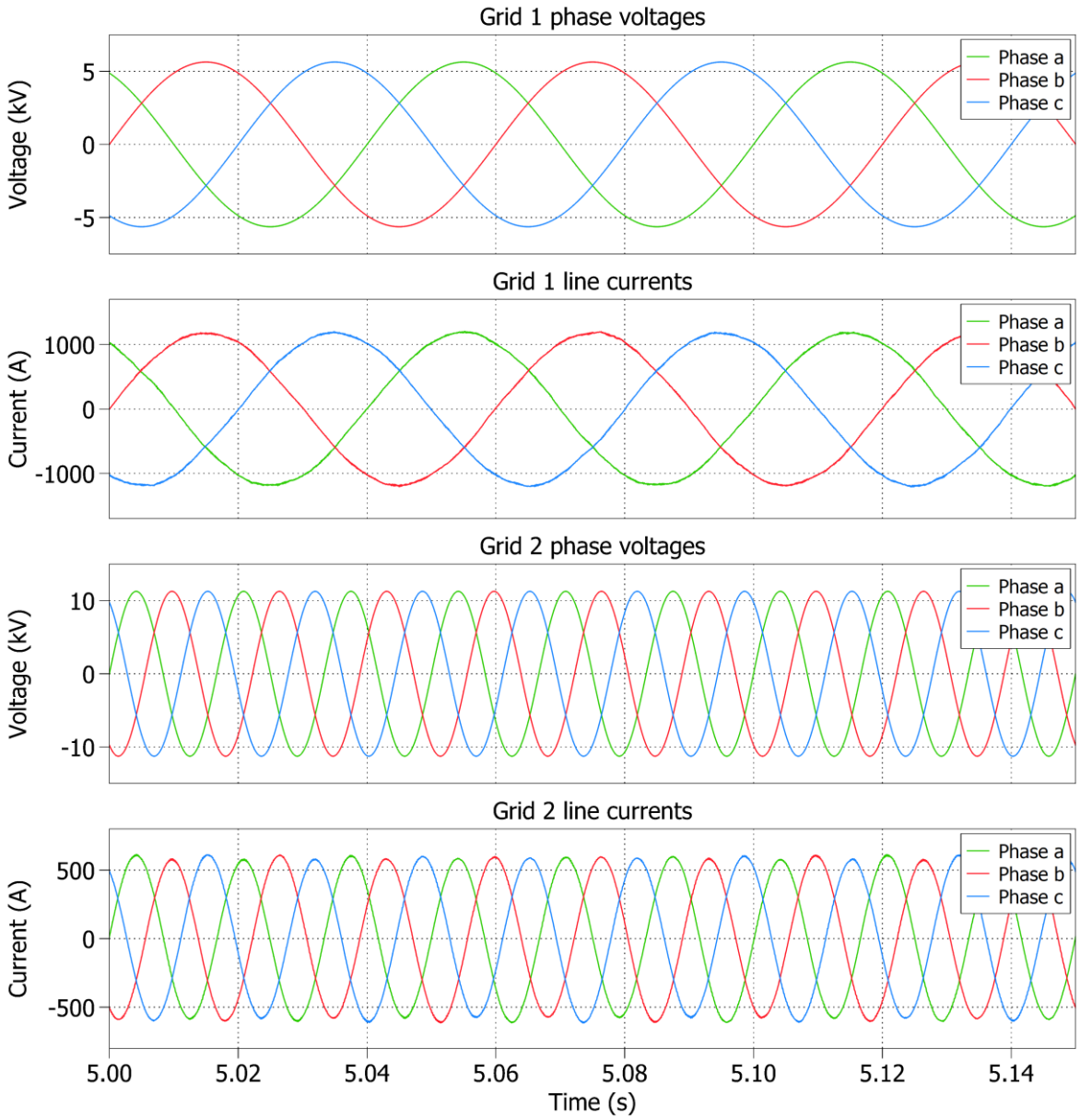

Figure 3.7: Steady-state grid voltage and current waveforms for f_1 = 50/3 Hz and f_2 = 60 Hz

Figure 3.8 shows the DW-M2AC capacitor voltages and arm voltages & currents in phase 'a' for f_1 = 50/3 Hz and f_2 = 60 Hz. The capacitor voltage ripples are now around 13.5 % which indicates that when the two AC systems frequencies are significantly apart, the demand for capacitive energy storage would be higher. As it can be seen from Figure 3.8, the arm voltage and current waveforms look different to previous case of 60/50 Hz operation since the Grid 1 frequency (f_1 = 50/3 Hz) is different now, but the max/min peak values are same as the previous scenario.

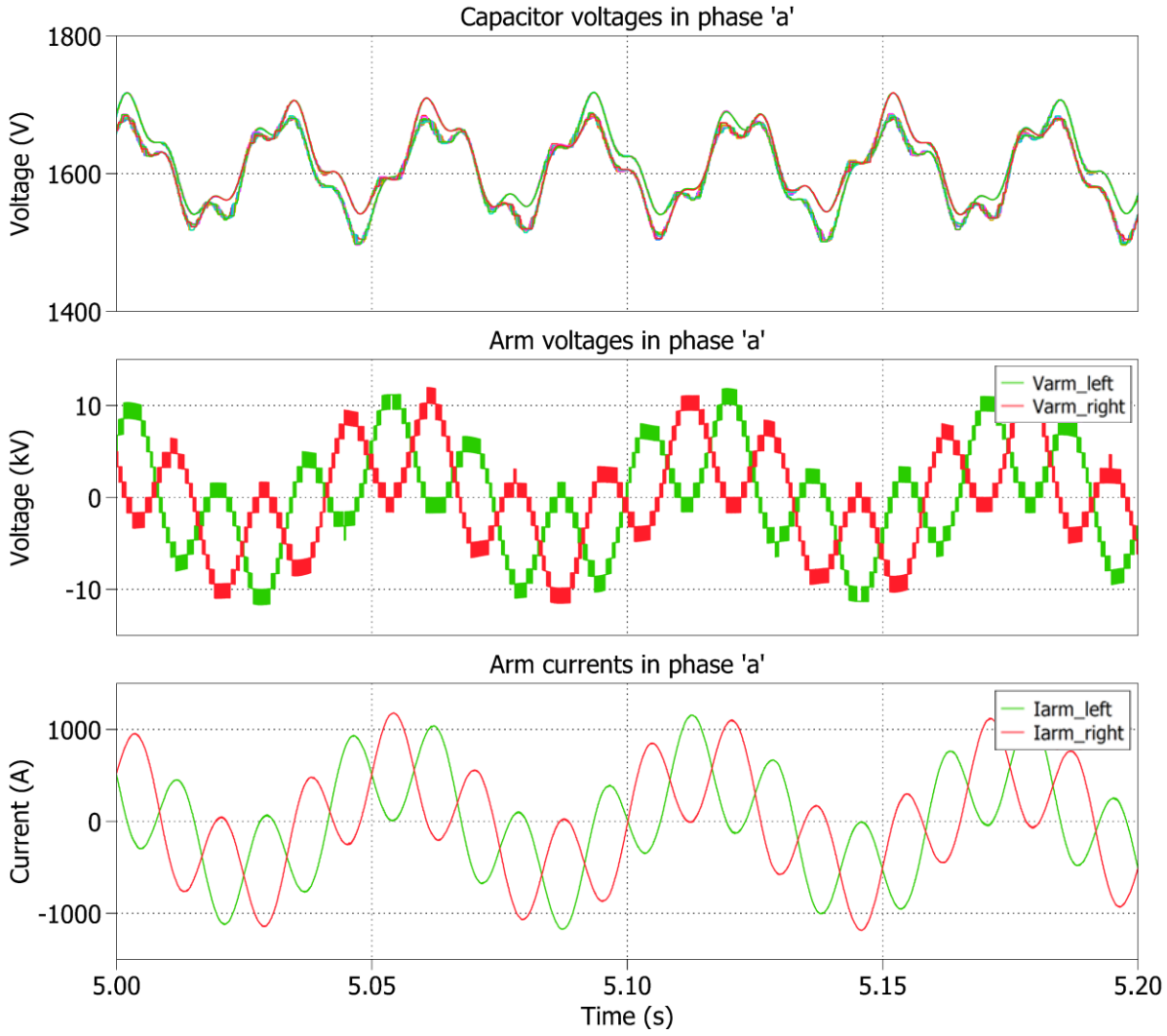

Figure 3.8: Steady-state DW-M2AC voltage and current waveforms for f_1 = 50/3 Hz and f_2 = 60 Hz

To study the transient response and the bidirectional power transferring capability of the DW-M2AC, active and reactive power references are changed when the converter is operating at f_1 = 50 Hz and f_2 = 60 Hz. In Figure 3.9a, the active power reference is changed with a ramp of 100 ms from +1 p.u. to -1 p.u. in steps of -0.5 p.u. at t = 4 s, 5 s, 6 s, 7s while the reactive power reference is set to zero. As shown in Figure 3.9a, the desired operating point for active power is properly followed by the controller. During each transient, the capacitor voltages fluctuate by a small margin but then it restores back to the original reference value in few cycles. The DW-M2AC is also capable of supplying/absorbing reactive power to/from the grid if required. In Figure 3.9b,

the converter is initially supplying 5 MW (0.5 p.u.) from Grid 1 to Grid 2. At t = 4 s, it is commanded to supply 5 MVAr (0.5 p.u.) to the grid and at t = 6 s, it absorbs 5 MVAr (-0.5 p.u.) from Grid 2. Peak-to-peak ripple in capacitor voltages are high when the converter is providing reactive power, Figure 3.9b.

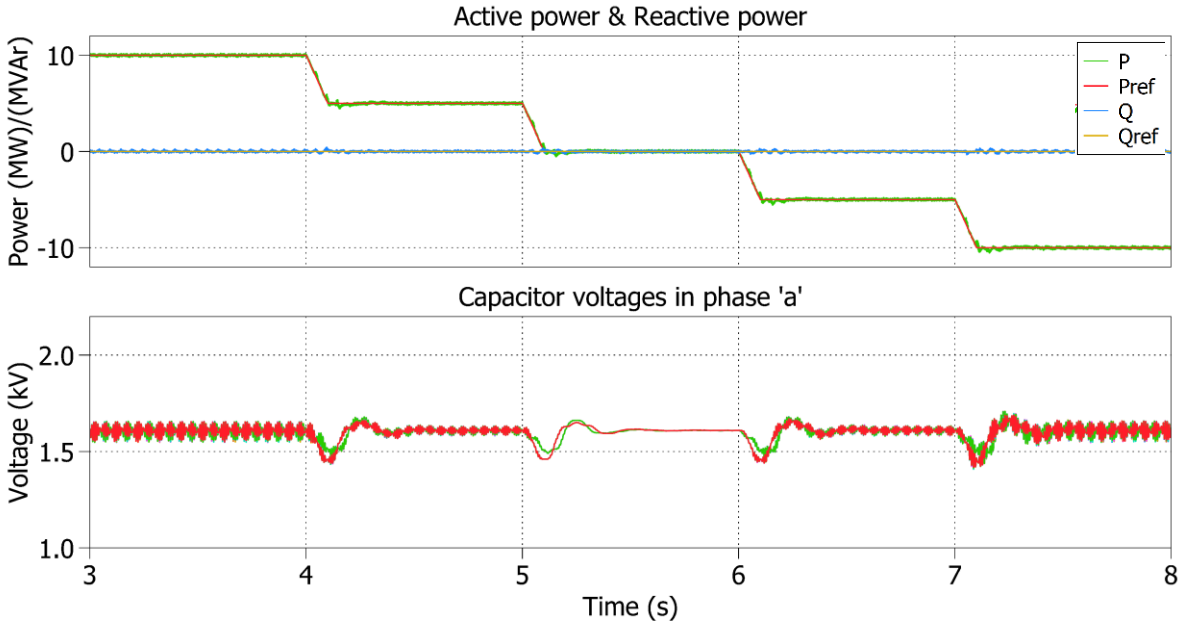

(a)

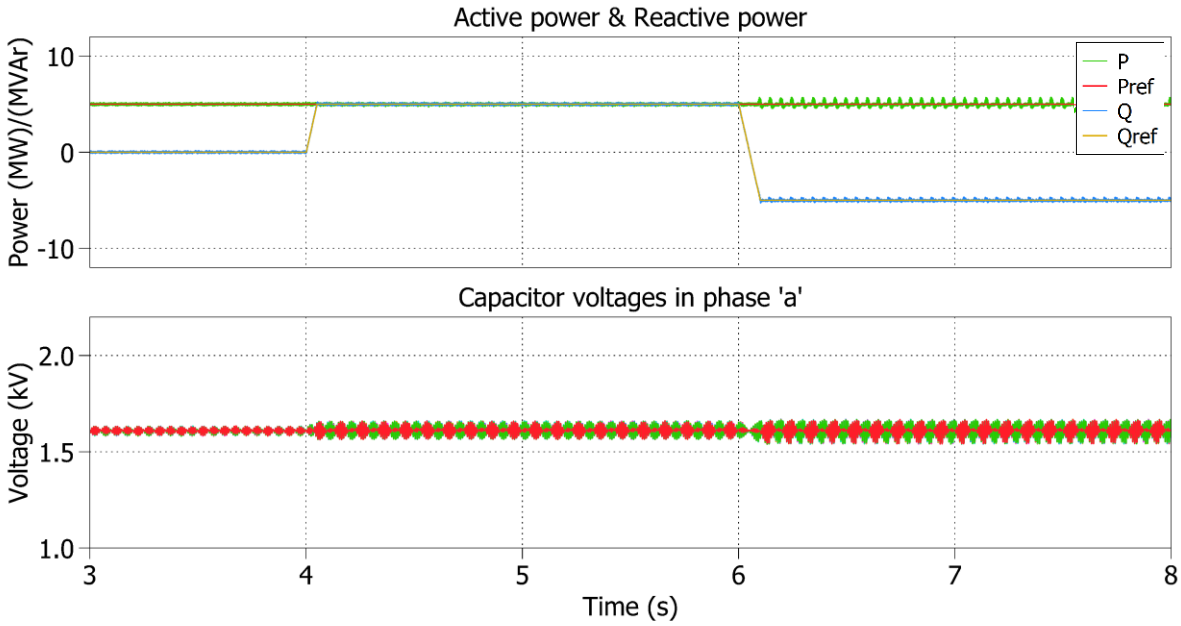

(b)

Figure 3.9: Converter transient waveforms under dynamic operation when (a) active power is changed (b) reactive power is changed at the operating point of f_1 = 50 Hz and f_2 = 60 Hz

3.4.2 DW-M2AC for Variable Frequency Operation

In order to demonstrate the variable frequency operation capability of the DW-M2AC, another case study scenario is simulated where the low voltage side of the converter (side 1) is connected to a resistive load (load side) while the high voltage side of the converter (side 2) is connected to a grid (supply side) operating at a fixed frequency. The main parameters used in this simulation are listed in Table 3.2. In this simulation case, power reference is set at the load side as 10 MW and the power factor is zero.

Table 3.2: Simulation parameters for three-phase variable frequency operation

Parameter	Symbol	Value
Three-phase DW-M2AC power rating	$S_{conv,3\emptyset}$	10 MVA
Grid 1 frequency	f_1	20 - 50 Hz
Grid 1 voltage (line-line rms)	V_{g1}	6.9 kV
Grid 2 frequency	f_2	60 Hz
Grid 2 voltage (line-line rms)	V_{g2}	13.8 kV
Transformer turns ratio	0.5:0.5:n	0.5:0.5:1
No. of submodules per arm	N_{sm}	7
Submodule capacitance	C_{sm}	10 mF
Average capacitor voltage	V_C	1.6 kV
Arm inductance	L_a	5 mH
Arm resistance	R_a	10 mΩ
Load resistance (per phase)	R_l	4.761 Ω

The frequency at the load side is reduced from 50 Hz to 20 Hz in steps of 10 Hz at time intervals of 100 ms. The steady-state grid voltage and current waveforms during the transition period is shown in Figure 3.10. As it can be seen from the Figure 3.10, during the time span of t = 4.9 s to t = 5 s, the load side frequency is 50 Hz and during the time span of t = 5.2 s to t = 5.3 s, the frequency is 20 Hz. Figure 3.11 shows the capacitor voltages in phase 'a' of the converter and the average capacitor voltage is maintained around 1600 V by the controller action. Also, it can be noted that when the frequency is going down, the peak-to-peak ripple in capacitor voltages are increasing, as would be expected.

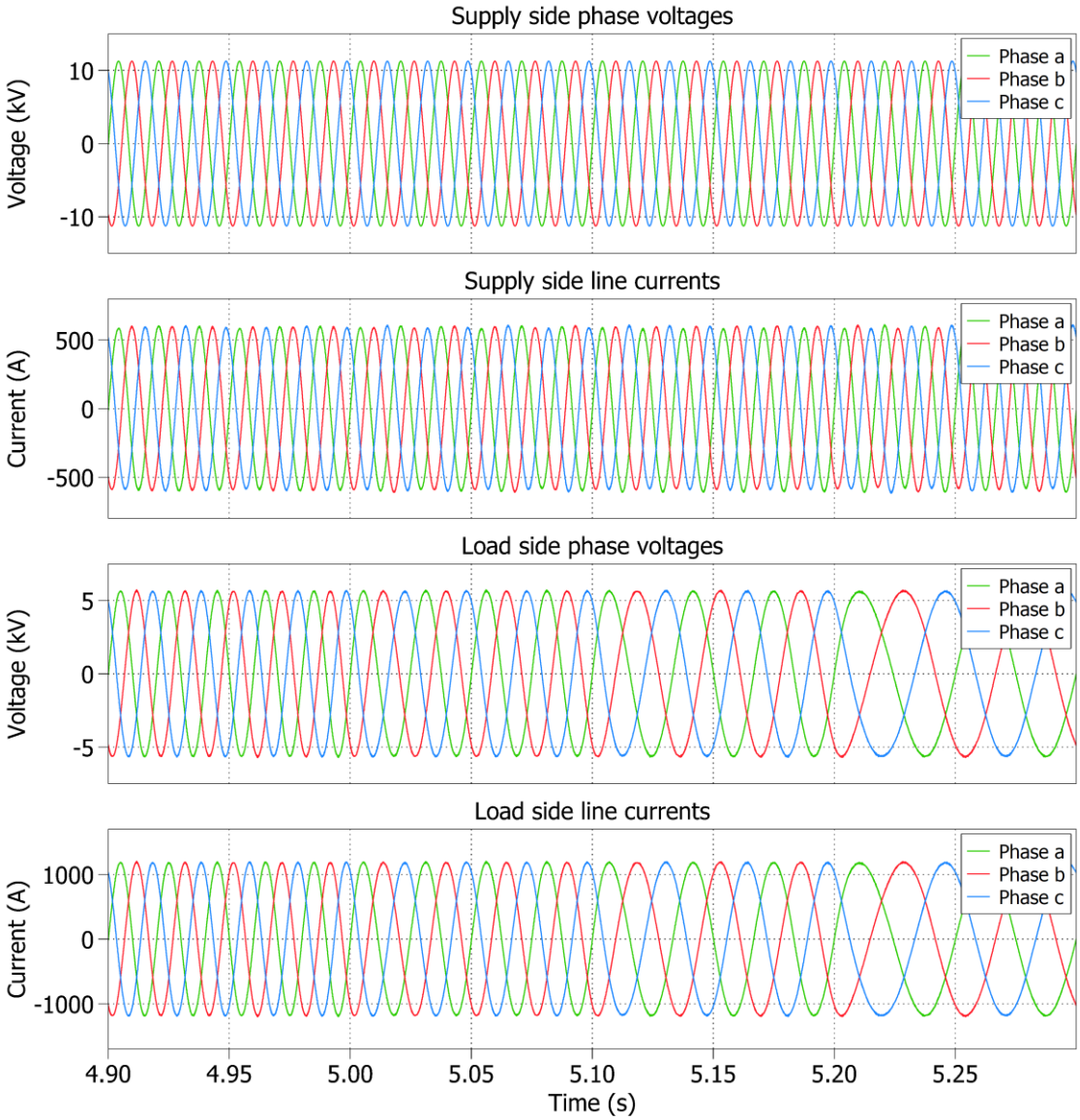

Figure 3.10: Steady-state grid voltage and current waveforms for variable frequency operation when frequency is changed from 50 Hz to 20 Hz

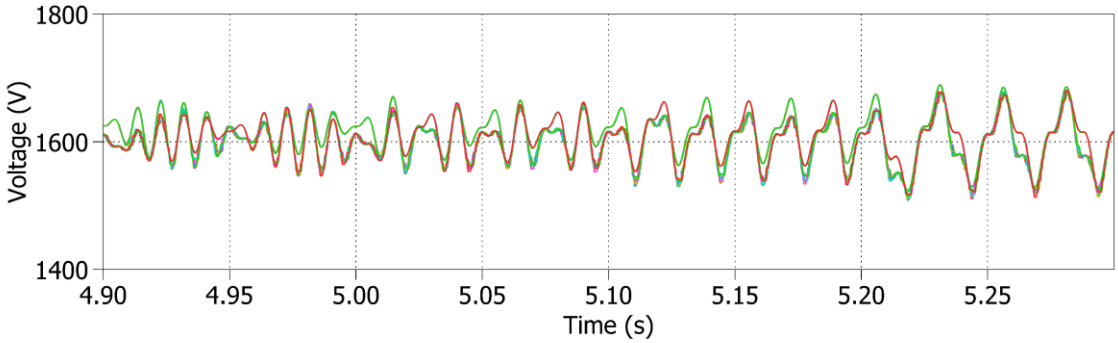

Figure 3.11: DW-M2AC capacitor voltage variations in phase ‘a’ when frequency is changed from 50 Hz to 20 Hz

3.5 Summary

A detailed description of the DW-M2AC control strategy and simulation results are presented in this chapter. The overall controller structure is introduced first and its sub-controllers are detailed subsequently. The performance of the DW-M2AC operation with the proposed control strategy is tested using two distinct case study scenarios. Under scenario 1: fixed frequency grid connected operation, active and reactive power transferring capability of the converter between two fixed frequency systems is tested. Converter steady-state waveforms are presented for 60 Hz to 50 Hz conversion and as well as for 60 Hz to 50/3 Hz conversion, where the latter imposes a larger mismatch in the two AC systems. In scenario 2: variable frequency operation, the converter's capability of transferring power from one fixed frequency to different other frequencies is tested. For this study, a 60 Hz grid is connected to a variable frequency load that changes from 50 Hz to 20 Hz. As expected, the capacitor voltage ripple increases when the frequency is reduced, which indicates a demand for higher capacitive energy storage requirement when the converter is operating at lower frequencies. The presented simulation results prove that the DW-M2AC can fulfill the requirement of a bidirectional AC/AC converter for interconnecting two AC systems with different frequencies and as well as an AC/AC converter for use in variable frequency motor drives/generators.

Chapter 4

Experimental Validation of the DW-M2AC

Performance of the DW-M2AC is validated through a series of experiments conducted using a scaled down laboratory prototype of the converter. The parameters of the experimental setup are dictated by the available components in the laboratory and hence the laboratory prototype is a low voltage three-phase 5-level DW-M2AC. The experimental results in this chapter include converter operational waveforms for different fixed frequencies and also for variable frequency operation. In addition to that, transient response of the converter for step change of output current is also presented.

4.1 Experimental Setup

The experimental setup is a three-phase 208V/104V rms line voltage, 1 kW prototype, Figure 4.1. PEH2015 full bridge modules from 'imperix' are used in this setup and there are 2 submodules per each arm. Since there are only 2 submodules used in each arm, the converter arm voltages will have 5 voltage levels. The converter control system is implemented using 'imperix' Boom Box controller and monitored through its associated real-time monitoring software. The high voltage side (side 2) of the converter is connected to the 208 V line-line rms AC supply operating at 60 Hz (f_2). The 60 Hz AC power supply is originating from NHR 9410-12 programmable power supply and connected via a three-phase variac to control the voltage input magnitudes accordingly. The low voltage side (side 1) is connected to a resistive load that can be operated at 104 V line-line rms with a variable frequency (f_1). The three-phase load consists of three load boxes valued at 10.6 Ω each. Three of 'Hammond' 1182T60P single-phase toroid power transformers each rated at 1500 VA, are used to build the three-phase integrated transformer for the converter and they are configured to use as center-tapped windings on the converter side as required. The transformer has a turns ratio of 0.5:0.5:1 and therefore the voltage step ratio (G_v) for the converter is 2. The

individual submodule capacitance is 5 mF and the individual average capacitor voltage is 88 V. The parameters used in the experimental setup are listed in Table 4.1.

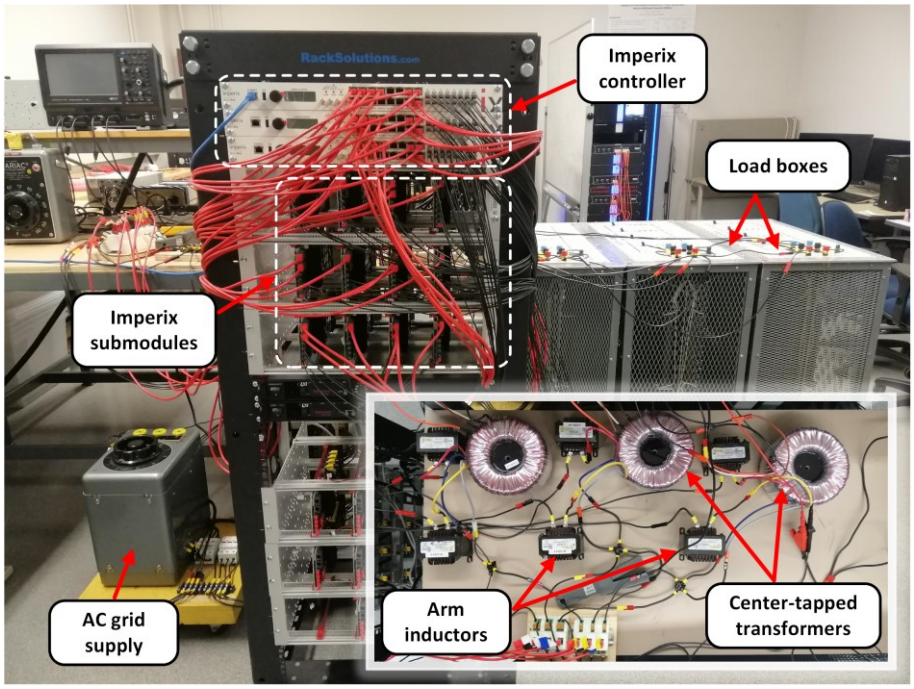

Figure 4.1: The experimental setup

Table 4.1: System parameters for the experimental setup

Parameter	Symbol	Value
Three-phase DW-M2AC power rating	$P_{conv,3\emptyset}$	1 kW
Load side frequency	f_1	10 - 50 Hz
Load side rated voltage (line-line rms)	V_{g1}	104 V
Supply side frequency	f_2	60 Hz
Supply side rated voltage (line-line rms)	V_{g2}	208 V
No. of submodules per arm	N_{sm}	2
Submodule capacitance	C_{sm}	5 mF
Average capacitor voltage	V_C	88 V
Arm inductance	L_a	2.5 mH
Transformer 3∅ power rating	$S_{tf,3\emptyset}$	4.5 kVA
Transformer turns ratio	0.5:0.5:n	0.5:0.5:1
Leakage inductance	L_l	0.085 mH
Magnetizing inductance	L_m	1.516 H
Load resistance (per phase)	R_l	10.6 Ω
Switching frequency	f_{sw}	5 kHz

4.2 Experimental Results for Fixed Frequency Operation

Figure 4.2 shows the steady-state results for the DW-M2AC operation when it is operating at fixed frequencies, f_1 = 50 Hz and f_2 = 60 Hz. The three-phase active power reference is set for 1 kW and the reactive power reference is set to zero. It can be seen that phase voltages and line currents at both sides are well synthesized with the expected amplitude and frequency.

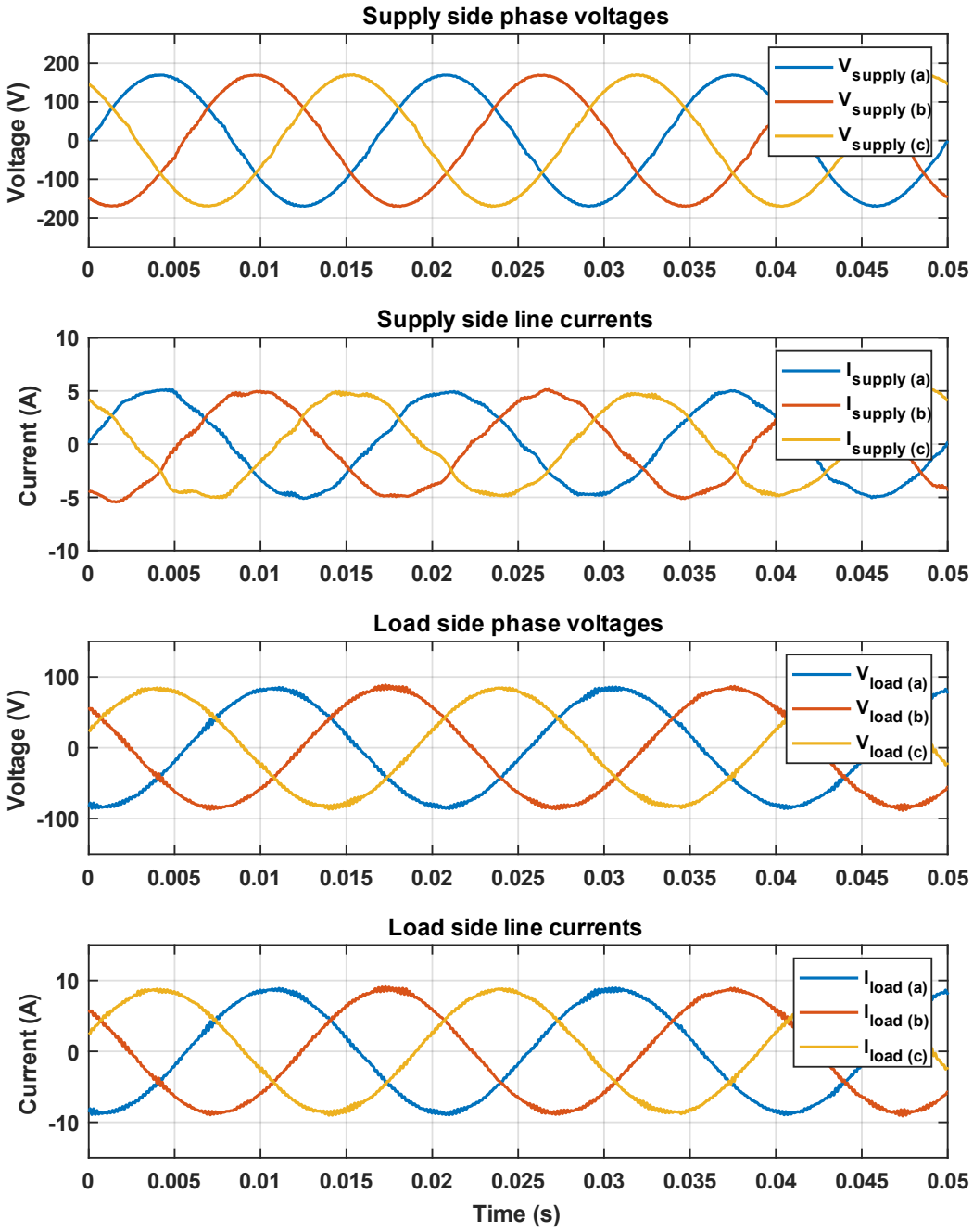

Figure 4.2: Steady-state voltage and current waveforms for f_1 = 50 Hz and f_2 = 60 Hz

As shown in Figure 4.3, the arm currents contain currents of both 50 Hz and 60 Hz frequencies. The average capacitor voltage is regulated at 88 V and the peak-to-peak capacitor ripple voltage is around 2.3%.

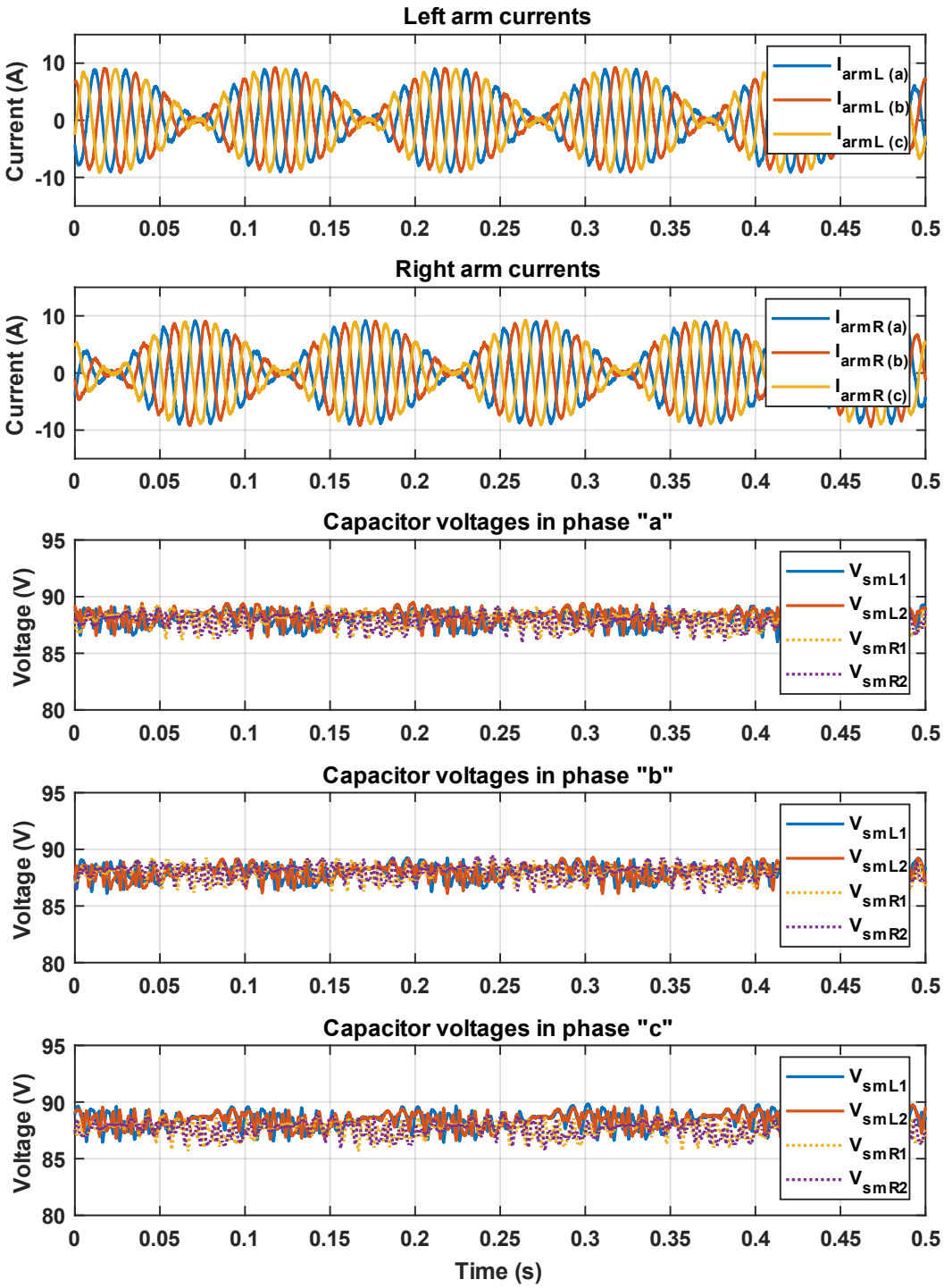

Figure 4.3: Arm currents and capacitor voltages for f_1 = 50 Hz and f_2 = 60 Hz

The first plot in Figure 4.4 shows the phase 'a' transformer winding currents of the center-tapped winding where the load is connected (side 1). Winding current in the left half of the winding is shown in blue colour and the winding current in right half is shown in red colour. The winding currents contain currents of two frequency components, 50 Hz and 60 Hz, as shown in Figure 4.4. The second plot in Figure 4.4 is obtained by subtracting the two winding currents and then dividing by 2 (i.e., $i_{\Delta} = \frac{i_{arm,R} - i_{arm,L}}{2}$). It can be clearly seen that the differential mode current passing through the center-tapped winding contains only one frequency, which is the supply side frequency of 60 Hz. This proves the concept of flux cancellation happening at the center-tapped winding. Most importantly, transformer core needs only to be rated for one AC frequency flux which is same as a conventional AC power transformer.

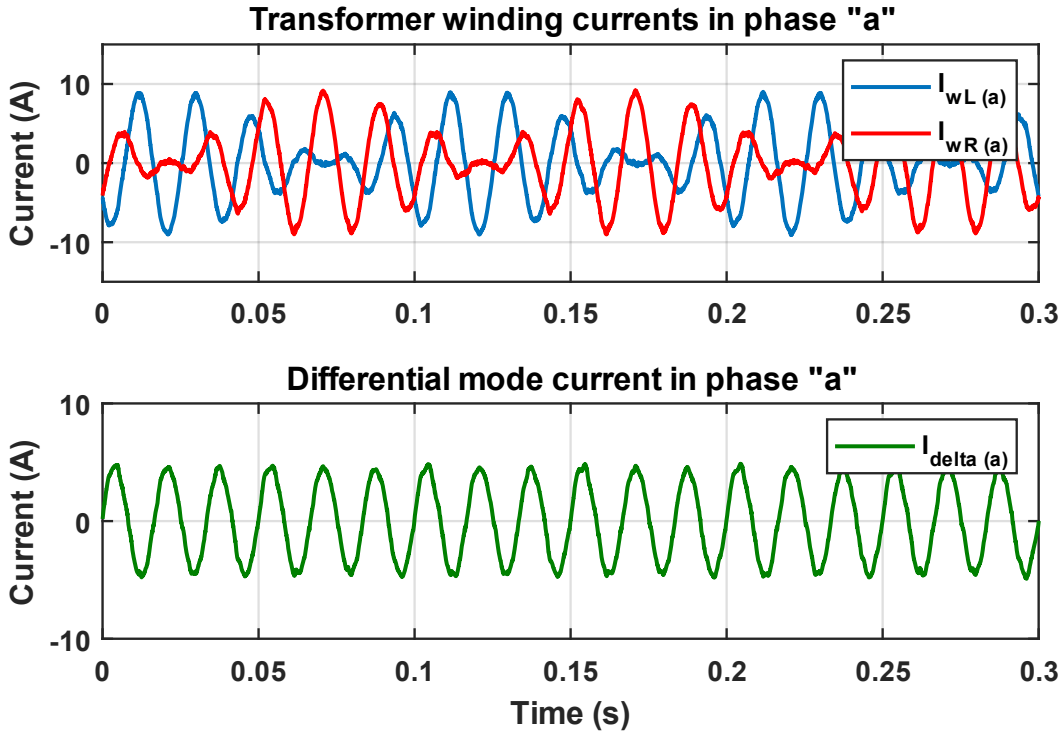

Figure 4.4: Transformer winding currents and differential mode current in phase 'a' for f_1 = 50 Hz and f_2 = 60 Hz

Representative oscilloscope waveforms obtained during the steady-state, when the converter is operating at f_1 = 50 Hz and f_2 = 60 Hz are presented in Figure 4.5. As it can be seen from the Figure 4.5b, the converter arm voltages have 5 voltage levels (i.e., $2N_{sm}$+1 levels where N_{sm} is the number of submodules per arm) which are imposed by the 2 submodules used in each arm. The max/min peak of arm voltage varies between ±170 V which is equivalent to the peak value of the supply side voltage.

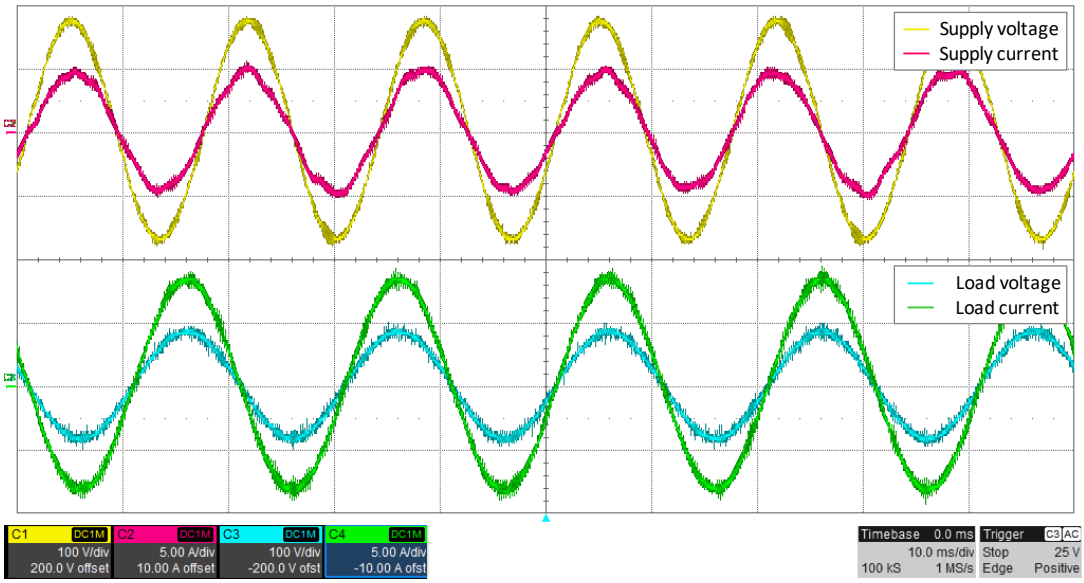

(a) Voltage and current waveforms in phase 'a' for supply and load

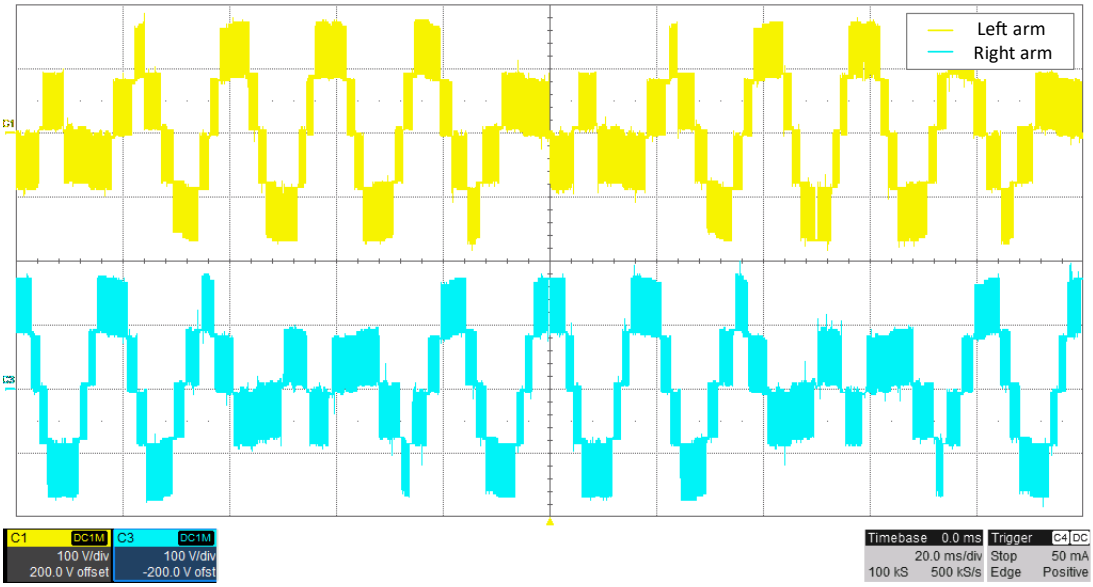

(b) Arm voltages in phase 'a'

Figure 4.5: Steady-state waveforms for f_1 = 50 Hz and f_2 = 60 Hz in phase 'a' for (a) voltages and currents in supply side and load side, (b) arm voltages

Converter operational waveforms for load side frequency of 50/3 Hz is shown in Figure 4.6. In Figure 4.7, the average capacitor voltage is regulated at 88 V as required, and the peak-to-peak capacitor ripple voltage is around 5.2%, which is approximately 2 times higher than the previous case. This confirms the fact that the converter needs higher energy storage requirement when the two frequencies are moving apart, as would be expected for any direct AC/AC converter.

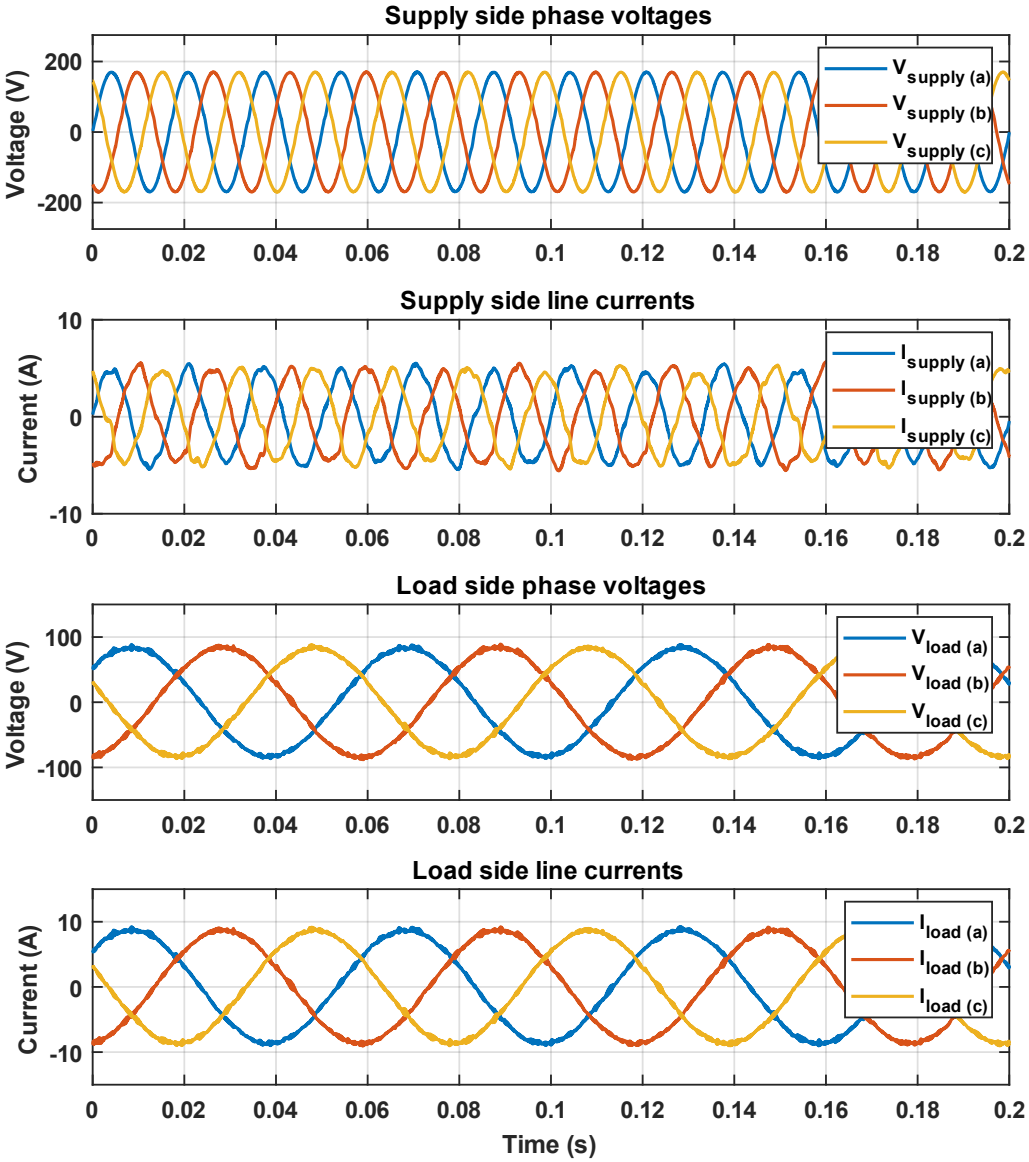

Figure 4.6: Steady-state voltage and current waveforms for f_1 = 50/3 Hz and f_2 = 60 Hz

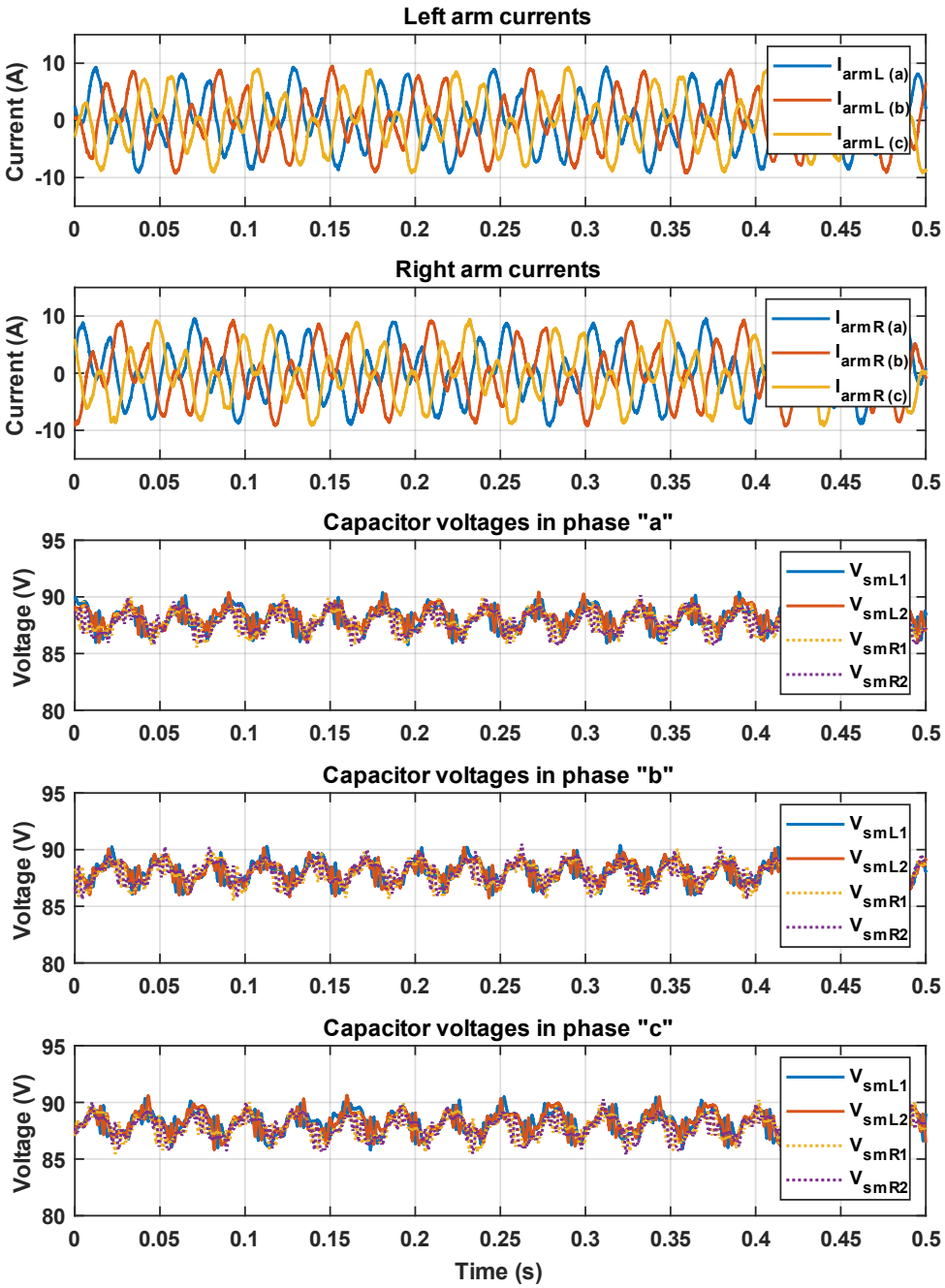

Figure 4.7: Arm currents and capacitor voltages for f_1 = 50/3 Hz and f_2 = 60 Hz

Steady-states results for several other frequency values for f_1 such as 40 Hz, 35 Hz, 25 Hz, 15 Hz and 10 Hz are included in Appendix A. These results include supply & load side voltages and currents, arm currents in and left and right arms, and capacitor voltages. Oscilloscope waveforms during steady-state operation for the above mentioned frequencies are also included in Appendix A.

4.3 Experimental Results for Variable Frequency Operation and Transient Response

The converter performance in variable frequency operation is tested changing the load side frequency, f_1. Figure *4.8* shows the steady-state voltage and current waveforms when load side frequency, f_1 is reduced from 50 Hz to 15 Hz. The frequency change starts at t = 1 s with a ramp from 50 Hz to 15 Hz in 500 ms. As it can be seen from Figure 4.8, the load side frequency is 50 Hz during the time span of t = 0.9 s to t = 1 s and after t = 1.5 s onwards the load side frequency is 15 Hz.

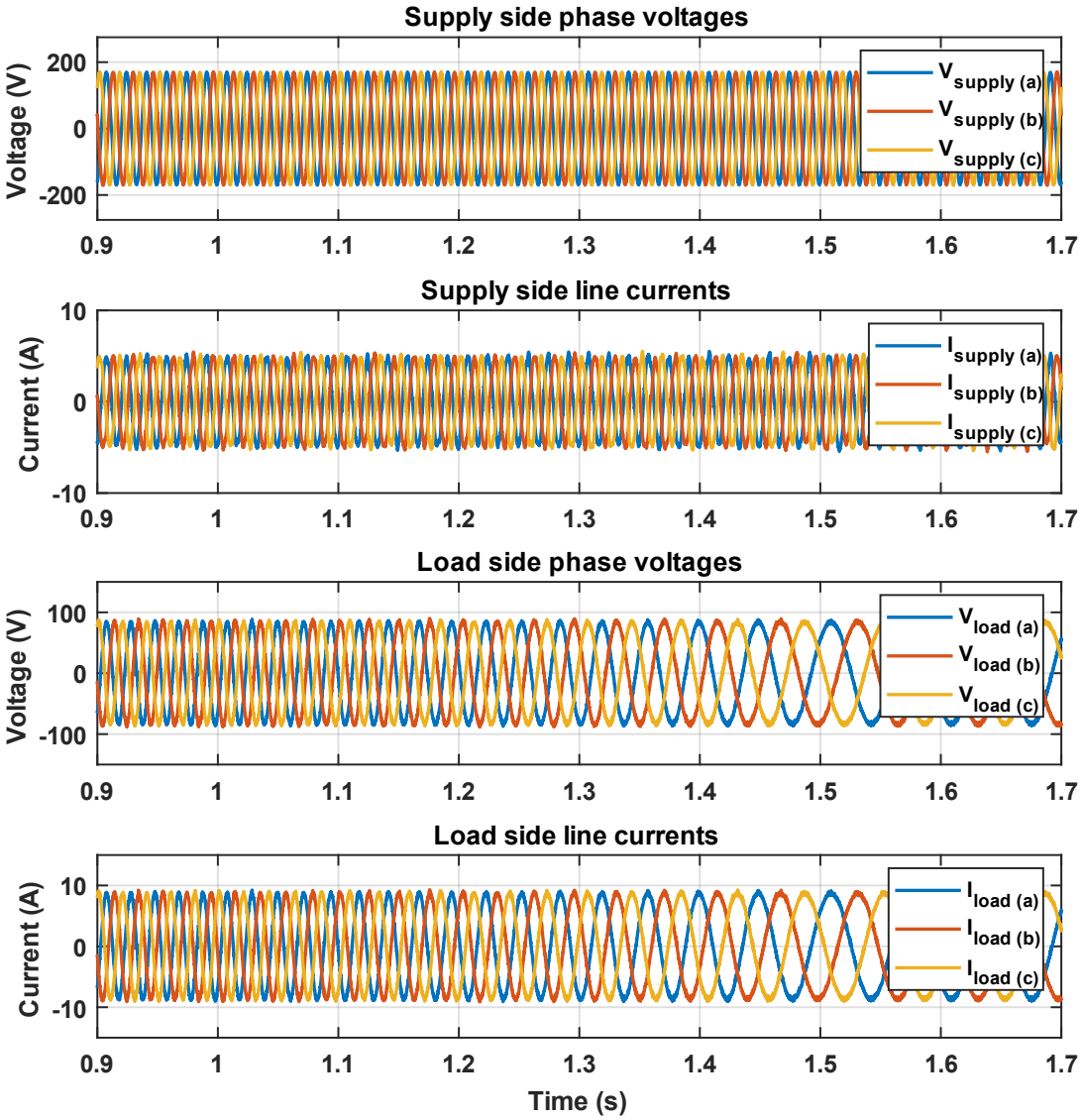

Figure 4.8: Steady-state voltage and current waveforms when f_1 is reduced from 50 Hz to 15 Hz and $f_2 = 60$ Hz

During the frequency ramp change, the average capacitor voltage is regulated at 88 V by the controller and it can be clearly seen that the peak-to-peak ripple in capacitor voltages are increasing as the load side frequency decreases, Figure 4.9.

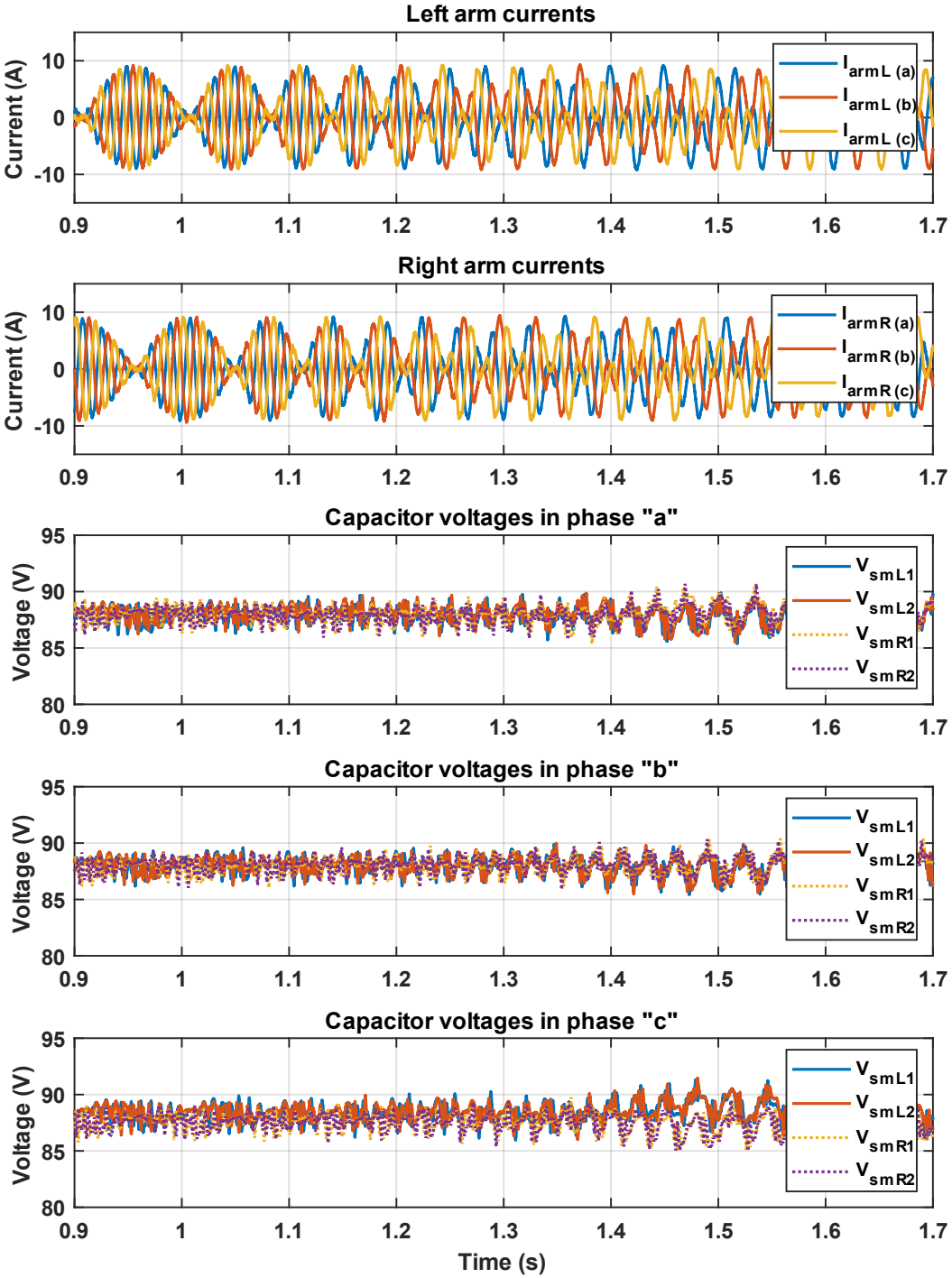

Figure 4.9: Arm currents and capacitor voltages when f_1 is reduced from 50 Hz to 15 Hz and $f_2 = 60$ Hz

In order to evaluate the dynamic response of the converter, at t = 1 s the current reference is changed resulting in converter power to be increased from 50% to 100% while the DW-M2AC is operating at f_1 = 25 Hz and f_2 = 60 Hz. As it can be seen from Figure 4.10, the load current jumps at t = 1 s and since the load resistance is kept constant load voltage is also expected to rise.

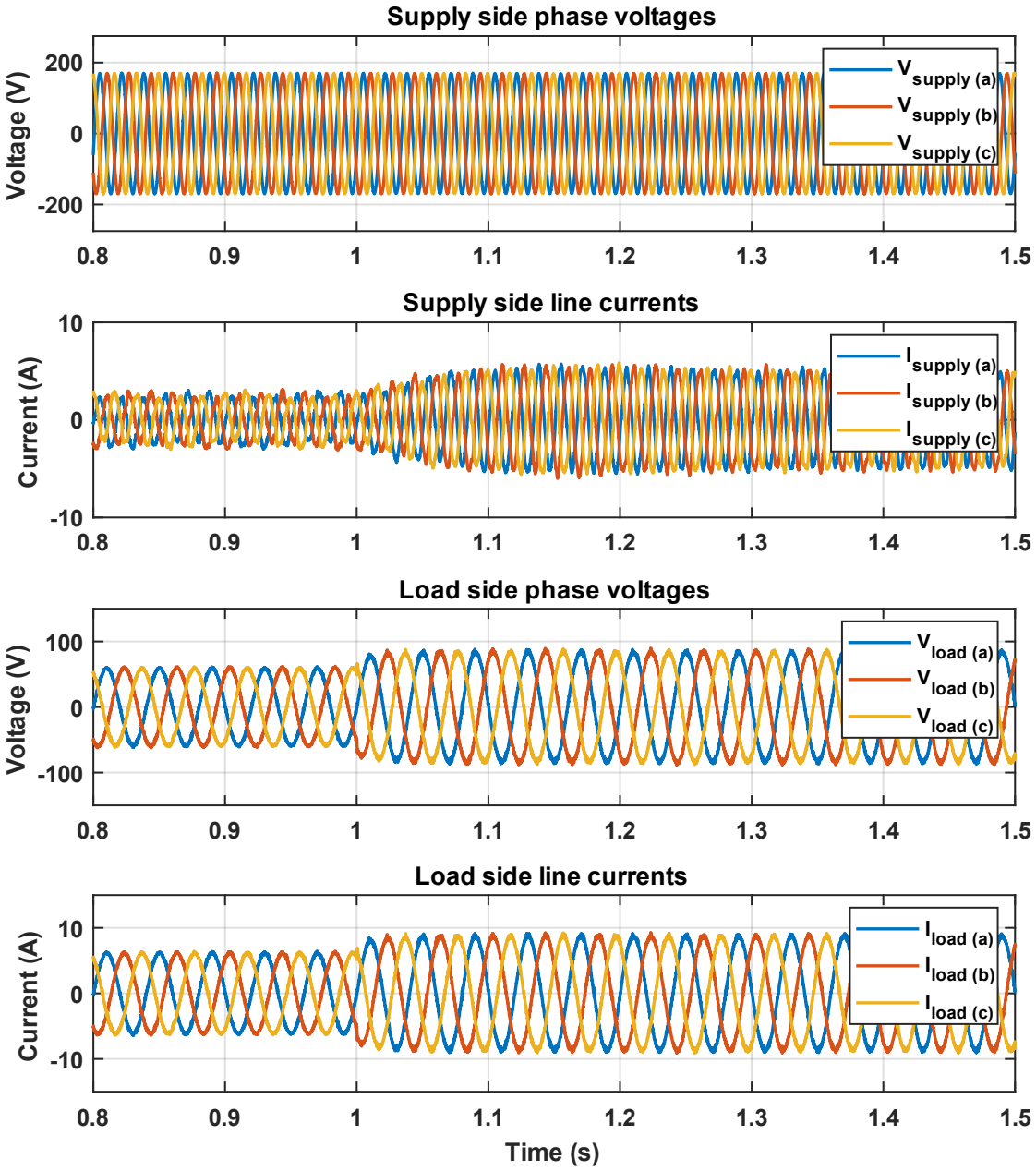

Figure 4.10: Steady-state voltage and current waveforms when rated power is changed from 50% to 100% at t = 1 s, for f_1 = 25 Hz and f_2 = 60 Hz

In Figure 4.11, when the transient happens, the capacitor voltage drops by around 3 V but then quickly restores back to the original reference value, 88 V, in less than 300 ms.

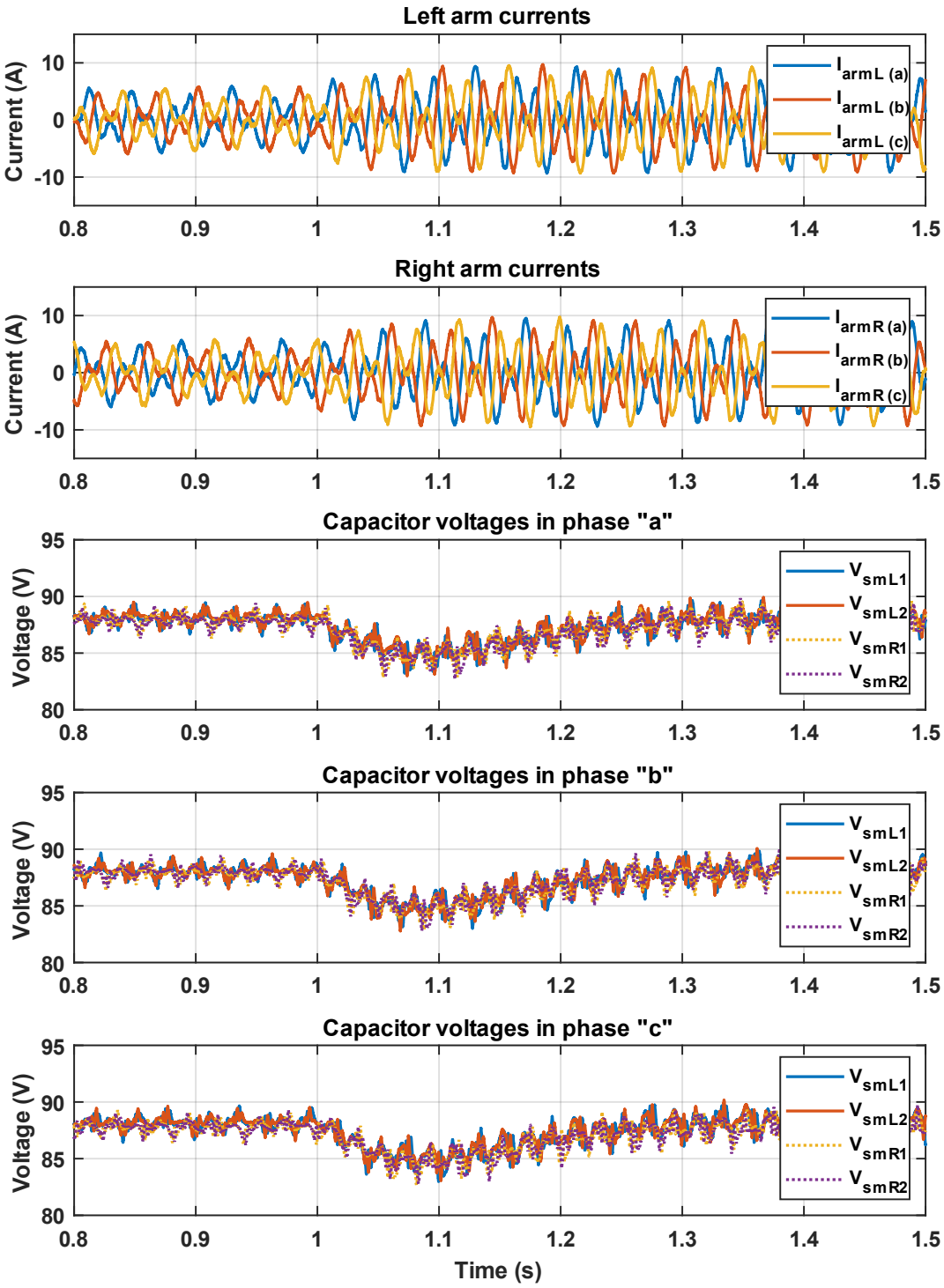

Figure 4.11: Arm currents and capacitor voltages when rated power is changed from 50% to 100% at t = 1 s, for f_1 = 25 Hz and f_2 = 60 Hz

4.4 Summary

The performance of the DW-M2AC and the proposed control strategy is validated through several experiments conducted using a 208/104 V, 1 kW three-phase laboratory prototype. The experimental results support the simulation results obtained in Chapter 3, further validating the converter operating principle and the power transfer mechanism discussed in Chapter 2. Steady-state results are presented for the converter operating at two different fixed frequencies, 60 Hz and 50 Hz. Another set of results are presented for fixed frequencies of 60 Hz and 50/3 Hz, to test the scenario where the two frequencies are significantly apart. Appendix A contains additional steady-state results obtained for several other fixed operating frequencies. The dynamic response of the converter controls is also tested by changing the output current reference when the converter is operating at 60 Hz and 25 Hz. An experiment is conducted by using varying frequencies at the load side to prove the suitability of the DW-M2AC as an AC/AC MMC for variable frequency motor drives. Arm inductors and the number of submodules used in this laboratory prototype are smaller in value compared to a typical MMC and hence the THD values in output waveforms are expected to be higher. Also, the imbalances in arm parameters in the converter leads to a certain amount of undesired harmonics in arm currents that can be addressed using more sophisticated controlling schemes.

Chapter 5

Conclusion and Future works

In this thesis work, a novel modular multilevel converter topology suitable for direct AC/AC power conversion is proposed. The proposed converter has an integrated transformer which can be used to match the voltages of two AC systems and also to provide necessary galvanic isolation. The converter power transferring mechanism is analyzed and proven with simulations. A control strategy is also proposed for three-phase closed loop operation of the converter and the performance of the control strategy and the converter operating principle are validated through a series of simulations and experiments. A summary of the research work and possible future works are presented in this chapter.

5.1 Summary

In the area of modular multilevel converters for AC/AC power conversion the B2B MMC, M3C and Hexverter have gained much attention in the previous literature. Among those mentioned MMC topologies, the M3C has a lesser number of arms compared to the B2B MMC and the Hexverter has even lesser number of arms. Therefore, developing AC/AC MMCs with fewer arms like the Hexverter has been a research trend due to the reasons such as lower number of components used in the converter (i.e., semiconductor switches, submodule capacitors, voltage and current sensors) and lesser control complexity led by low number of control states currents.

This thesis proposes a novel direct AC/AC MMC topology which also has a lesser number of arms and an integrated transformer which can provide galvanic separation for two AC systems. The lower number of arms provide the advantage of saving space in the converter station and cost savings in measuring equipment. The proposed converter has differentially connected converter arms across the center tapped transformer windings hence the name for the converter is derived as Differential-Wye Modular Multilevel AC Converter (DW-M2AC). Like many other direct AC/AC

MMCs, the DW-M2AC uses full bridge submodules stacked together inside the converter arms. One of the salient features in this converter system architecture is that the converter arms are connected in such a way that they are in series with the transformer winding. This will provide the benefit for the DW-M2AC to use transformer leakage inductance as converter arm inductance hence the cost of having a separate arm inductor is reduced here. Also, the DW-M2AC has adapted a novel power transfer mechanism with this center-tapped transformer winding arrangement where the flux is cancelled at one side of the transformer winding. This will allow the converter arm currents to carry multiple frequencies but the core needs to be rated only for a single frequency component like the conventional transformers used in power systems. However, the area product of the transformer will be somewhat higher as the transformer winding carries current of two frequency components leading to a higher rms current value in the winding than the normal case.

The comparative analysis done with two of prominent direct AC/AC MMCs (the M3C and Hexverter) provides some interesting findings in favor of the DW-M2AC. While the semiconductor effort for the DW-M2AC is in par with the M3C, it has a significantly lower semiconductor effort than the Hexverter which has a similar number of converter arms as the DW-M2AC. Therefore, the DW-M2AC stands above the Hexverter in terms of semiconductor effort. The DW-M2AC would be better alternative for the M3C also since the number of converter arms is lower than the M3C and the DW-M2AC can be benefited through the above mentioned benefits with lesser arms in the converter. And also, it is found that the DW-M2AC only requires half of turns ratio compared to a transformer used with the M3C or Hexverter. Therefore, when the voltage magnitude of one AC system is several times higher than the other, the DW-M2AC would require a lower transformer turns ratio while operating at its optimal operating point where the semiconductor effort is minimized.

Based on the dynamic equations derived for the converter operation, a control strategy is developed. In this control scheme, converter arm currents are decoupled into common mode and differential mode components. These common mode current and differential mode current are analogues to grid 1 and grid 2 currents respectively and therefore active power and reactive power transfer between two AC systems can be controlled by employing two independent current controllers. Two design case study scenarios are used to simulate the converter operation which covers two areas of possible applications for the DW-M2AC. In the grid connected operation two

AC systems with two distinct fixed frequencies (50 Hz and 60 Hz) are connected using the DW-M2AC. Steady-state results for the converter operation proves the proper power transferring happened from one frequency to the other as discussed in the converter operating principle analysis. Another simulation is performed considering AC system frequencies of 60 Hz and 50/3 Hz where the 50/3 Hz is selected specially to demonstrate the application of Fractional Frequency Transmission Systems. In this scenario, it is found that the capacitor voltage ripple is 2 times higher than the previous case which indicates the converter would require a higher capacitive energy storage if it is going to operate at frequencies where the two frequencies are significantly distant from each other. Converter transient response is evaluated by changing the active and reactive power references when the converter is operating at 60/50 Hz and the converter controls act promptly for the changes in power references by regulating the capacitor voltages at the desired value. For the variable frequency operation scenario, load side frequency is reduced from 50 Hz to 20 Hz and the simulation results shows a clear indication of capacitor voltage ripple getting bigger when the frequency is reduced.

In order to further validate the performance of the DW-M2AC, a low voltage three-phase 208/104 V, 1 kW laboratory prototype is developed using two full bridge submodules per arm. A series of experiments are conducted using two fixed frequency systems and also generating variable frequencies at the load side. Then the converter dynamic response is also tested by changing the output current reference. The experiment result includes steady-state waveforms for several discrete frequencies at load side ranging from 50Hz to 10 Hz, waveforms for variable frequency operation from 50 to 50/3 Hz and the transient waveforms when the current reference is changed during the fixed 50/25 Hz operation. As a conclusion, converter operating principle with power transferring mechanism is validated from both simulation and experimental results and the DW-M2AC can be identified as a suitable candidate in direct AC/AC power conversion when high stepping ratios are needed.

5.2 Future Works

This thesis work validates a novel MMC topology for direct AC/AC power conversion and there are number of directions which this research work could lead to. Some of these future developments are outlined below.

- The proposed DW-M2AC is a 3ph-3ph converter topology like many other direct and indirect MMCs discussed in the literature. With slight modification at the terminal where the center-tapped connections are connected to the three-phase system, a 3ph-1ph version of this converter can be derived. This can be employed in railway traction applications where 3ph-1ph AC/AC converters have gained much attention in the literature.

- While conserving the existing system architecture with the center-tapped transformer winding arrangement, there is an alternative way of connecting one side of the converter arms as a delta connection as shown in Figure 5.1. This will lead to a completely new set

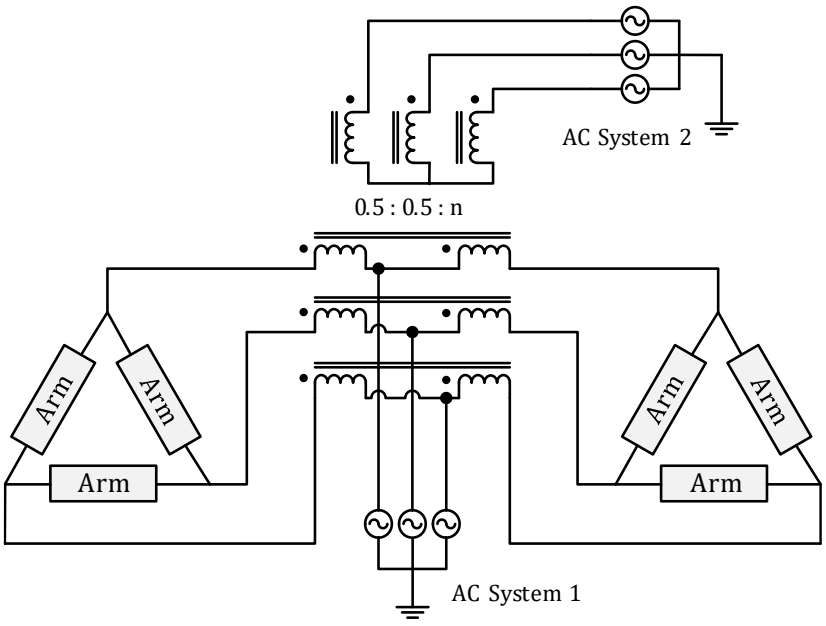

Figure 5.1: An alternative way of connecting one side of converter arms; as a delta connection

of arm voltage and current derivations which may lead to a different semiconductor effort for the converter. Most importantly there will be an internal loop created by the delta connection and this can be used as a possible way to have circulating currents local to the converter without affecting the grid currents. Having such circulating currents can be used as a method to control the energy balance between each arm and also, they can be used to suppress undesired harmonics leading to better THD values.

- During the experiments, low order harmonics appeared on the capacitor voltage ripples and arm currents leading to higher THD values which were not visible in the simulations where it had identical arm parameters. These negative effects were reduced to a certain level by selecting converter arm inductance as close as possible to each other. Therefore, efforts could be made to employ more sophisticated controlling methods to overcome the undesired harmonics due to asymmetric arm parameters.

- In the laboratory experiments, one side of the converter was connected to a restive load and single direction power flow (i.e., power flow from source to load) was tested. As an extension to the experimental works, an actual motor can be connected at the load side and more advanced controller schemes can be incorporated such as field oriented control. This arrangement will allow to test the converter's performance at low frequency operation as well as the bidirectional power flow when the motor is operating in regenerative mode. Another option would be to use the programmable power supply to generate variable frequencies so that it will emulate the action of a wind generator in Wind Energy Conversion Systems (WECS). Also, by using two power supplies, bidirectional power flow capability of the DW-M2AC can be tested experimentally.

Bibliography

[1] K. Sharifabadi, L. Harnefors, H. P. Nee, S. Norrga, and R. Teodorescu, *Design, control and application of modular multilevel converters for HVDC transmission systems*, 2016.

[2] Y. Zhang, G. P. Adam, T. C. Lim, S. J. Finney, and B. W. Williams, "Voltage source converter in high voltage applications: Multilevel versus two-level converters," *IET Conf. Publ.*, vol. 2010, no. 570 CP, 2010.

[3] A. Nabae, I. Takahashi, and H. Akagi, "A New Neutral-Point-Clamped PWM Inverter," *IEEE Trans. Ind. Appl.*, vol. IA-17, no. 5, pp. 518–523, 1981.

[4] T. A. Meynard and H. Foch, "Multi-level conversion: High voltage choppers and voltage-source inverters," *PESC Rec. - IEEE Annu. Power Electron. Spec. Conf.*, pp. 397–403, 1992.

[5] J. S. Lai and F. Z. Peng, "Multilevel converters - A new breed of power converters," *IEEE Trans. Ind. Appl.*, vol. 32, no. 3, pp. 509–517, 1996.

[6] A. Lesnicar and R. Marquardt, "An innovative modular multilevel converter topology suitable for a wide power range," *2003 IEEE Bol. PowerTech - Conf. Proc.*, vol. 3, pp. 6–11, 2003.

[7] "SIEMENS MVD (SINAMICS PERFECT HARMONY GH150)." https://new.siemens.com/global/en/products/drives/sinamics/medium-voltage-converters/sinamics-perfect-harmony-gh150.html (accessed May 19, 2022).

[8] F. T. Ghetti, A. A. Ferreira, H. A. C. Braga, and P. G. Barbosa, "A study of shunt active power filter based on modular multilevel converter (MMC)," *2012 10th IEEE/IAS Int. Conf. Ind. Appl. INDUSCON 2012*, 2012.

[9] A. K. Sahoo and N. Mohan, "High frequency link multi-winding power electronic transformer using modular multilevel converter for renewable energy integration," *IECON Proc. (Industrial Electron. Conf.*, pp. 4642–4648, 2014.

[10] Y. Gang, G. Yichang, Z. Lidan, L. Dongdong, and L. Xing, “Multi-Phase Permanent Magnet Synchronous Generator Variable Speed Constant Frequency Offshore Wind System Based on Modular Multilevel Converter,” *2019 IEEE PES Innov. Smart Grid Technol. Asia, ISGT 2019*, pp. 2127–2132, 2019.

[11] “SIEMENS HVDC PLUS.” https://www.siemens-energy.com/global/en/offerings/power-transmission/portfolio/high-voltage-direct-current-transmission-solutions/hvdc-plus.html (accessed May 19, 2022).

[12] J. Peralta, H. Saad, S. Dennetière, J. Mahseredjian, and S. Nguefeu, “Detailed and averaged models for a 401-level MMC-HVDC system,” *IEEE Trans. Power Deliv.*, vol. 27, no. 3, pp. 1501–1508, 2012.

[13] S. Allebrod, R. Hamerski, and R. Marquardt, “New T ransformerless , S calable Modular Mu l tilevel Converters for HVDC- T ransmission,” pp. 174–179, 2008.

[14] A. Dekka, B. Wu, R. L. Fuentes, M. Perez, and N. R. Zargari, “Evolution of Topologies, Modeling, Control Schemes, and Applications of Modular Multilevel Converters,” *IEEE J. Emerg. Sel. Top. Power Electron.*, vol. 5, no. 4, pp. 1631–1656, 2017.

[15] A. Nami, J. Liang, F. Dijkhuizen, and G. D. Demetriades, “Modular multilevel converters for HVDC applications: Review on converter cells and functionalities,” *IEEE Trans. Power Electron.*, vol. 30, no. 1, pp. 18–36, 2015.

[16] M. Glinka and R. Marquardt, “A new AC/AC multilevel converter family,” *IEEE Trans. Ind. Electron.*, vol. 52, no. 3, pp. 662–669, 2005.

[17] I. Krastev, P. Tricoli, S. Hillmansen, and M. Chen, “Future of Electric Railways,” *IEEE Electrif. Mag.*, no. 9, pp. 6–14, 2016.

[18] Y. S. Kumar and G. Poddar, “Control of Medium-Voltage AC Motor Drive for Wide Speed Range Using Modular Multilevel Converter,” *IEEE Trans. Ind. Electron.*, vol. 64, no. 4, pp. 2742–2749, 2017.

[19] R. W. Erickson and O. A. Al-Naseem, “A new family of matrix converters,” *IECON Proc. (Industrial Electron. Conf.*, vol. 2, no. Xcx, pp. 1515–1520, 2001.

[20] L. Baruschka and A. Mertens, “A new three-phase AC/AC modular multilevel converter with six branches in hexagonal configuration,” *IEEE Trans. Ind. Appl.*, vol. 49, no. 3, pp. 1400–1410, 2013.

[21] B. Liu, Y. Meng, and S. Bai, “A Novel High-Power ACIAC Modular Multilevel Converter in Y Configuration and Its Control Strategy,” *2016 IEEE PES Asia-Pacific Power Energy Eng. Conf.*, vol. 6, pp. 973–977, 2016.

[22] W. Kawamura, M. Hagiwara, and H. Akagi, “Control and experiment of a 380-V, 15-kW motor drive using modular multilevel cascade converter based on triple-star bridge cells (MMCC-TSBC),” *Int. Power Electron. Conf. (IPEC-Hiroshima 2014 - ECCE ASIA)*, pp. 3742–3749, 2014.

[23] B. Fan, K. Wang, P. Wheeler, C. Gu, and Y. Li, “A Branch Current Reallocation Based Energy Balancing Strategy for the Modular Multilevel Matrix Converter Operating Around Equal Frequency,” *IEEE Trans. Power Electron.*, vol. 33, no. 2, pp. 1105–1117, 2018.

[24] W. Kawamura, Y. Chiba, M. Hagiwara, and H. Akagi, “Experimental Verification of an Electrical Drive Fed by a Modular Multilevel TSBC Converter When the Motor Frequency Gets Closer or Equal to the Supply Frequency,” *IEEE Trans. Ind. Appl.*, vol. 53, no. 3, pp. 2297–2306, 2017.

[25] A. Wijesekera, Y. Li, and G. Kish, “A Partial Power Processing MMC Topology for Direct AC/AC Power Conversion,” *2021 IEEE 22nd Work. Control Model. Power Electron. COMPEL 2021*, 2021.

[26] M. Spichartz, V. Staudt, and A. Steimel, “Analysis of the module-voltage fluctuations of the Modular Multilevel Converter at variable speed drive applications,” *Proc. Int. Conf. Optim. Electr. Electron. Equipment, OPTIM*, pp. 751–758, 2012.

[27] A. J. Korn, M. Winkelnkemper, and P. Steimer, “Low output frequency operation of the Modular Multi-Level Converter,” *2010 IEEE Energy Convers. Congr. Expo. ECCE 2010 - Proc.*, pp. 3993–3997, 2010.

[28] M. Hagiwara, I. Hasegawa, and H. Akagi, “Start-up and low-speed operation of an electric motor driven by a modular multilevel cascade inverter,” *IEEE Trans. Ind. Appl.*, vol. 49, no. 4, pp. 1556– 1565, 2013.

[29] Y. Wang, Q. Xu, S. Liao, L. Wang, and J. M. Guerrero, “Impedance Modeling and Stability Analysis of AC/AC Modular Multilevel Converter for Railway System,” *IEEE Trans. Transp. Electrif.*, vol. 7782, no. c, 2020.

[30] F. Rong, S. Xu, L. Pan, and Z. Sun, “Transformerless Grid Connected Control of Wind Turbine Based on H-MMC,” *IEEE J. Emerg. Sel. Top. Power Electron.*, vol. 10, no. 2, pp. 2126–2137, 2022.

[31] F. Qin, T. Hao, and F. Gao, “A Railway Power Conditioner Using Direct AC-AC Modular Multilevel Converter,” *2nd Int. Conf. Smart Grid Renew. Energy, SGRE 2019 - Proc.*, vol. 1, pp. 20–24, 2019.

[32] R. Tsuruta, T. Hosaka, and H. Fujita, “A new power flow controller using six multilevel cascaded converters for distribution systems,” *2014 Int. Power Electron. Conf. IPEC-Hiroshima - ECCE Asia 2014*, pp. 1350–1356, 2014.

[33] Y. Meng, K. Wu, F. Jia, S. Yan, Y. Yang, and X. Wang, “Grid integration and fault ride-through of fractional frequency offshore wind power system based on Y-connected modular multilevel converter,” no. November 2021, pp. 1–12, 2022.

[34] G. F. Gontijo, S. Wang, T. Kerekes, and R. Teodorescu, “Novel converter topology with reduced cost, size and weight for high-power medium-voltage machine drives: 3x3 modular multilevel series converter,” *IEEE Access*, vol. 9, pp. 49082–49097, 2021.

[35] G. Gontijo, S. Wang, T. Kerekes, and R. Teodorescu, “New ac-ac modular multilevel converter solution for medium-voltage machine-drive applications: Modular multilevel series converter,” *Energies*, vol. 13, no. 14, 2020.

[36] K. Ilves, L. Bessegato, and S. Norrga, “Comparison of cascaded multilevel converter topologies for AC/AC conversion,” *2014 Int. Power Electron. Conf. IPEC-Hiroshima - ECCE Asia 2014*, pp. 1087–1094, 2014.

[37] Y. S. Kumar and G. Poddar, “Balanced Submodule Operation of Modular Multilevel Converter-Based Induction Motor Drive for Wide-Speed Range,” *IEEE Trans. Power Electron.*, vol. 35, no. 4, pp. 3918–3927, 2020.

[38] B. Li, “Hybrid Back-to-Back MMC System for Variable Speed AC Machine Drives,” *CPSS Trans. Power Electron. Appl.*, vol. 5, no. 2, pp. 114–125, 2020.

[39] S. Liu, X. Wang, B. Wang, P. Sun, Q. Zhou, and Y. Cui, “Comparison between back-to-back MMC and M3C as high power AC/AC converters,” *Asia-Pacific Power Energy Eng. Conf. APPEEC*, vol. 2016-Decem, pp. 671–676, 2016.

[40] K. Wang, Y. Li, Z. Zheng, and L. Xu, “Voltage balancing and fluctuation-suppression methods of floating capacitors in a new modular multilevel converter,” *IEEE Trans. Ind. Electron.*, vol. 60, no. 5, pp. 1943–1954, 2013.

[41] M. Diaz *et al.*, “An overview of applications of the modular multilevel matrix converter,” *Energies*, vol. 13, no. 21, pp. 1–37, 2020.

[42] P. Blaszczyk, “Hex-Y - A New Modular Multilevel Converter Topology for a Direct AC-AC Power Conversion,” *2018 20th Eur. Conf. Power Electron. Appl. EPE 2018 ECCE Eur.*, pp. 1–10, 2018.

[43] R. Alaei, S. Member, S. A. Khajehoddin, and W. Xu, “Sparse AC / AC Modular Multilevel Converter,” *IEEE Trans. Power Deliv.*, vol. 31, no. 3, pp. 1195–1202, 2016.

[44] W. Liu, F. Liu, H. Gao, Y. Zhuang, and X. Zha, “A Transformerless Three-Port Nonagonal MMC for the Grid Connection and Local Consumption of Distributed Generation,” *IEEE J. Emerg. Sel. Top. Power Electron.*, vol. 7, no. 1, pp. 108–117, 2019.

[45] A. Christe and D. Dujic, “Galvanically isolated modular converter,” *IET Power Electron.*, vol. 9, no. 12, pp. 2318–2328, 2016.

[46] M. Abbasi and J. Lam, “A Very High-Gain-Modular Three-Phase AC/DC Soft-Switched Converter Featuring High-Gain ZCS Output Rectifier Modules Without Using Step-Up Transformers for a DC Grid in Wind Systems,” *IEEE Trans. Ind. Appl.*, vol. 54, no. 4, pp. 3723–3736, 2018.

[47] Y. Tang, P. B. Wyllie, J. Yu, X. M. Wang, L. Ran, and O. Alatise, “Offshore low frequency AC transmission with back-to-back modular multilevel converter (MMC),” *IET Semin. Dig.*, vol. 2015, no. CP654, pp. 1–8, 2015.

[48] C. McLyman, *Transformer and Inductor Design Handbook*, 4 th ed. Boca Raton, FL, USA: CRC Press, 2011.

Appendix A

A.1 Steady-state Results

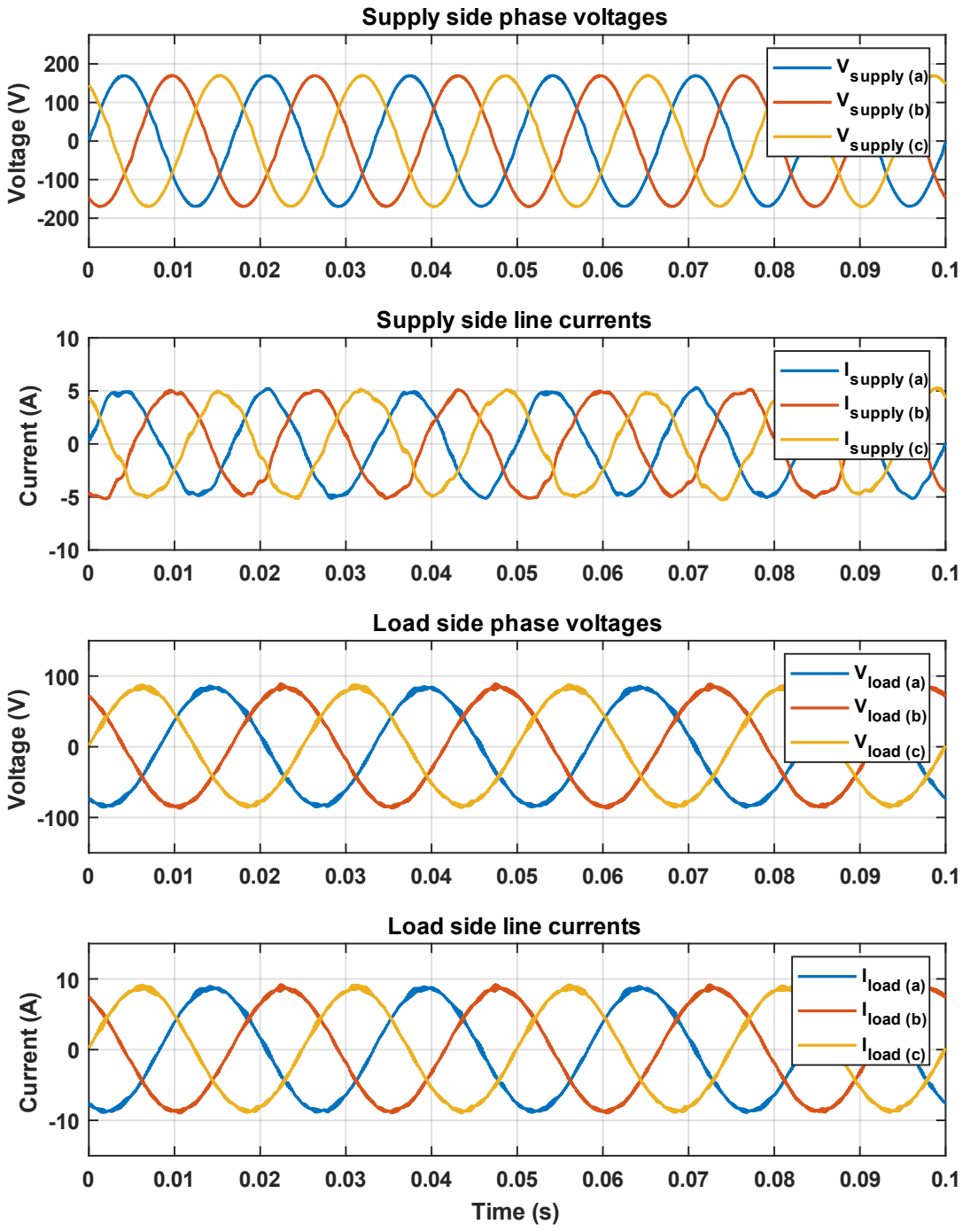

Figure A.1.1: Steady-state voltage and current waveforms for $f_1 = 40$ Hz and $f_2 = 60$ Hz

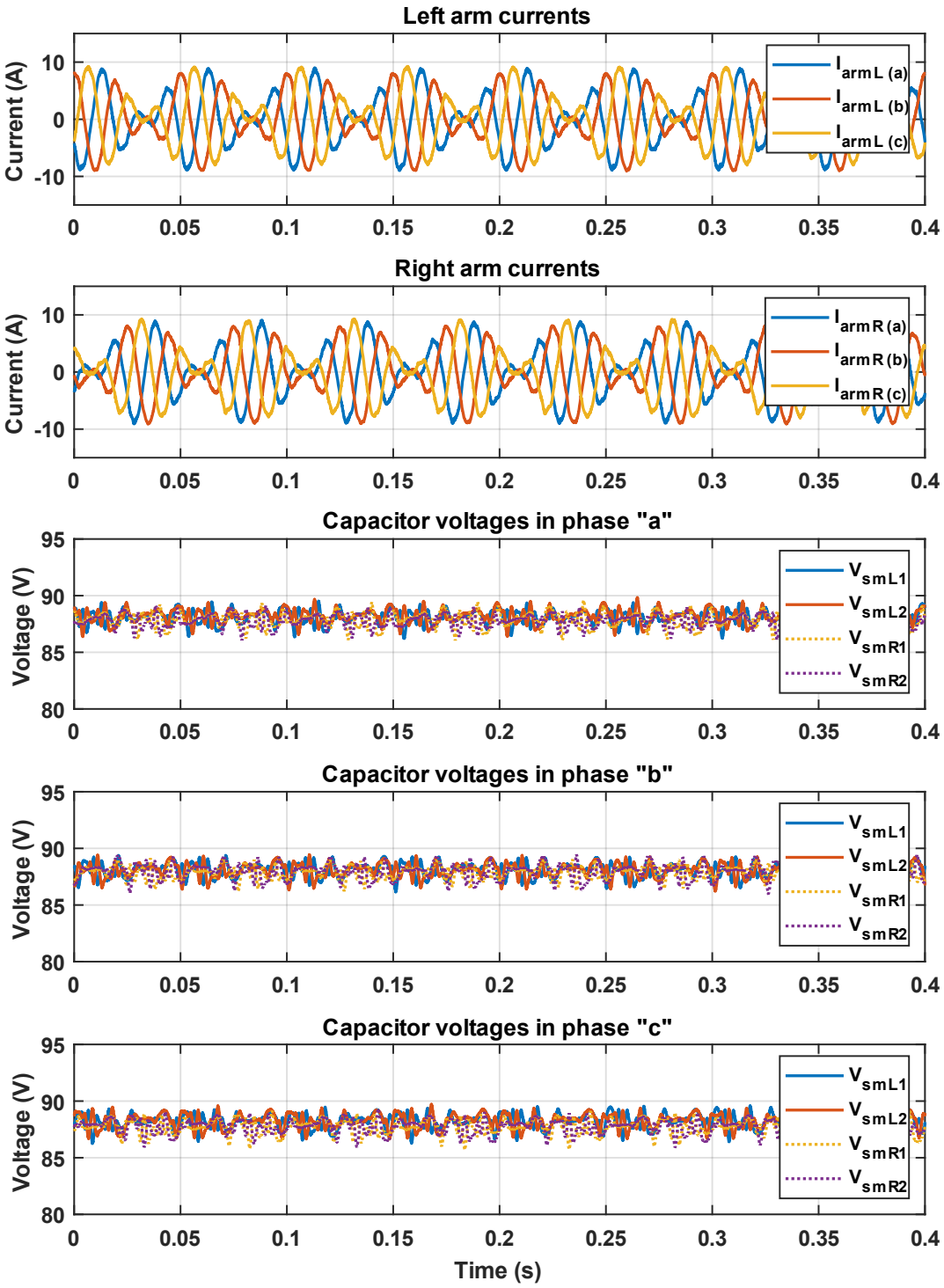

Figure A.1.2: Arm currents and capacitor voltages for f_1 = 40 Hz and f_2 = 60 Hz

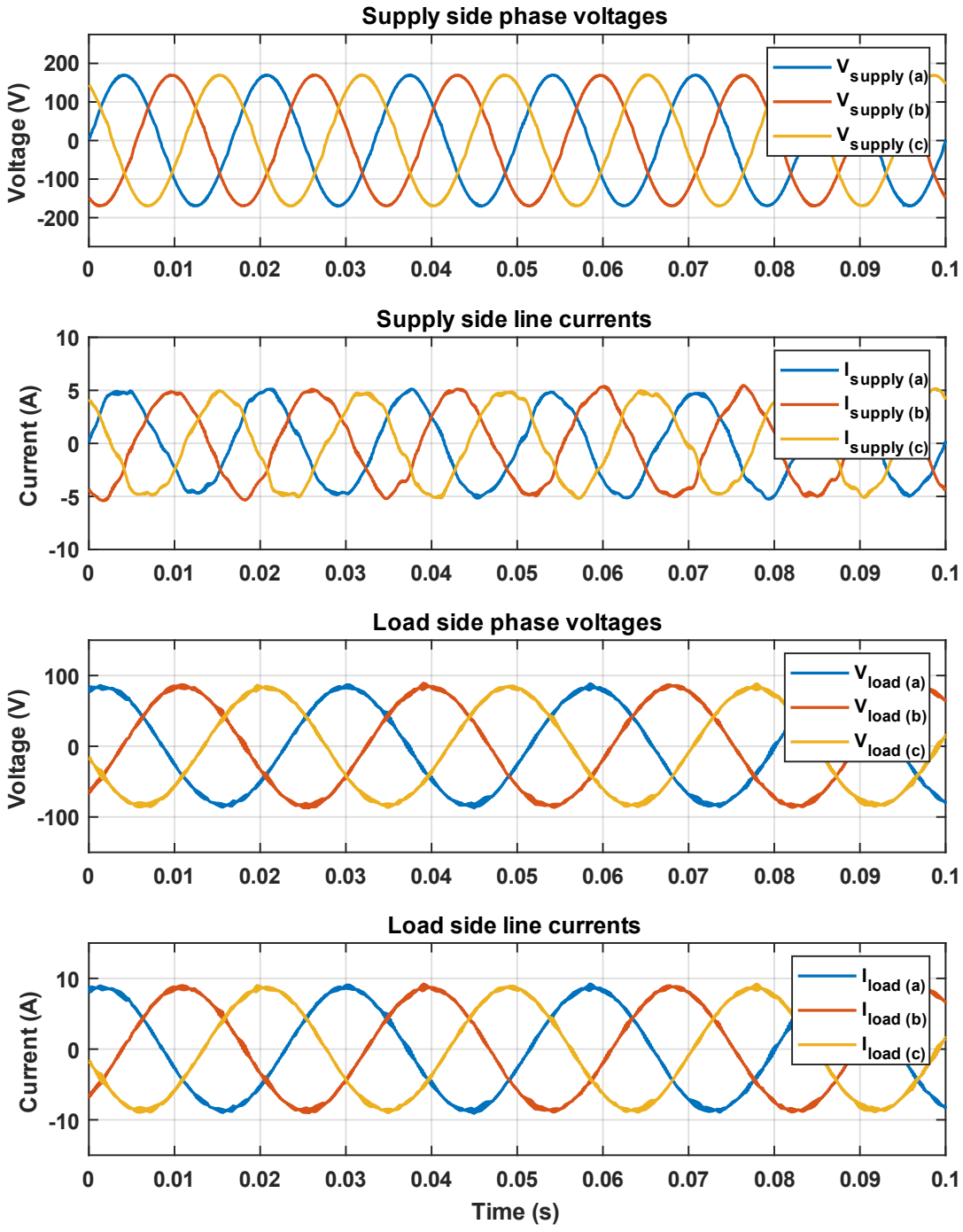

Figure A.1.3: Steady-state voltage and current waveforms for f_1 = 35 Hz and f_2 = 60 Hz

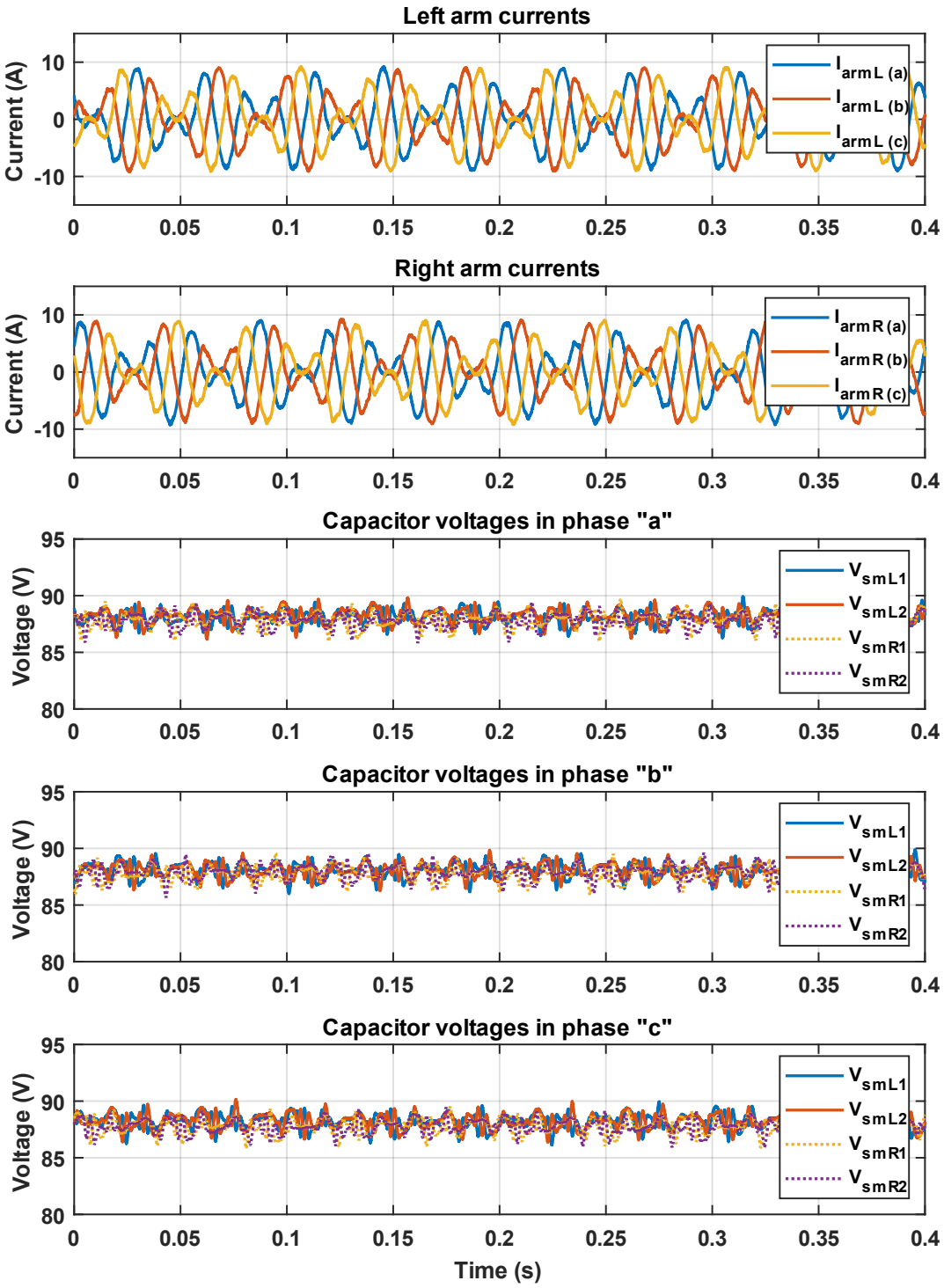

Figure A.1.4: Arm currents and capacitor voltages for f_1 = 35 Hz and f_2 = 60 Hz

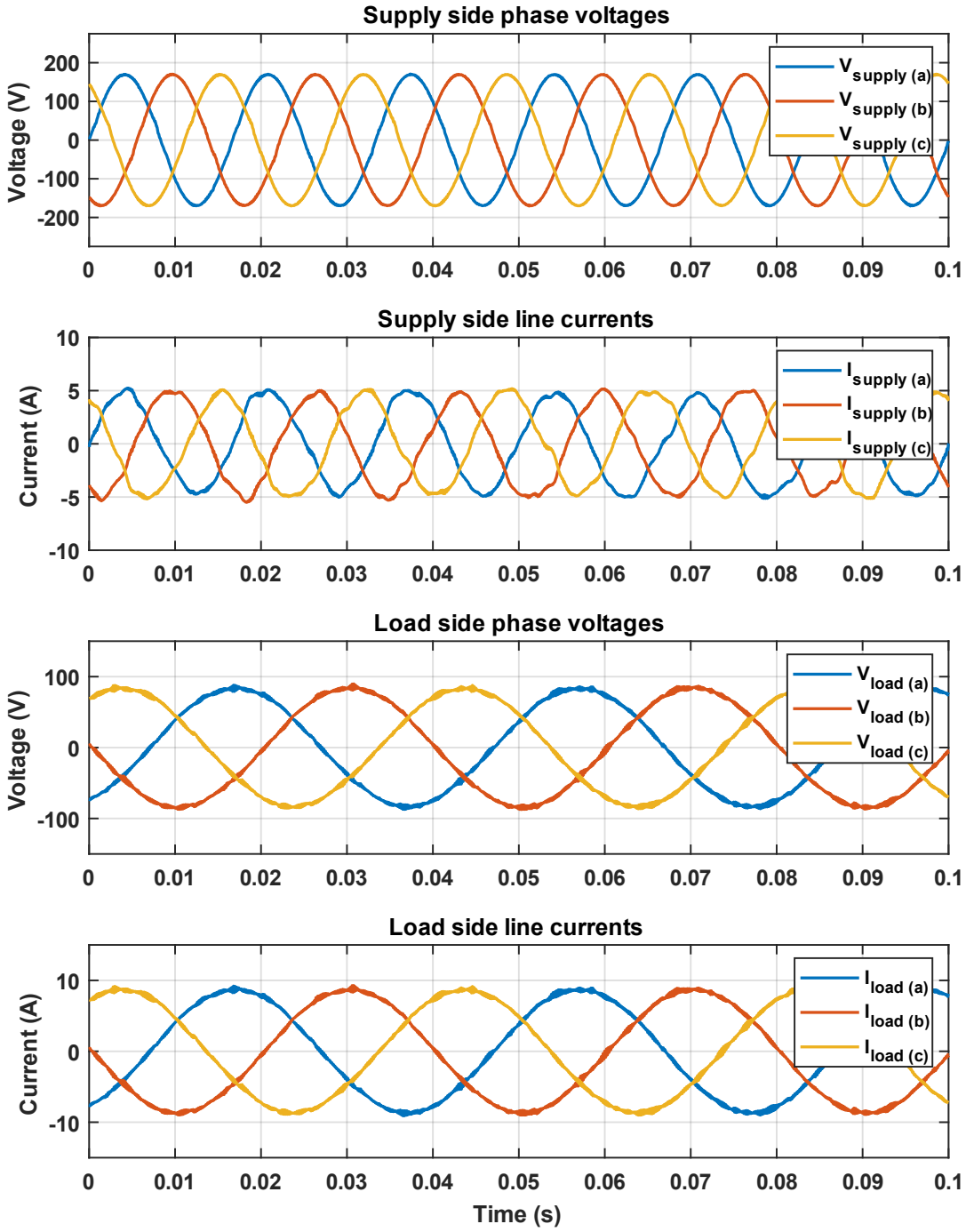

Figure A.1.5: Steady-state voltage and current waveforms for f_1 = 25 Hz and f_2 = 60 Hz

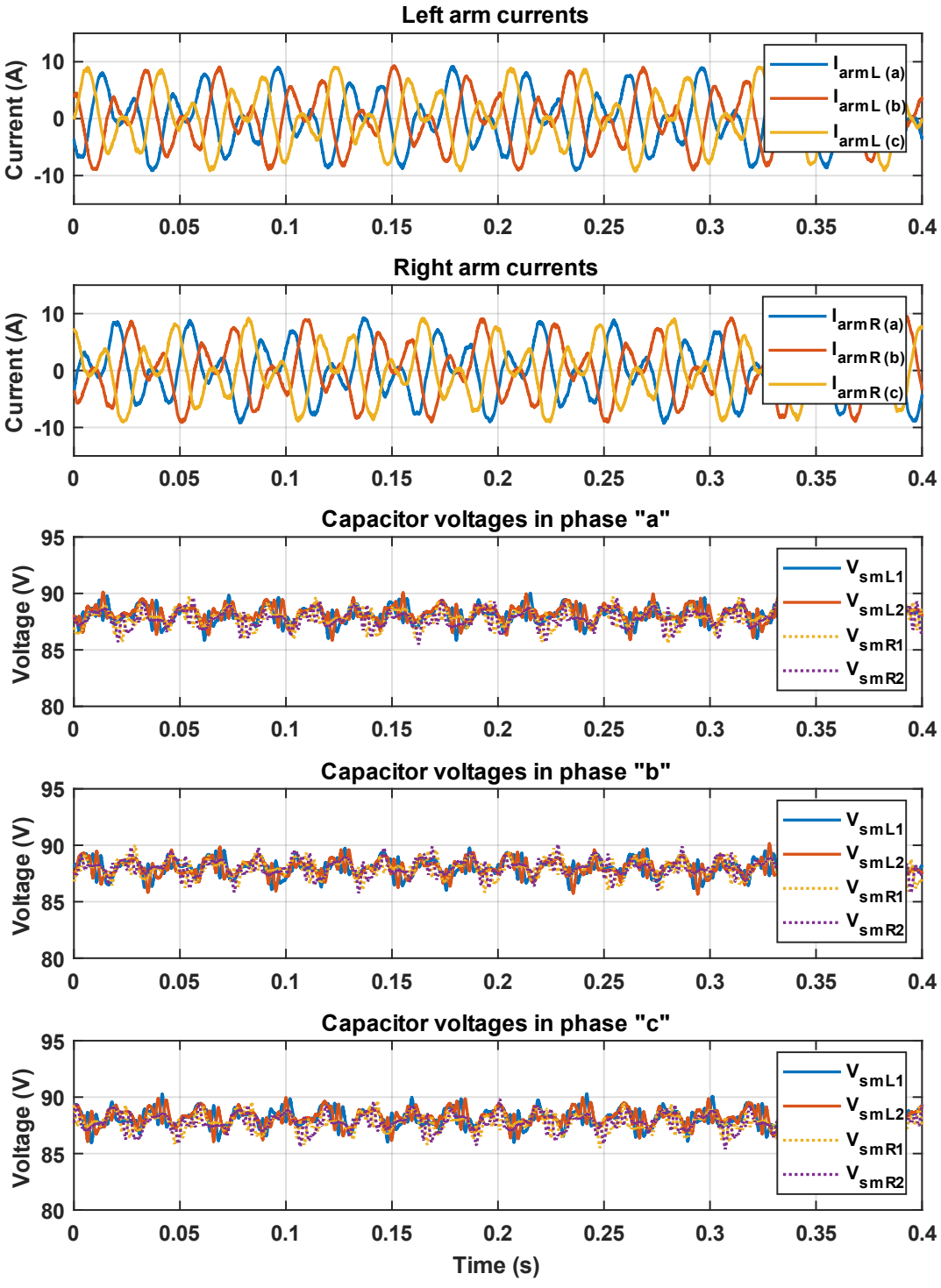

Figure A.1.6: Arm currents and capacitor voltages for f_1 = 25 Hz and f_2 = 60 Hz

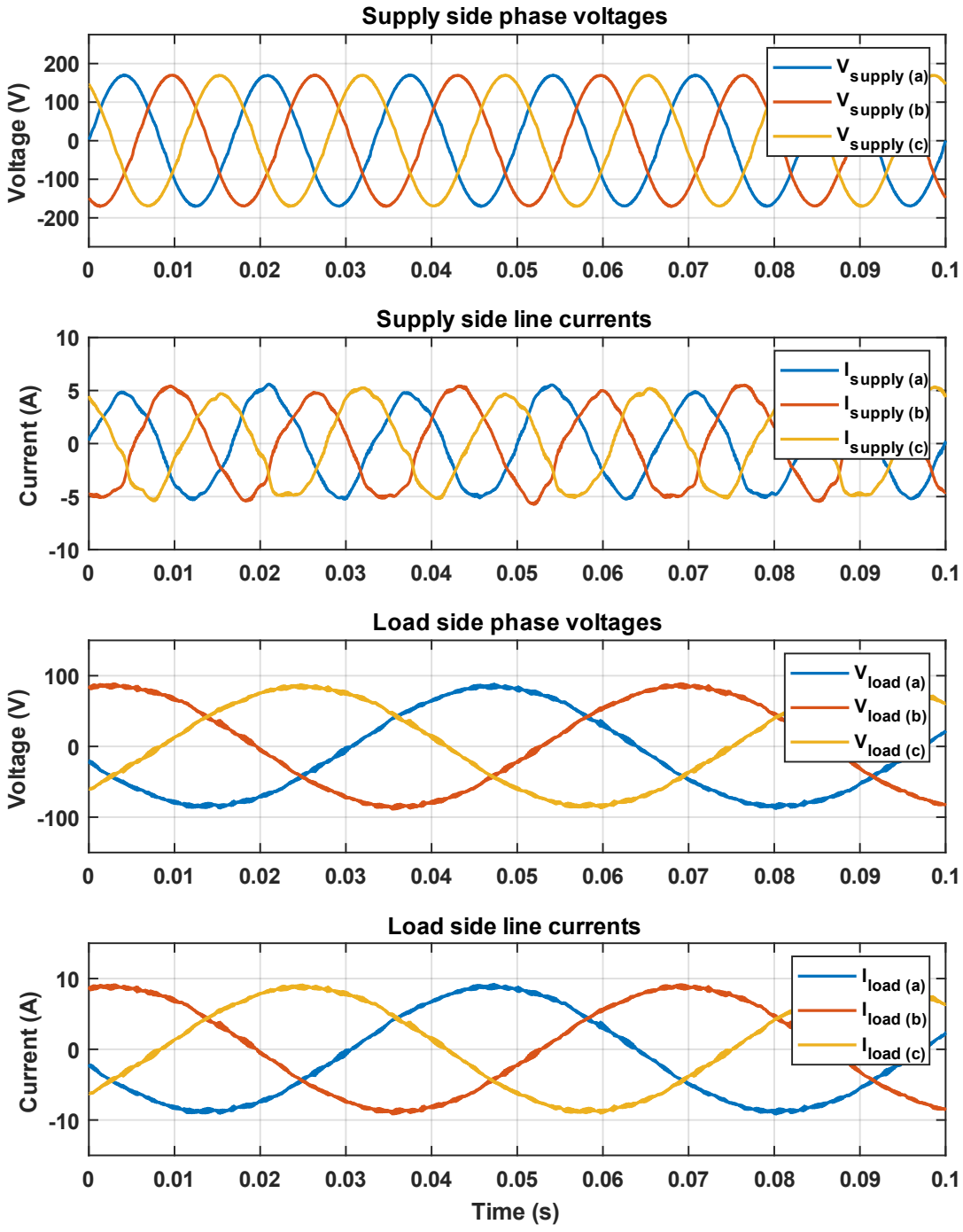

Figure A.1.7: Steady-state voltage and current waveforms for f_1 = 15 Hz and f_2 = 60 Hz

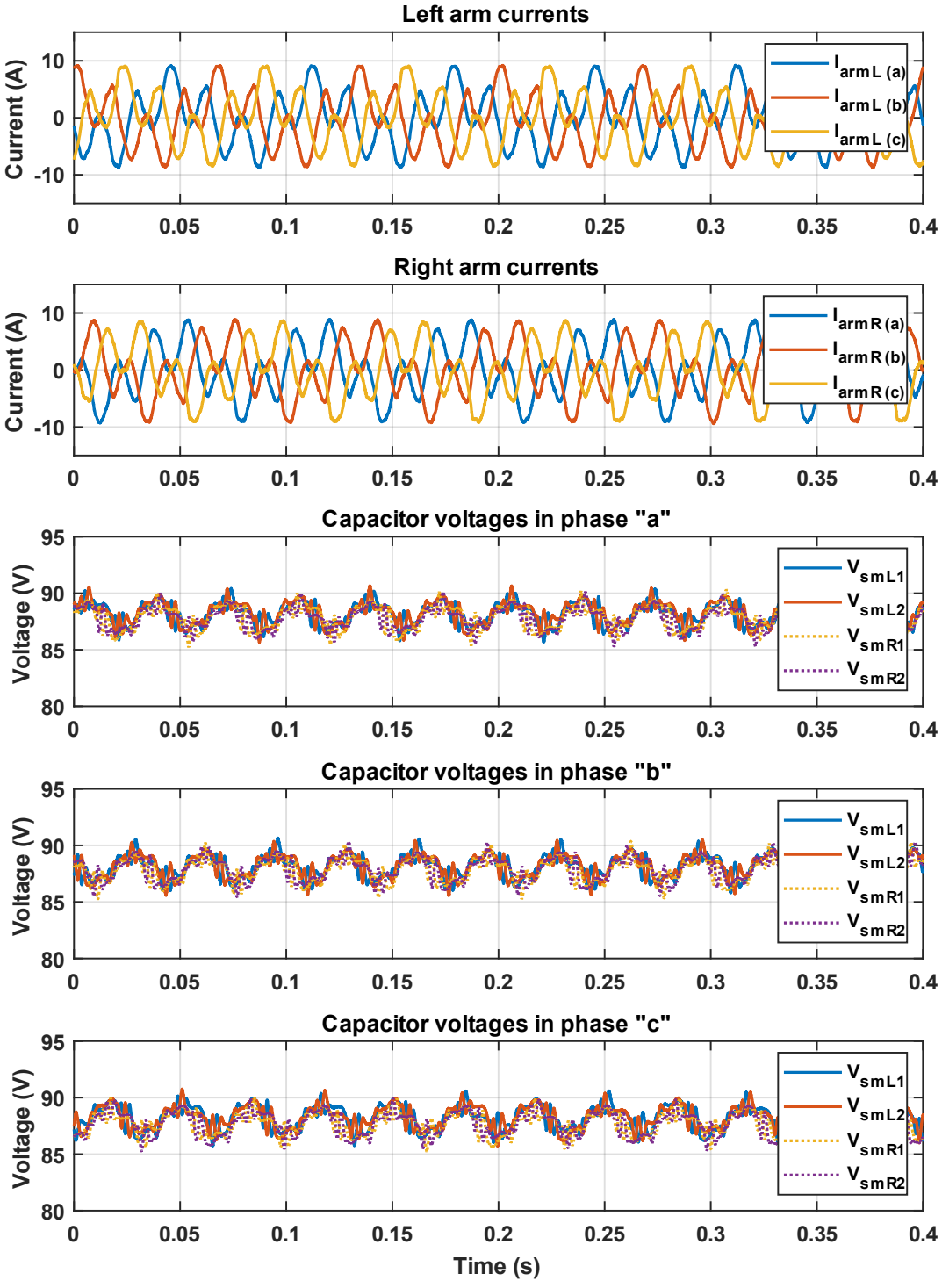

Figure A.1.8: Arm currents and capacitor voltages for f_1 = 15 Hz and f_2 = 60 Hz

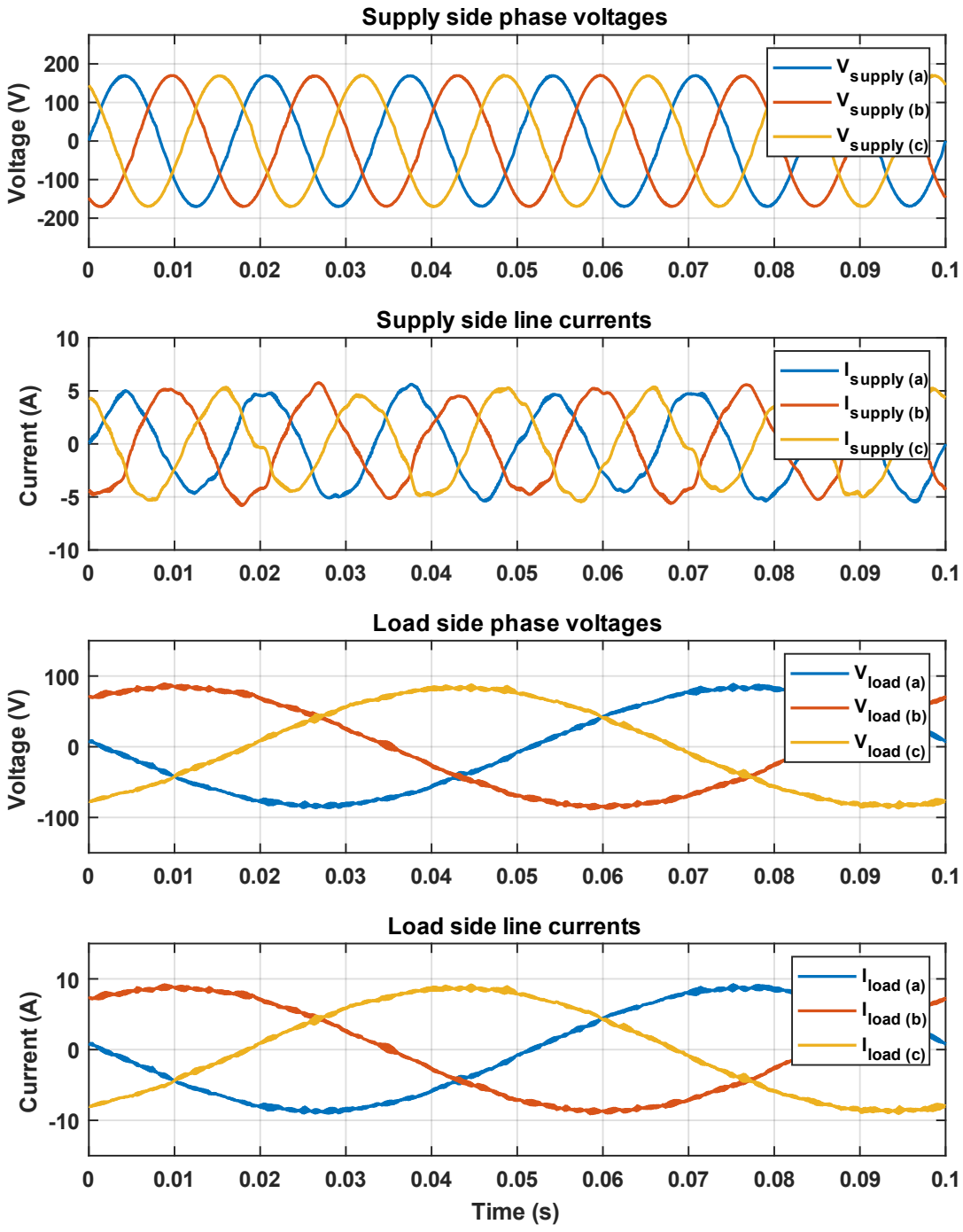

Figure A.1.9: Steady-state voltage and current waveforms for f_1 = 10 Hz and f_2 = 60 Hz

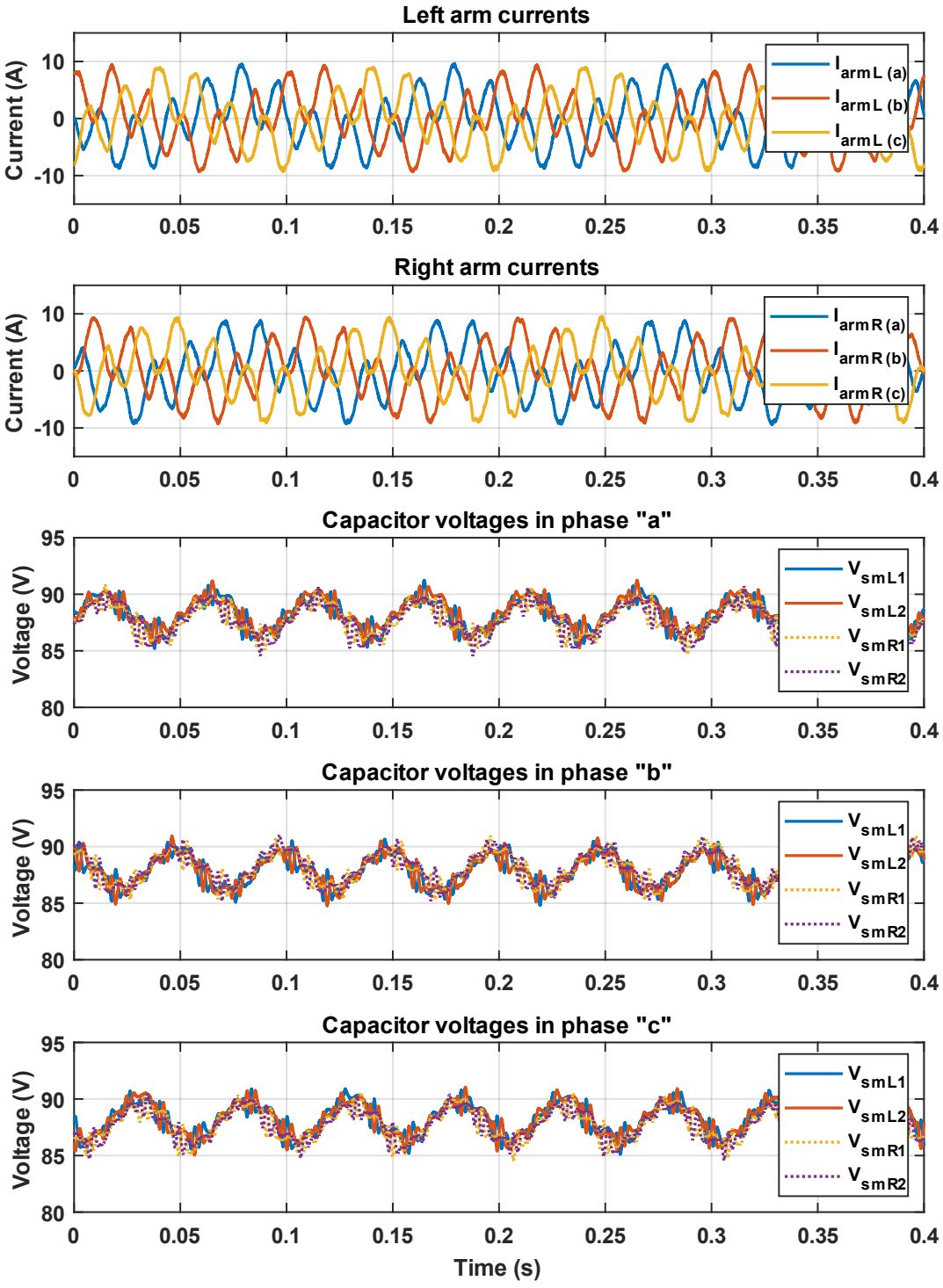

Figure A.1.10: Arm currents and capacitor voltages for f_1 = 10 Hz and f_2 = 60 Hz

A.2 Oscilloscope Waveforms

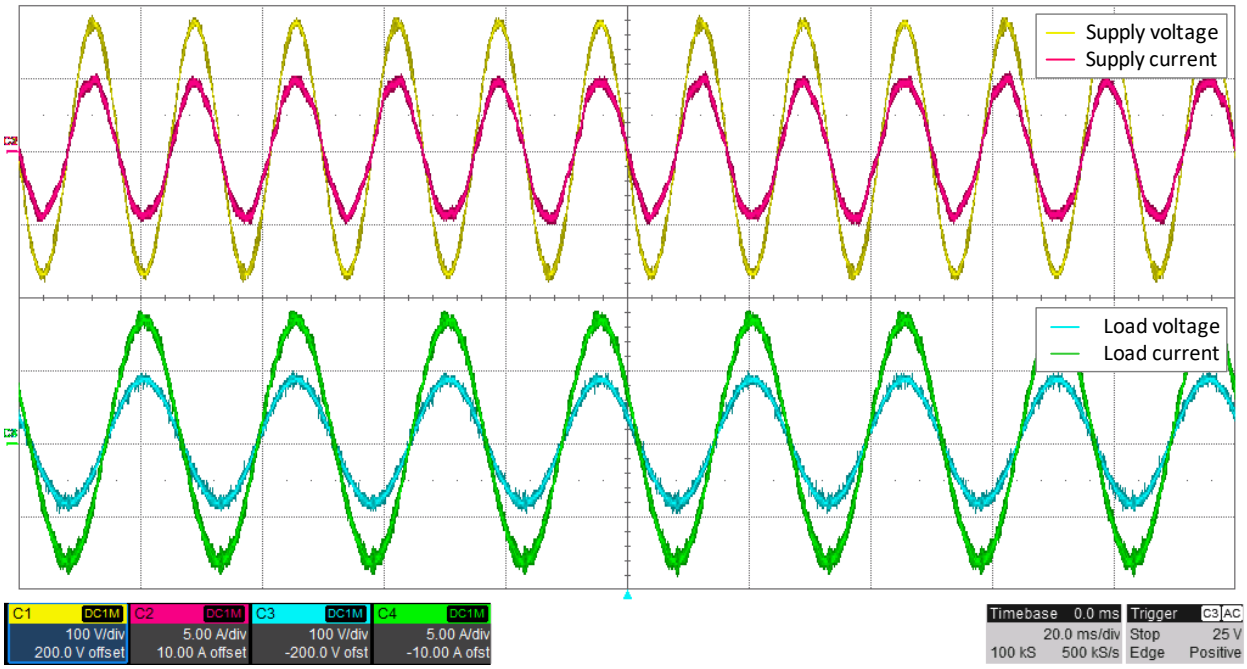

Figure A.2.1: Voltage and current waveforms for supply and load in phase 'a' at f_1 = 40 Hz and f_2 = 60 Hz

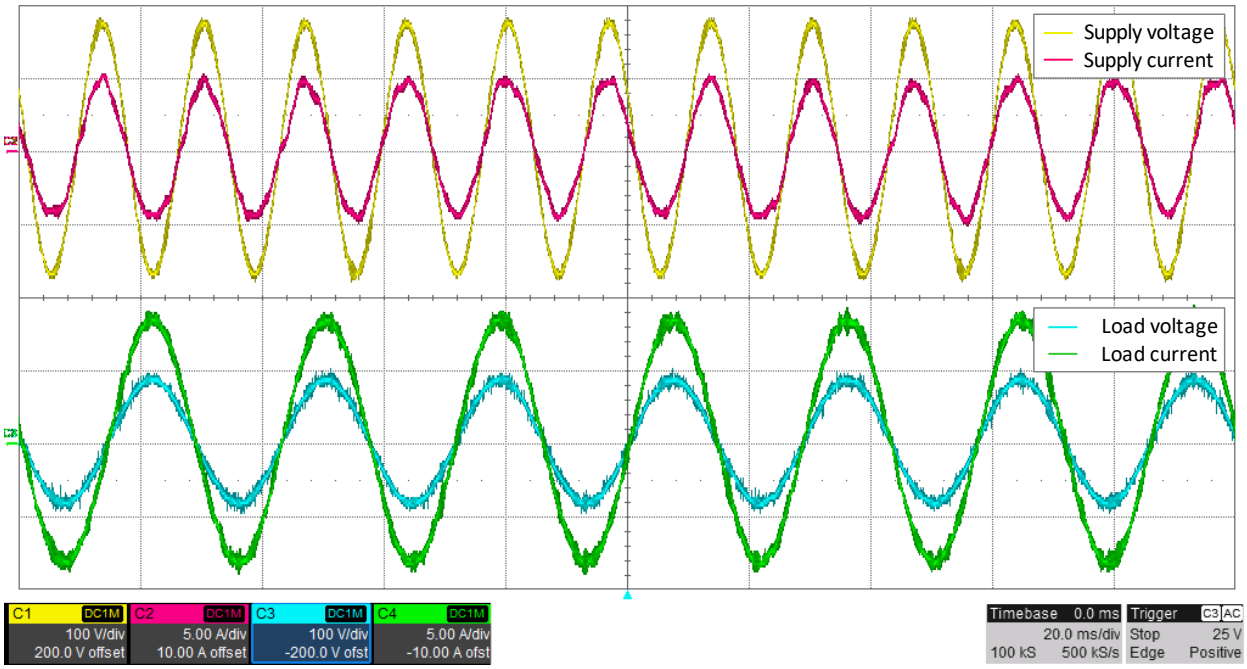

Figure A.2.2: Voltage and current waveforms for supply and load in phase 'a' at f_1 = 35 Hz and f_2 = 60 Hz

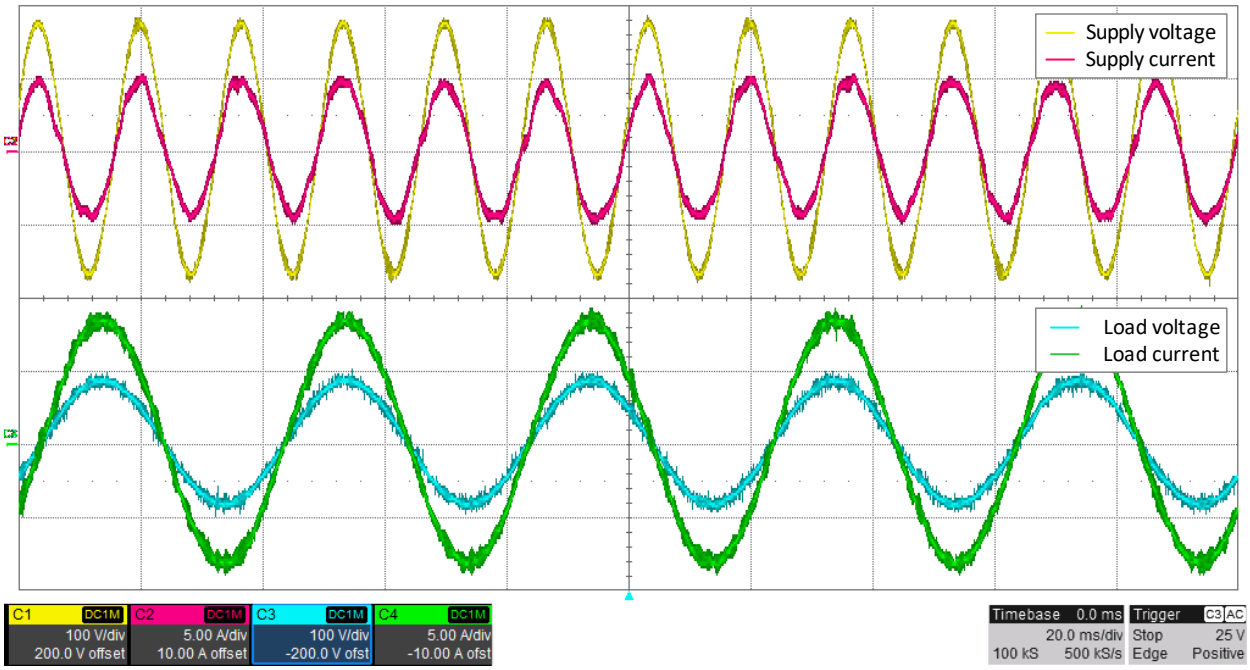

Figure A.2.3: Voltage and current waveforms for supply and load in phase 'a' at f_1 = 25 Hz and f_2 = 60 Hz

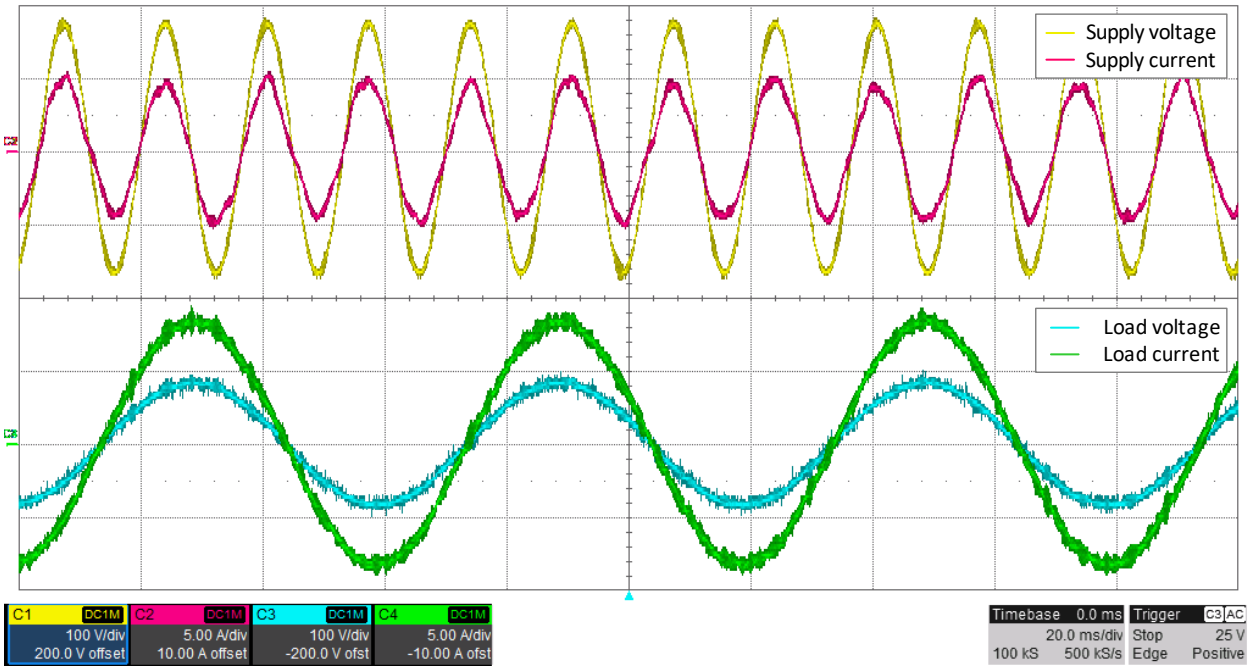

Figure A.2.4: Voltage and current waveforms for supply and load in phase 'a' at f_1 = 50/3 Hz and f_2 = 60 Hz

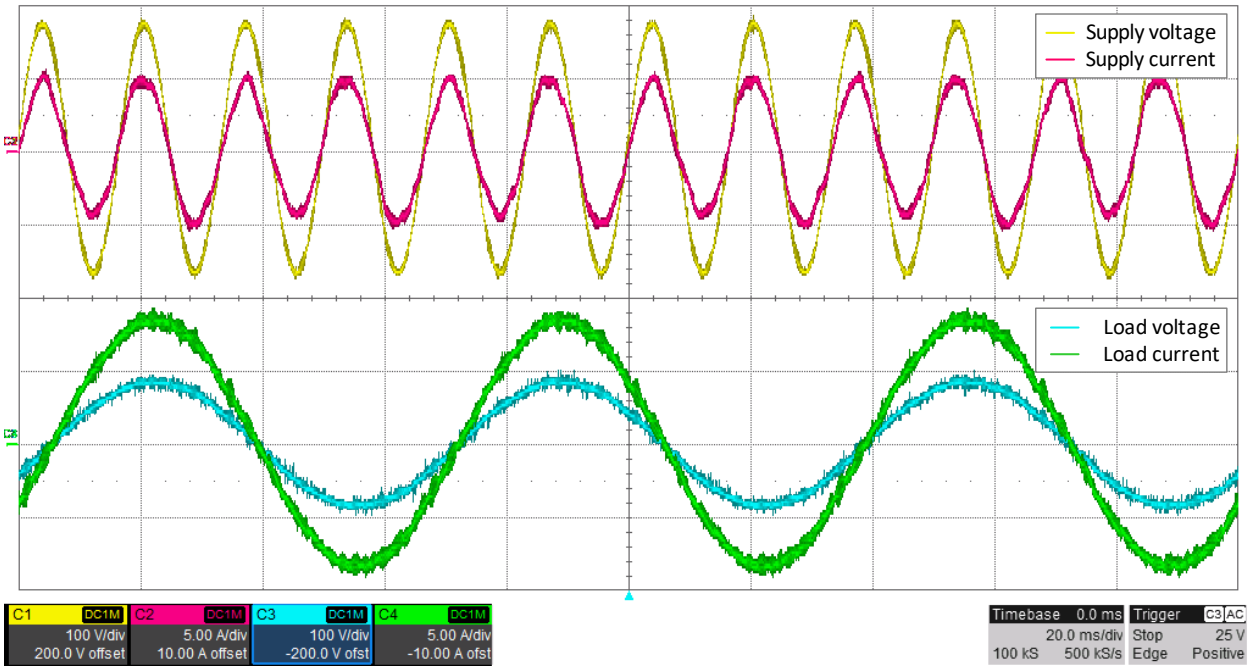

Figure A.2.5: Voltage and current waveforms for supply and load in phase 'a'
at f_1 = 15 Hz and f_2 = 60 Hz

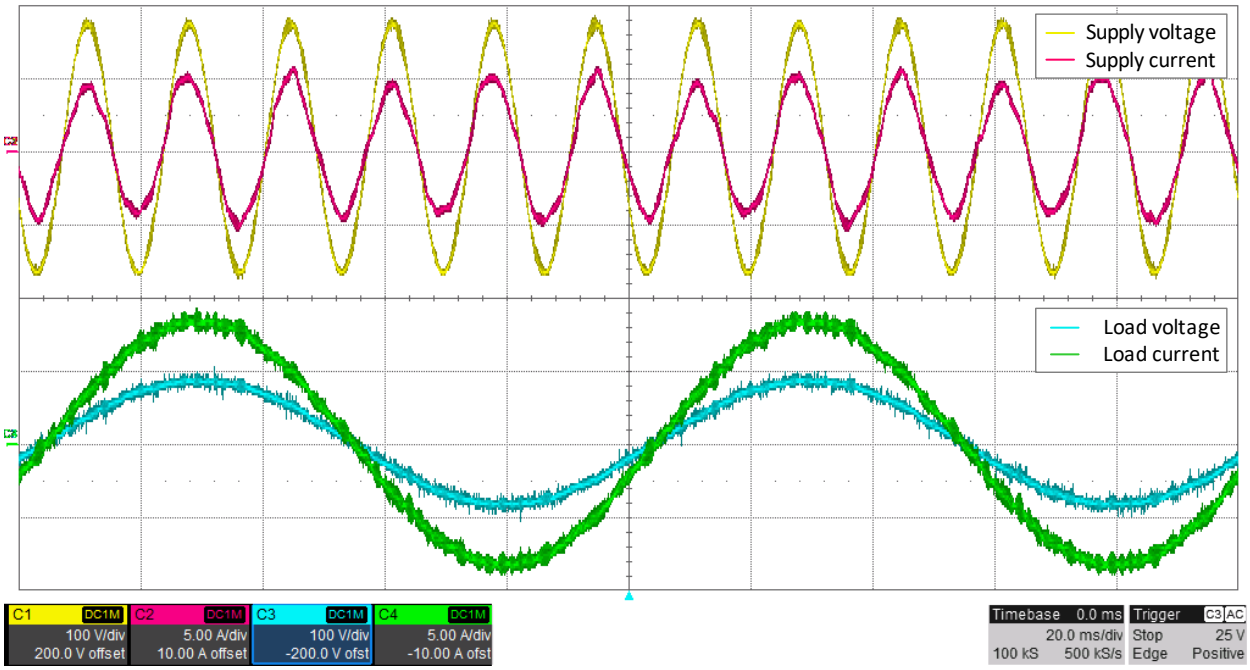

Figure A.2.6: Voltage and current waveforms for supply and load in phase 'a'
at f_1 = 10 Hz and f_2 = 60 Hz